

เสถียรภาพของกริดขนาดเล็กที่มีแหล่งผลิตกำลังไฟฟ้าจากลม



นาย ไชวาน เสง

## ศูนย์วิทยทรัพยากร

วิทยานิพนธ์นี้เป็นส่วนหนึ่งของการศึกษาตามหลักสูตรปริญญาวิศวกรรมศาสตรมหาบัณฑิต  
สาขาวิชาวิศวกรรมไฟฟ้า ภาควิชาวิศวกรรมไฟฟ้า  
คณะวิศวกรรมศาสตร์ จุฬาลงกรณ์มหาวิทยาลัย

ปีการศึกษา 2551

ลิขสิทธิ์ของจุฬาลงกรณ์มหาวิทยาลัย

# STABILITY OF A MICROGRID WITH WIND POWER GENERATION



Mr. Sovannarith Leng

A Thesis Submitted in Partial Fulfillment of the Requirements  
for the Degree of Master of Engineering Program in Electrical Engineering

Department of Electrical Engineering

Faculty of Engineering

Chulalongkorn University

Academic Year 2008

Copyright of Chulalongkorn University

Thesis Title STABILITY OF A MICROGRID WITH WIND POWER GENERATION

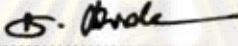
By Mr. Sovannarith Leng

Field of Study Electrical Engineering

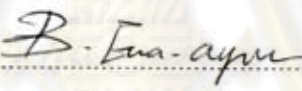
Thesis Principal Advisor Naebboon Hoonchareon, Ph. D.

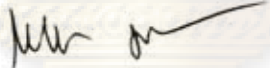
---

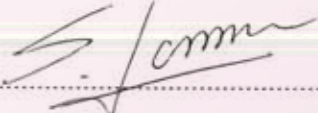
Accepted by the Faculty of Engineering, Chulalongkorn University in Partial Fulfillment of the Requirements for the Master's Degree

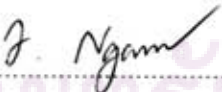
  
..... Dean of the Faculty of Engineering  
(Associate Professor Boonsom Lerdhirunwong, Dr. Ing)

THESIS COMMITTEE

  
..... Chairman  
(Professor Bundhit Eua-arporn, Ph.D.)

  
..... Thesis Principal Advisor  
(Naebboon Hoonchareon, Ph.D.)

  
..... Member  
(Somboon Sangwongwanich, Dr. of Eng.)

  
..... External Member  
(Associate Professor Issarachai Ngamroo, Ph. D.)

ศูนย์วิจัยทรัพยากรชีวภาพ  
จุฬาลงกรณ์มหาวิทยาลัย

ชิวาน เลข: เสถียรภาพของกริดขนาดเล็กที่มีแหล่งผลิตกำลังไฟฟ้าจากลม. (STABILITY OF A MICROGRID WITH WIND POWER GENERATION) อ. ที่ปรึกษาวิทยานิพนธ์: ดร. แนนบุญ หนูเจริญ, 78 หน้า.

วิทยานิพนธ์นี้ นำเสนอการพัฒนาแบบจำลองเชิงพลวัตของกริดขนาดเล็ก ที่ประกอบด้วยกังหันลม ขับเคลื่อนเครื่องกำเนิดไฟฟ้าเหนี่ยวนำแบบกรงกระรอก และแบบดับลิเฟด (Doubly-fed) เครื่องกำเนิดไฟฟ้าแบบซิงโครนัส และโหลดที่มีองค์ประกอบบางส่วนเป็นแบบโหลดกำลังไฟฟ้าคงที่ การแปรผันของความถี่ลมตามธรรมชาติถูกจำลองด้วยค่าสุ่มที่มีการกระจายแบบไวน์บูล ทำการศึกษาสมรรถนะเชิงพลวัตของระบบดังกล่าวภายใต้การรบกวนทั้งขนาดใหญ่และขนาดเล็ก รวมถึงสมรรถนะของระบบภายใต้การทำงานแบบแยกอิสระจากกริดหลัก พร้อมทั้งเปรียบเทียบระหว่างการควบคุมกังหันลมและเครื่องกำเนิดไฟฟ้าเหนี่ยวนำที่ต่างกันไปในสามแบบ ได้แก่ แบบความเร็วโรเตอร์คงที่ แบบความเร็วโรเตอร์แปรผัน เพื่อควบคุมค่ากำลังไฟฟ้ารีแอกทีฟ และแบบความเร็วโรเตอร์แปรผัน เพื่อควบคุมขนาดแรงดันที่ขั้วเครื่องกำเนิดไฟฟ้า โดยให้ความสำคัญเป็นพิเศษกับการแกว่งของกำลังไฟฟ้าที่ผลิตได้จากกังหันลม และผลกระทบของการแกว่งของกำลังไฟฟ้างกล่าวต่อกำลังไฟฟ้าที่ไหลผ่านจุดเชื่อมต่อกับกริดหลัก เพื่อรักษาเสถียรภาพของควมถี่ในกริดขนาดเล็กนั้น นอกจากนี้ยังได้ศึกษาผลของการสับปลดตัวเก็บประจุที่ติดตั้งไว้บริเวณสถานีไฟฟ้าพลังงานลมเพื่อชดเชยกำลังไฟฟ้ารีแอกทีฟที่มีต่อเสถียรภาพของกริดขนาดเล็กนี้ด้วย

นอกจากการศึกษาด้วยการจำลองแบบเชิงเวลาแล้ว ยังได้วิเคราะห์สัญญาณขนาดเล็กของระบบที่ทำให้เป็นเชิงเส้น เพื่อศึกษาพฤติกรรมที่เกี่ยวข้องกับเสถียรภาพเชิงสัญญาณขนาดเล็กของระบบ

ผลจากการศึกษานี้ สามารถนำไปประยุกต์เพื่อใช้กำหนดความต้องการเชิงสมรรถนะของการควบคุมกริดขนาดเล็กที่ผลิตไฟฟ้าจากพลังงานลมนี้ เพื่อให้สามารถทำงานได้อย่างน่าเชื่อถือและมีเสถียรภาพต่อไปในอนาคต

# ศูนย์วิทยทรัพยากร จุฬาลงกรณ์มหาวิทยาลัย

ภาควิชา.....วิศวกรรมไฟฟ้า..... ลายมือชื่อนิลิต.....  
สาขาวิชา.....วิศวกรรมไฟฟ้า..... ลายมือชื่อ อ.ที่ปรึกษาวิทยานิพนธ์หลัก.....  
ปีการศึกษา 2551

##4970766521: MAJOR ELECTRICAL ENGINEERING

KEYWORDS : MICROGRID/ WIND POWER GENERATION/ DOUBLY-FED  
INDUCTION GENERATOR/STABILITY

SOVANNARITH LENG: STABILITY OF A MICROGRID WITH WIND  
POWER GENERATION. THESIS PRINCIPAL ADVISOR: NAEBBOON  
HOONCHAREON, Ph.D. 78 pp.

This thesis presents dynamic modeling of the microgrid with wind-turbine driven squirrel cage induction generator and doubly-fed induction generator, synchronous generator, and some constant-power load. The natural fluctuation of wind speed is modeled using Weibull distribution. The system dynamic performances under both small and large disturbances, including islanding mode of operation have been examined, and compared among the three different control schemes: fixed-speed, variable-speed with VAR control and variable-speed with voltage control. Special attention has been paid to the resulting fluctuations of generated power from wind station and its impact, especially under short-circuit on the tie-line stabilizing flow and frequency fluctuation of the microgrid. Moreover it also investigates the impact of local capacitor switching, for conventional reactive power compensator, on the stability of the microgrid system.

In addition to the time domain simulation, the small signal analysis of the linearized system has been conducted in order to examine the small signal stability of the microgrid.

The test results here could be applied to addressing appropriate control performance requirements to ensure reliable and stable operation of the microgrid with wind power generation in the future.

ศูนย์วิทยทรัพยากร  
จุฬาลงกรณ์มหาวิทยาลัย

Department: Electrical Engineering

Field of Study: Electrical Engineering

Academic Year: 2008

Student's Signature: \_\_\_\_\_

Principal Advisor's Signature: \_\_\_\_\_

*Sovannarith*

*Naebboon*

## ACKNOWLEDGEMENTS

I express, from bottom of heart, my deepest and sincerest appreciation and gratitude to my beloved adviser, Dr. Naebboon Hoonchareon for his instructions, guidance, care, friendly discussion, and continuous encouragement. In my life, I will not forget encouragement and helpful advice for my study at Chulalongkorn University.

I especially wish to thank my thesis committee: Professor Dr. Bundhit Eua-Arporn, Dr. Somboon Sangwongwanich, and Assoc. Prof. Dr. Issarachai Ngamroo, for their invaluable advices, thesis supervision, and instructive encouragement.

Thanks also to the lecturers and professors at the Department of Electrical Engineering, Chulalongkorn University, for their invaluable sources of knowledge, and wisdoms.

Very special and profound thanks and gratitude to my beloved parent for their love, constant moral encouragement, and their sacrifice of everything for their sons and daughters. They always support and hold me when I am down so I never lost my spirit. No word I can say about their goodness. I am very proud to be their son. I also thank to my brothers and sister for caring and support. It is to them that I dedicate this thesis.

The last but not least, I would like to express my deepest appreciation to JICA for AUN/SEED-Net project for my financial support, to officers and staffs of International School of Engineering (ISE) and AUN/SEED-Net for their kindness and help during my study.



ศูนย์วิทยทรัพยากร  
จุฬาลงกรณ์มหาวิทยาลัย

# CONTENTS

<b>ABSTRACT (THAI)</b> .....	<b>iv</b>
<b>ABSTRACT (ENGLISH)</b> .....	<b>v</b>
<b>ACKNOWLEDGEMENTS</b> .....	<b>vi</b>
<b>CONTENTS</b> .....	<b>vii</b>
<b>LIST OF FIGURES</b> .....	<b>ix</b>
<b>LIST OF TABLES</b> .....	<b>x</b>
<b>CHAPTER I INTRODUCTION</b> .....	<b>1</b>
1.1 Motivation .....	1
1.2 Objective of Research.....	2
1.3 Scope of Research .....	2
1.4 Research Methodology .....	2
1.5 Expected Contribution.....	3
<b>CHAPTER II MICROGRID OPERATION</b> .....	<b>4</b>
2.1 Definition.....	4
2.2 Structure.....	4
2.3 Modes of Operation .....	5
2.4 Applications.....	6
2.5 Practical Issues .....	6
2.6 Microgrid Stability .....	7
<b>CHAPTER III WIND POWER GENERATION</b> .....	<b>8</b>
3.1 Aerodynamic System.....	8
3.1.1 Tip Speed Ratio .....	9
3.1.2 Power Coefficient.....	10
3.2 Wind Turbine Technologies .....	11
3.2.1 Fixed-Speed Wind Turbines.....	11
3.2.2 Variable-Speed Wind Turbines .....	11
3.3 Wind Turbine Configurations.....	12
3.3.1 Type A: Fixed Speed.....	12
3.3.2 Type B: Limited Variable Speed.....	13
3.3.3 Type C: Variable Speed With Partial Scale Frequency Converter .....	13
3.3.4 Type D: Variable Speed With Full-Scale Frequency Converter.....	14
3.4 Voltage Control Capability of Wind Turbine.....	14
3.4.1 Current Wind Turbine Types .....	14
3.4.2 Wind Turbine Voltage Control Capabilities .....	15
3.5 Induction Generator .....	17
3.5.1 Principle of Operation .....	17
3.5.2 Induction Machine Equivalent .....	18
3.5.3 Steady State Performance Equations of an Induction Machine .....	21
3.5.4 Steady State Performance.....	22

<b>CHAPTER IV SYSTEM MODELED .....</b>	<b>25</b>
4.1 Microgrid System Model.....	25
4.2 Wind Power System Model.....	26
4.2.1 Wind Speed Model.....	26
4.2.2 Rotor Model .....	27
4.2.3 Doubly-Fed Induction Generator Model.....	29
4.2.4 Converter Model .....	32
4.2.5 Rotor-Side PWM Controller Model.....	36
4.2.6 Grid-Side PWM Control Model.....	40
4.2.7 Pitch Angle Controller Model.....	42
4.3 Synchronous Machine Model.....	42
4.3.1 Generator Model .....	42
4.3.2 Governor Model .....	47
4.4 Load Model.....	47
4.5 Network Model.....	48
<b>CHAPTER V TEST RESULTS AND DISCUSSION.....</b>	<b>53</b>
5.1 Validation of System Model.....	53
5.1.1 WT-SCIG without Local VAr Compensation.....	53
5.1.2 WT-SCIG with Local VAr Compensation.....	55
5.2 Dynamic Responses under Local Capacitor Switching.....	60
5.3 Dynamic Responses Under Small Disturbance .....	64
5.4 Dynamic Responses Under Temporary Fault.....	66
5.5 Dynamic Responses Under Permanent Fault .....	68
5.6 Impact of Load Model .....	70
5.7 Small Signal Analysis.....	71
<b>CHAPTER VI CONCLUSION .....</b>	<b>74</b>
6.1 Conclusion .....	74
6.2 Future Works .....	74
<b>REFERENCES.....</b>	<b>75</b>
<b>APPENDIX.....</b>	<b>76</b>
<b>BIOGRAPHY.....</b>	<b>78</b>

ศูนย์วิทยทรัพยากร  
จุฬาลงกรณ์มหาวิทยาลัย

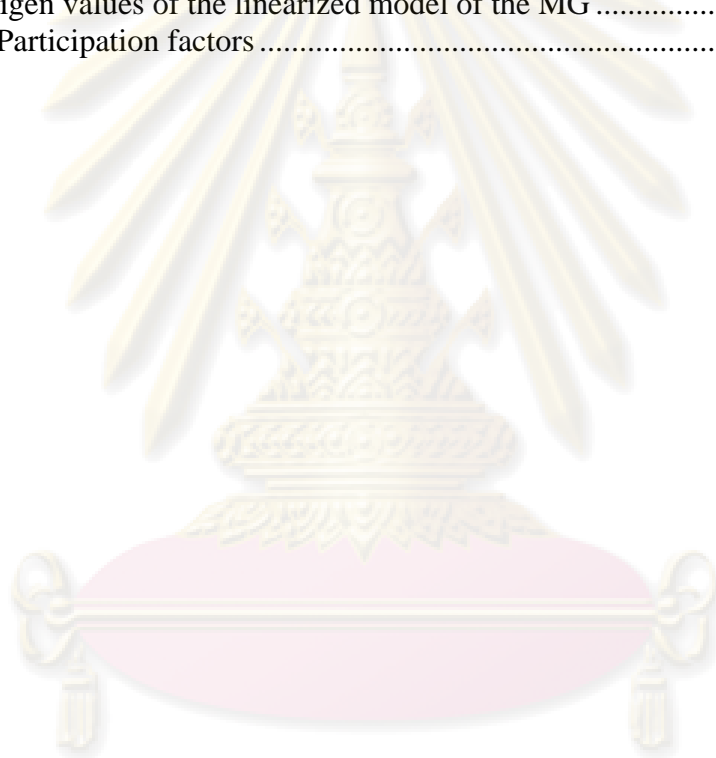


## LIST OF FIGURES

Figure 2.1 Microgrid architecture.....	5
Figure 3.1 Illustration of wind conditions around the moving blade.....	10
Figure 3.2 Wind turbine type A.....	12
Figure 3.3 Wind turbine type B.....	13
Figure 3.4 Wind turbine type C.....	13
Figure 3.5 Wind turbine type D.....	14
Figure 3.6 Widely used wind turbine types.....	15
Figure 3.7 Dependence of (a) active and (b) reactive power of a squirrel cage induction generator.....	16
Figure 3.8 Elementary equivalent circuit for induction machine.....	19
Figure 3.9 Equivalent circuit for an induction machine.....	20
Figure 3.10 Equivalent circuit with rotor at stator frequency.....	20
Figure 3.11 Induction machine speed-torque characteristic.....	23
Figure 3.12 Generation and braking characteristics of the induction machine.....	24
Figure 4.1 Single line diagram of the studied microgrid system.....	25
Figure 4.2 Wind power system.....	26
Figure 4.3 Wind speed simulation.....	27
Figure 4.4 Weibull distribution at each wind speed.....	27
Figure 4.5 Performance coefficient of wind turbine.....	28
Figure 4.6 Turbine characteristic.....	28
Figure 4.7 Block diagram of rotor model.....	29
Figure 4.8 Full-bridge dc-dc converter.....	33
Figure 4.9 PWM with bipolar voltage switching.....	33
Figure 4.10 One-leg switch-mode inverter.....	34
Figure 4.11 Pulse-width modulation (PWM).....	35
Figure 4.12 Sinusoidal PWM.....	36
Figure 4.13 Turbine characteristic and optimal power tracking curves.....	38
Figure 4.14 V-I characteristic.....	39
Figure 4.15 Block diagram of rotor-side converter control.....	40
Figure 4.16 Schematic of grid-side converter.....	40
Figure 4.17 Block diagram of grid-side converter control.....	41
Figure 4.18 Pitch angle control model.....	42
Figure 4.19 Droop characteristic.....	47
Figure 4.20 Constant power dynamic load model.....	48
Figure 4.21 Transformation reference frame.....	51
Figure 5.1 Simulink block of microgrid with WT-SCIG.....	53
Figure 5.2 Dynamic responses of SCIG without local VAR compensation.....	55
Figure 5.3 Mechanical torque of wind turbine.....	57
Figure 5.4 Dynamic responses of SCIG with var compensation.....	59
Figure 5.5 Simulink block of microgrid with WT-SCIG and SG.....	60
Figure 5.6 Impact of local compensator on stability of MG.....	63
Figure 5.7 Simulink block of MG with DFIG and a constant power load model.....	64
Figure 5.8 Dynamic performances under small disturbance.....	65
Figure 5.9 Active power fluctuation.....	66
Figure 5.10 Dynamic performances under temporary fault.....	68
Figure 5.11 Dynamic performances under permanent fault.....	69
Figure 5.12 Simulink block of MG with all constant power loads.....	70
Figure 5.13 Frequency of the MG.....	71

## LIST OF TABLES

Table 2.1 Relative sizes of distributed generation .....	7
Table 3.1 Approximation of power curves .....	10
Table 3.2 Wind turbine types .....	12
Table 4.1 Nominal values of wind turbine rotor .....	29
Table 5.1 Load flow initialization without local VAR compensation .....	54
Table 5.2 Line flow and losses without local VAR compensation .....	54
Table 5.3 Load flow initialization with local VAR compensation .....	55
Table 5.4 Line flow and losses with local VAR compensation .....	55
Table 5.5 Load flow initialization without local VAR compensation .....	61
Table 5.6 Line flow and losses without local VAR compensation .....	61
Table 5.7 Load flow initialization with local VAR compensation .....	62
Table 5.8 Line flow and losses with local VAR compensation .....	62
Table 5.9 Eigen values of the linearized model of the MG .....	72
Table 5.10 Participation factors .....	72



ศูนย์วิทยทรัพยากร  
จุฬาลงกรณ์มหาวิทยาลัย

# CHAPTER I

## INTRODUCTION

### 1.1 Motivation

Current research topics relating to microgrid application have gained increasing attention recently due to the continued advancement of distributed generation (DG) technology and the environmental incentives of such a small-scaled power system. This could significantly change the structure of electric power industry to which power engineers are accustomed. Some large power plants could soon be disconnected from the grid because of their deteriorating efficiency and adverse impacts on the environment, whereas the total amount of power generated by modern DG technologies is expected to increase significantly. Hence, it requires attention of power system engineers and researchers to look into issues pertinent to system performance of the micro-grid, including stability performance.

Most emerging technologies to be employed in the micro-grid such as wind turbine, photovoltaic, micro-turbine, fuel cell, as well as high-performance energy storage have their dynamical characteristics quite different from one another, and from those of conventional technology. Hence, modeling dynamical performance of a microgrid system is rather a complex task. In this thesis, it examines stability of a microgrid which is primarily supplied by one of the most likely to be utilized sources, that is wind power generation.

Wind power generation employing a doubly-fed induction generator (DFIG) is one of the fastest growing sources of power generation worldwide because of the following crucial features: ample and widespread resources, clean and suitable for remote areas, and fast technology advancement [1]. The salient characteristics of DFIG for this application are its capabilities to optimize the output electrical power and to minimize impact of the fluctuation of wind velocity on the generated power, simultaneously.

In Thailand, it is expected to see the increasing number of DGs within distribution systems in response to the government policy on promoting the uses of renewable energy and of high-efficiency combined heat and power (CHP) technology, through the scheme of purchasing electric power from Very Small Power Producers (VSPP). In Cambodia, with the country's distributed structure of power systems having already existed, it could see more prevalent uses of DGs, especially in the types of wind power and small hydro power in the near future.

Although penetration of DGs currently has not yet reached the significant level, that situation is changing quite rapidly and requires attention to issues related to high penetration of DG within the distribution systems. Indiscriminant application of individual DG could cause quite technical challenges, such as voltage regulation, protection coordination, and distribution system reliability, for operating an entire distribution system. To that end, a better way to realize the emerging potential of DG is to take a system-based approach which views a group of DGs and the associated loads as a subsystem, referred to as "Microgrid".

Many researches are being undertaken relating Microgrid (MG). Some model architectures have been proposed. Although the components of a MG are fairly well understood, the system as a whole is not. When several sources are connected to form a MG, the system behavior remains unpredictable. This being the case, modeling the

system and examining its dynamical behaviors in order to develop an appropriate control system is crucial to the success of MG operation.

## 1.2 Objective of Research

The specific objectives of this thesis are devoted to

1. Modeling and analyzing dynamic performances of a microgrid with wind power generation.
2. Investigating stability performances of the microgrid under small and large disturbances, including islanding mode of operation in order to try to address the control performance requirement for maintaining the MG stability.

## 1.3 Scope of Research

The scope of this research is limited to

1. Modeling of MG's main components, of which it includes:
  - Wind Power: wind speed, rotor turbine, squirrel cage induction generator (SCIG), doubly-fed induction generator (DFIG) and its control system that encompasses both mechanical control with pitch control scheme and electrical control by using PWM with current control scheme.
  - Synchronous Generator: governor and excitation
  - Load: constant power
  - Network
2. Study the stability issues pertinent to small signal stability caused by wind fluctuation and transient stability caused by temporary and permanent faults, respectively.

## 1.4 Research Methodology

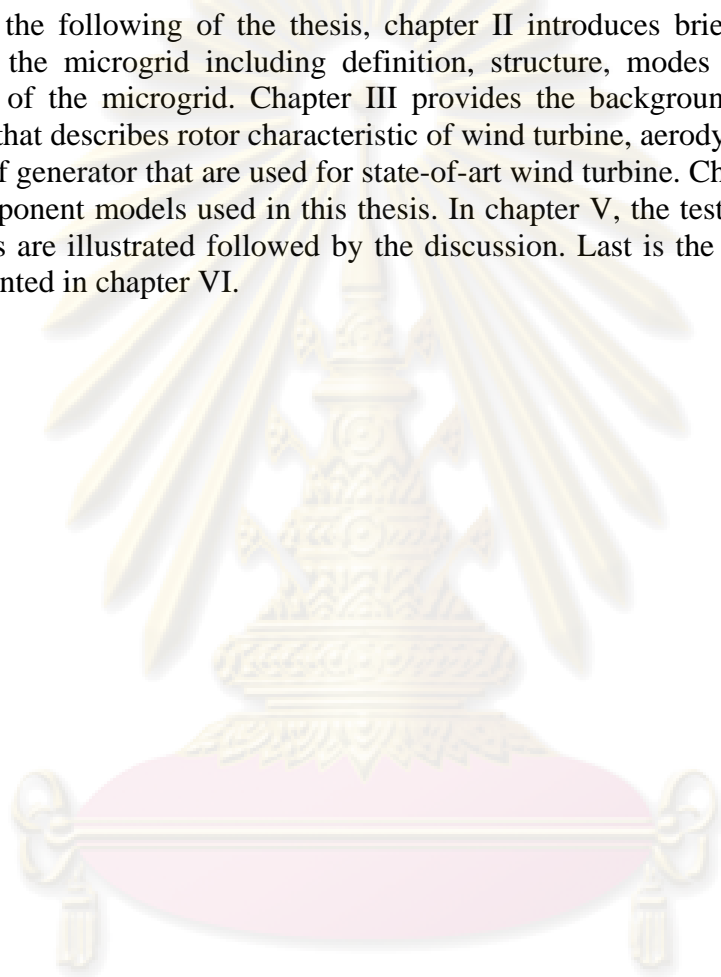
1. Literature reviews of background knowledge relevant to Micro-grid system structure, generation components, control components, applications and modes of operation.
2. Identify salient features of microgrid dynamic performance and technical problems associated with system stability.
3. Develop a software program capable of simulating dynamic behavior of the system modeled of microgrid of interest in order to get acquaintance with microgrid dynamic performance.
4. Validate the constructed model using relevant data from reference articles.
5. Define the thesis problem statement and revise or fine-tune the specific objective and scope of study as appropriate: What a microgrid system to model is, how to analyze and evaluate microgrid stability, what the control performance requirement(s) is to ensure the stability of the microgrid operation.
6. Classify case studies according to various probable scenarios of disturbances both inside and outside the microgrid.
7. Analyze simulated test results, make critical discussion, and revise experimental design as necessary.
8. Make conclusion, and document for a thesis report and publication.

### 1.5 Expected Contribution

The contribution of this thesis study may include:

1. Get dynamic models of MG's components consisting of wind power generation equipped with squirrel cage induction generator (SCIG), wind power generation equipped with doubly-fed induction generator (DFIG), constant power load, and synchronous generation with governor and constant excitation model.
2. Obtain a tool for MG stability investigation under both small and large disturbances.

For the following of the thesis, chapter II introduces briefly to the general concept of the microgrid including definition, structure, modes of operation, and application of the microgrid. Chapter III provides the background on wind power generation that describes rotor characteristic of wind turbine, aerodynamic of the wind and types of generator that are used for state-of-art wind turbine. Chapter IV describes all the component models used in this thesis. In chapter V, the test results of various case studies are illustrated followed by the discussion. Last is the conclusion of this thesis presented in chapter VI.



ศูนย์วิทยทรัพยากร  
จุฬาลงกรณ์มหาวิทยาลัย

## CHAPTER II

### MICROGRID OPERATION

One class of dynamic effects of immediate concern is the possibility for distributed generation (DG) to alter the local dynamics of a specific subsystem or distribution feeder. This becomes a concern when there is a significant penetration of DG relative to the total load on that feeder. Such localized concentrations are likely to occur even before DG becomes more commonplace. Thus, there is some urgency for the power industry to understand the possible effects of locally high concentrations of DG. One concept that shows promise as a means of taking full advantage of DG is the microgrid (MG). MG has currently receiving considerable interest from the power community [2]. In this section, the general concept of the microgrid is emphasized including its definition, operation and application.

#### 2.1 Definition

Microgrid is a cluster of loads and micro-sources, operating as a single controllable system that provides both power and heat to its local area enabling a more efficient use of renewable resources, which boosts efficiency and lowers emissions [3].

The main incentives of MG operation is that it can provide

- Reduction in green-house gas emissions; hence, mitigating climate change
- Increased energy efficiency
- Deregulation or competition policy
- Diversification of energy resources

#### 2.2 Structure

Figure2. 1 shows the MG architecture. It consists of a group of feeders with a single point of connection to the main distribution utility which is referred to as point of common coupling (POCC), a separation device (SD) that can disconnect the MG immediately when a fault occurs in the distribution grid. The sensitive loads are located at the feeder 1, 2 and require the local generation. The traditional loads are connected to the feeder 3 and have no requirement of any local generation. The local controllers (LC) are equipped with each local generation similar to conventional controllers such as AVR or governor. Additionally, in the MG system it has also the communication network to exchange information among LCs and upper central controller to achieve the advanced control [3].

จุฬาลงกรณ์มหาวิทยาลัย

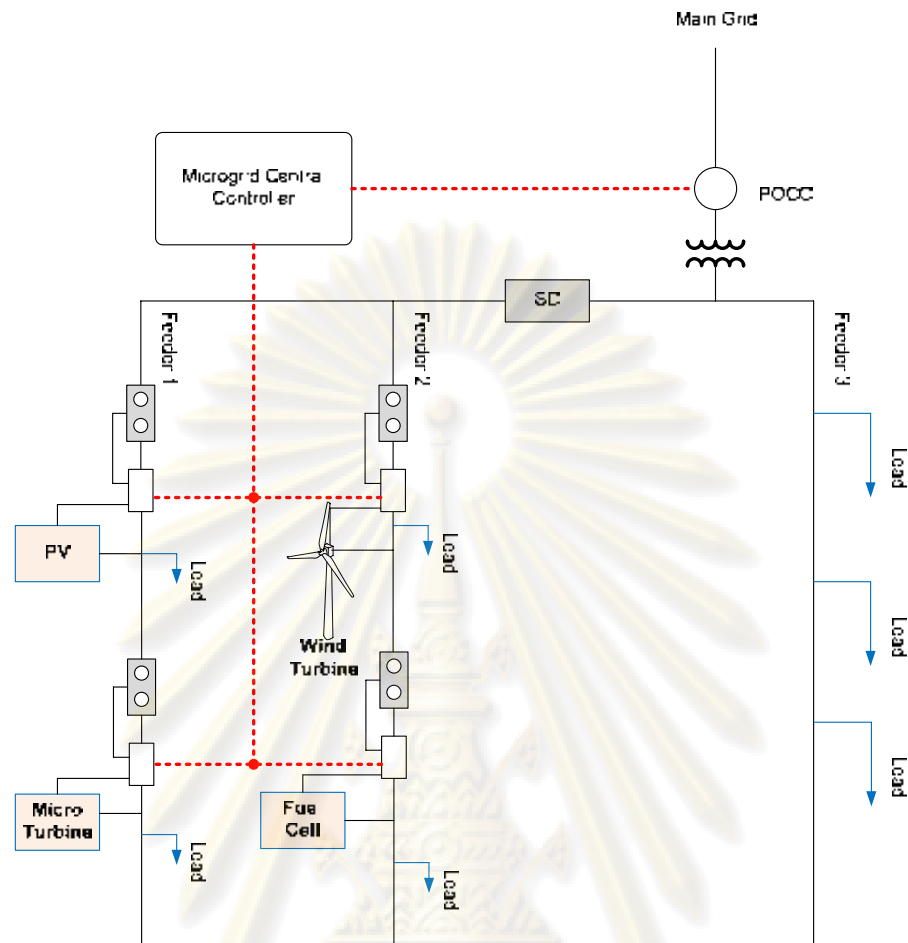


Figure 2. 1 Microgrid architecture [3].

### 2.3 Modes of Operation

Concepts for micro-grids fall into two general categories [4]:

- Systems that are intended to always be operated isolating from a large utility grid.
- Systems that are normally connected to a larger grid.

Conceptually, the isolated microgrid is like a scaled-down version of a large scale utility grid. Many of the technical requirements are the same. In order to supply reliability, and quality of power, the microgrid must have mechanisms to regulate voltage and frequency in response to changes in customer loads and in response to disturbances.

For the grid-connected microgrid, the distinction is more subtle. The basic concept is that the microgrid is designed and operated such that it behaves like a single, predictable and orderly load or generator to the main grid at the point of interconnection. This arrangement provides several potential advantages for all of the stakeholders, this includes

- DG owners may be able to size and operate their generation more economically, by being able to export (or import) power to the micro-grid.
- The micro-grid takes advantage of load diversity to reduce the total installed DG capacity required.
- The customers load may be able to have a continued service, possibly at a reduced level, when connection to the host utility is lost.

- The host utility may be able to depend on the microgrid to serve customers load in such a fashion that substation and bulk power infrastructure need not be rated (or expanded) to meet the entire connected load, as in the case if the DG were not present.
- The microgrid could be controlled in such a fashion as to be active asset to bulk system reliability. For example, it can provide spinning reserve or black start services to the main grid.

## 2.4 Applications

The microgrid concept is an advanced approach for enabling integration of, in principle, an unlimited quantity of distributed energy resources (DER) into the electricity grid. The micro-grid concept is driven by two fundamental principles:

- 1) A *system* perspective is necessary for customers, utilities, and society to capture the full benefits of integrating distributed energy resources into an energy system
- 2) The *business development* for accelerating adoption of these advanced concepts will be driven, primarily, by lowering the cost and enhancing the value of microgrid.

Each innovation embodied in the microgrid concept, e.g., intelligent power electronic interfaces a single, smart switch for grid disconnect and resynchronization, has been created specifically to lower the cost and improve the reliability of smaller-scale distributed generation (DG) systems. The goal of this thesis is to accelerate realization of the many benefits offered by smaller-scale DG, such as their ability to supply waste heat at the point of need (avoiding extensive thermal distribution networks) or to provide higher power quality to some but not all loads within a facility. From a grid perspective, the micro-grid concept is attractive because it recognizes the reality that the conventional distribution system is extensive, old, and will change very slowly. The micro-grid concept enables high penetration of DER without requiring re-design or re-engineering of the distribution system, itself.

During disturbances, the generation and load can autonomously separate from the distribution system to isolate the micro-grid's load from the disturbance (and thereby maintaining high level of service) without harming the transmission grid's integrity. Intentional islanding of generation and loads has the potential to provide a higher local reliability than that provided by the power system as a whole. The smaller size of emerging generation technologies permits generators to be placed optimally in relation to heat loads allowing for use of waste heat. Such applications give more than double the overall efficiencies of the systems [5].

## 2.5 Practical Issues

From [6] the two barriers of the microgrid operation are highlighted as follows:

### Technical

- Limited availability of advanced DG options that can compete economically.
- Need streamlined analysis tools for evaluating high penetration effects on distribution system.
- Need verified and recognized safety/protective relaying methods for both: grid connected and isolated operations of MG.



### Economic & Regulatory

- Emerging DG technologies must achieve aggressive commercialization and cost goals.
- Need interconnection standards that address microgrid systems.
- Utility policies create barriers to market. In fact, they should participate and provide the ability to enhance and support the new form of such power system generation such as microgrid.
- No comprehensive method in place to monetize combined benefits to users, utilities, and society.

From the above, it can be seen that DG is one of the main components inside the microgrid operation. Table 2.1 provides the size classification of DG for further clarify about the concept of distributed generation.

Table 2. 1 Relative sizes of distributed generation [7]

Micro distributed generation	~ 1 watt < 5 kW
Small distributed generation	5 kW < 5 MW
Medium distributed generation	5 MW < 50 MW
Large distributed generation	50 MW < ~ 300 MW

From the power generation and control perspectives, DG units can be divided into two main categories: *dispatchable* and *non-dispatchable* sources.

A dispatchable DG source is defined as a fast-response energy source which has adequate capacity to meet the real and reactive power commands within specified limits. Such a source may interface through a power converter and include storage devices on its DC side, e.g. a variable-speed wind-turbine based power generation unit connected through a back-to-back converter to utility systems, or a fuel-cell powered converter.

A non-dispatchable source is either a slow-response source in terms of its response time to variations in real and reactive power references during transients, e.g. a gas-turbine generator with the response time in the order of 50 ms to a few seconds, or acts as an uncontrollable source which is highly dependent on the power provided by its prime source, e.g. photovoltaic source that relies only on solar radiations or a fix-speed wind-turbine based power generation source that rely on wind resources with unpredicted, time-varying nature, as the input energy [1].

## 2.6 Microgrid Stability

The growing concern about interaction of distributed energy resources (DER) has been raised, especially the issue associated with system stability under the high penetration of DER [8]. Extra burdens have been added to the microgrid operation because of some requirement such as power electronic inverters and protection design for maintaining the safety and stability of the microgrid during both grid-connected mode and islanded mode. The stability of the microgrid is affected by some vital factors such as the control strategies of micro-sources and energy storage system, types of load in the MG, location of fault and inertia constant of rotating machine [9].

## CHAPTER III

### WIND POWER GENERATION

As a result of increasing environmental concern, the impact of conventional electricity generation on the environment is being minimized and efforts are made to generate electricity from renewable sources. The main advantages of electricity generation from renewable sources are the absence of harmful emissions and the infinite availability of the prime mover that is converted into electricity. One way of generating electricity from renewable sources is to use wind turbines to convert the energy contained in flowing air into electricity.

Wind turbines often do not take part in voltage and frequency control. Hence when a disturbance occurs, the wind turbines are disconnected, and reconnected when normal operation has been resumed. Thus, notwithstanding the presence of wind turbines, frequency and voltage are maintained by controlling the large power plants as would have been the case without any wind turbines present. This is possible, as long as wind power penetration is still low.

However, a tendency to increase the amount of electricity generated from wind turbines can be observed. Therefore, the penetration of wind turbines in electrical power systems will increase and they may begin to influence overall power system behavior, making it impossible to run a power system by only controlling large scale power plant. It is therefore important to study the behavior of wind turbines in an electrical power system and their interaction with other generation equipment and with loads.

The three typical types of machines to be used with wind turbine that are often used in power generation are:

- Squirrel cage induction generator
- Direct drive synchronous generator, and
- Doubly-fed induction generator

#### 3.1 Aerodynamic System [10]

Unlike different type modeling of generators, converters, mechanical shaft systems and control systems, the aerodynamic system is the novel and unfamiliar modeling system for the electromechanical engineers and will be represented and outlined in this section.

##### Wind Turbine Rotor

From a physical point of view, the static characteristics of a wind turbine rotor can be described by the relationships between the total power in the wind and the mechanical power of the wind turbine. These relationships are readily described starting with the incoming wind in the rotor swept area. It can be shown that the kinetic energy of a cylinder of air of radius  $R$  travelling with wind speed  $V_{wind}$  corresponds to a total wind power  $P_{wind}$  within the rotor swept area of the wind turbine. This power,  $P_{wind}$ , can be expressed by:

$$P_{wind} = \frac{1}{2} \rho_{AIR} \pi R^2 V_{wind}^3 \quad (3.1)$$

Where  $\rho_{AIR}$  is the air density ( $=1.225 \text{ kg/m}^3$ )  
 $R$  is the rotor radius  
 $V_{wind}$  is the wind speed

It is not possible to extract all the kinetic energy of the wind, since this would mean that the air would standstill directly behind the wind turbine. This would not allow the air to flow away from the wind turbine, and clearly this cannot represent a physical steady-state condition. The wind speed is only reduced by the wind turbine, which thus extracts a fraction of the power in the wind. This fraction is denoted as the power efficiency coefficient,  $C_P$ , of the wind turbine. The mechanical power,  $P_{mech}$ , of the wind turbine is therefore – by the definition of  $C_P$  – given by the total power in the wind  $P_{wind}$  according to the following equation:

$$P_{mech} = C_P P_{wind} \quad (3.2)$$

It can be shown that the theoretical, as being described by [14], static upper limit of  $C_P$  is  $16/27$  (approximately 0.593). That is, it is theoretically possible to extract approximately 59% of the kinetic energy of the wind. This is known as Betz's limit. For a comparison, modern three-bladed wind turbines have an optimal  $C_P$  value in the range of 0.52–0.55 when measured at the hub of the turbine.

In some cases,  $C_P$  is specified with respect to the electrical power at the generator terminals rather than regarding the mechanical power at the turbine hub; that is, the losses in the gear and the generator are deducted from the  $C_P$  value. When specified in this way, modern three-bladed wind turbines have an optimal  $C_P$  value in the range of 0.46–0.48. It is therefore necessary to understand whether  $C_P$  values are specified as a mechanical or as an electrical power efficiency coefficient.

If the torque  $T_{mech}$  is to be applied instead of the power  $P_{mech}$ , it is conveniently calculated from the power  $P_{mech}$  by using the turbine rotational speed  $\omega_{turb}$ :

$$T_{mech} = \frac{P_{mech}}{\omega_{turb}} \quad (3.3)$$

It is clear that the power,  $P_{mech}$ , that is extracted from the wind will depend on rotational turbine speed, wind speed and blade angle,  $\beta$ . Therefore,  $P_{mech}$ , and hence  $C_P$  can be represented as functions of these quantities.

$$P_{mech} = f_{P_{mech}}(\omega_{turb}, V_{wind}, \beta) \quad (3.4)$$

### 3.1.1 Tip Speed Ratio

From Figure 3.1, the possible energy extraction will depend on the angle of incidence  $\varphi$  between the plane of moving rotor blade and relative wind speed  $V_{rel}$  seen from the moving blades. The angle of incidence  $\varphi$  is determined by the incoming wind speed  $V_{wind}$  and the speed of blades. Another commonly used term in the aerodynamics of wind turbines is the tip-speed ratio (TSR),  $\lambda$  which is defined by:

$$\lambda = \frac{\omega_{turb} R}{V_{wind}} \quad (3.5)$$

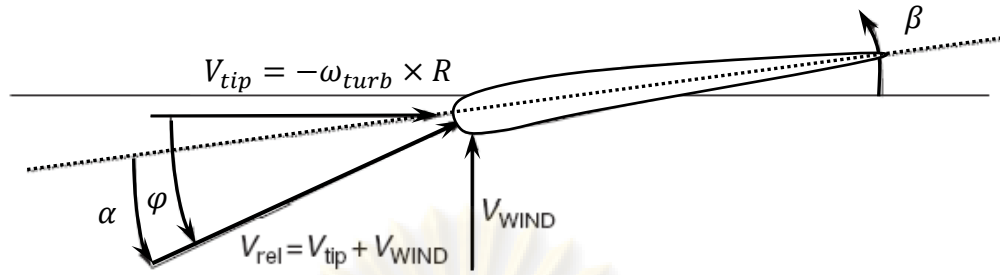


Figure 3.1 Illustration of wind conditions around the moving blade [10]

Therefore, the angle of incidence can be calculated as:

$$\varphi = \tan^{-1}\left(\frac{1}{\lambda}\right) = \tan^{-1}\left(\frac{V_{wind}}{\omega_{turb}R}\right) \quad (3.6)$$

Note:  $V_{tip}$  = tip speed;  $\omega_{turb}$  = turbine rotational speed;  $R$  = rotor radius;  $V_{rel}$  = relative wind speed;  $V_{wind}$  = wind speed;  $\alpha$  = angle of attach;  $\varphi$  = angle of incidence between the plane of the rotor and  $V_{rel}$ ;  $\beta$  = blade angle.

### 3.1.2 Power Coefficient

The power coefficient  $C_p$  can be expressed as a function of tip speed ratio  $\lambda$  and pitch angle  $\beta$ . The highest value of  $C_p$  is typically obtained for  $\lambda$  value in the range of 8 to 9, i.e. when the tip of the blades moves 8 to 9 times faster than the incoming wind. Manufacturer documentation shows that the power curves of individual wind turbines are very similar, so a general approximation can be used for computation of power coefficient  $C_p$  of both constant-speed and variable-speed wind turbines [10]:

$$C_p(\lambda, \beta) = c1 \left( \frac{c2}{\lambda_i} - c3\beta - c4\beta^{c5} - c6 \right) \exp\left(\frac{-c7}{\lambda_i}\right) \quad (3.7)$$

Where

$$\lambda_i = \left[ \left( \frac{1}{\lambda + c8\beta} \right) - \left( \frac{c9}{\beta^3 + 1} \right) \right]^{-1} \quad (3.8)$$

The table 3.1 shows the value of parameters  $c1$  to  $c9$  with the original parameters used by [10].

Table 3. 1 Approximation of power curves

	c1	c2	c3	c4	c5	c6	c7	c8	c9
Heier (1998)	0.5	116	0.4	0	—	5	21	0.08	0.035
Constant-speed wind turbine	0.44	125	0	0	0	6.94	16.5	0	-0.002
Variable-speed wind turbine	0.73	151	0.58	0.002	2.14	13.2	18.4	-0.02	-0.003

Alternatively, the reference [11] provides different mathematical approach given by (3.9) and (3.10), which will be used in this thesis. Nevertheless, both sets of equations generate the curves with the same fundamental shape as those of the physical wind turbine.

$$C_p(\lambda, \beta) = c_1 \left( \frac{c_2}{\lambda_i} - c_3\beta - c_4 \right) \exp\left(\frac{-c_5}{\lambda_i}\right) + c_6\lambda \quad (3.9)$$

Where

$$\lambda_i = \left[ \left( \frac{1}{\lambda + 0.08\beta} \right) - \left( \frac{0.035}{\beta^3 + 1} \right) \right]^{-1} \quad (3.10)$$

With the coefficient  $c_1$  to  $c_6$  are:  $c_1 = 0.5176$ ,  $c_2 = 116$ ,  $c_3 = 0.4$ ,  $c_4 = 5$ ,  $c_5 = 21$  and  $c_6 = 0.0068$ .

### 3.2 Wind Turbine Technologies [10]

Wind turbines can operate either with a fixed speed or a variable speed.

#### 3.2.1 Fixed-Speed Wind Turbines

The standard installed wind turbines, since early 1990s, operate at fix speed. That means regardless of the wind speed, the wind turbine rotor speed is fixed and determined by the frequency of the supply grid, the gear ratio and the generator design. They are designed to achieve maximum efficiency at one particular wind speed.

The fixed-speed wind turbine has advantage of being simple, robust and reliable. In addition, cost of its electrical parts is low. Its disadvantages are an uncontrolled reactive power consumption, mechanical stress and limited power quality control.

Owing to its fixed-speed operation, all fluctuations in the wind speed are transmitted as fluctuations in the mechanical torque and then as fluctuations in the electrical power to the grid. So in the case of weak grid, the power fluctuations can also lead to large voltage fluctuations.

#### 3.2.2 Variable-Speed Wind Turbines

In the modern wind turbine application, the variable-speed wind turbines have become dominant type among the installed wind turbines.

Variable-speed wind turbines are designed to achieve maximum aerodynamic efficiency over a wide range of wind speeds. With a variable-speed operation it has become possible continuously to adapt accelerating or decelerating the rotational speed  $\omega_{rm}$  of the wind turbine to the wind speed  $v$ . In this way, the tip speed ratio  $\lambda$  is kept constant at a predefined value corresponding to the maximum power coefficient. Contrary to a fixed-speed system, a variable-speed system keeps the generator torque fairly constant and the variations in the wind speed are absorbed by change in the generator speed.

The electrical system of a variable-speed wind turbine is more complicated than that of fixed-speed wind turbine. It is typically equipped with an induction or synchronous generator and connected to the grid through a power converter. The power converter controls the generator speed, that is the power fluctuations caused by wind variations are absorbed mainly by changes in the rotor generator speed and consequently in the wind turbine rotor speed.

### 3.3 Wind Turbine Configurations

There are various types of wind turbine configurations and they are classified both by their ability to control speed and by the type of power control.

Applying speed control criterion, there are four different dominating types of wind turbines. The sub-category classifications of wind turbines correspond to power (blade) control: stall, pitch, active control. Table 3.2 indicates different types of wind turbine configurations.

Table 3. 2 Wind turbine types

Control		Power Control		
		Stall	Pitch	Active Stall
Fixed Speed	Type A	Type A0	Type A1	Type A2
	Type B	Type B0	Type B1	Type B2
Variable Speed	Type C	Type C0	Type C1	Type C2
	Type D	Type D0	Type D1	Type D2

Note: The gray zones are not used in the wind turbine today.

#### 3.3.1 Type A: Fixed Speed

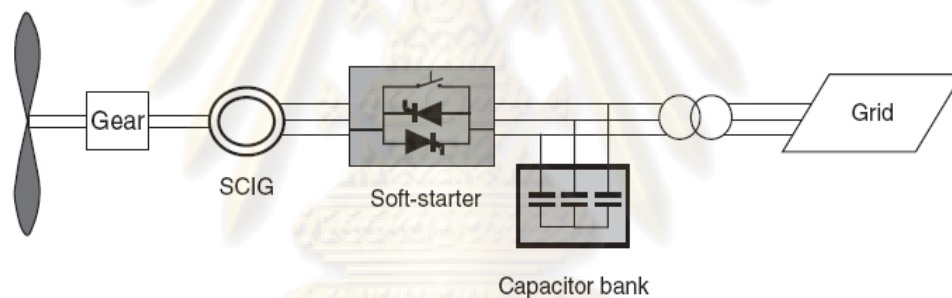


Figure 3.2 Wind turbine type A [10]

This configuration denotes the fixed-speed wind turbine with an asynchronous squirrel cage induction generator (SCIG) directly connected to the grid. Since the SCIG always draws reactive power from the grid, this configuration uses a capacitor bank for reactive power compensation. A smoother grid connection is achieved by using a soft-starter.

Regardless of the power control principle in a fixed-speed wind turbine, the wind fluctuations are converted into mechanical fluctuations and consequently into electrical power fluctuations. In the case of a weak grid, these can yield voltage fluctuations at the point of connection. Because of these voltage fluctuations, the fixed-speed wind turbine draws varying amounts of reactive power from the utility grid (unless there is a capacitor bank), which increases both the voltage fluctuations and the line losses. Thus the main drawbacks of this concept are that it does not support any speed control.

### 3.3.2 Type B: Limited Variable Speed

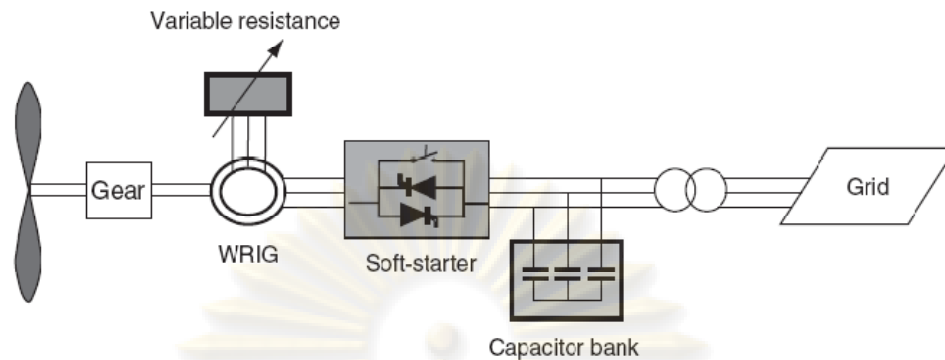


Figure 3.3 Wind turbine type B [10]

It uses a wound rotor induction generator (WRIG). Unlike wind turbine type A, the unique feature of this concept is that it has a variable additional rotor resistance, which can be changed by an optically controlled converter mounted on the rotor shaft. Thus, the total rotor resistance is controllable. The rotor resistance can be changed and thus controls the slip. This way, the power output in the system is controlled. The range of the dynamic speed control depends on the size of the variable rotor resistance. Typically, the speed range is 0–10% above synchronous speed. The energy coming from the external power conversion unit is dumped as heat loss.

### 3.3.3 Type C: Variable Speed With Partial Scale Frequency Converter

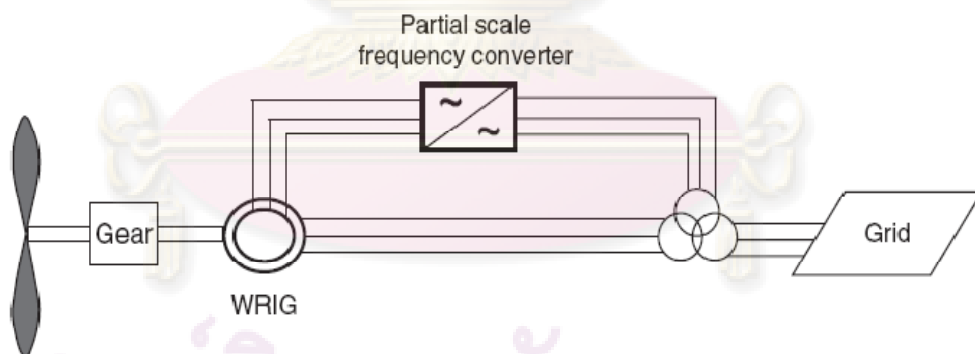


Figure 3.4 Wind turbine type C [10]

This configuration, known as the doubly fed induction generator (DFIG) concept, corresponds to the limited variable speed wind turbine with a wound rotor induction generator (WRIG) and partial scale frequency converter on the rotor circuit. The partial scale frequency converter performs the reactive power compensation and the smoother grid connection. It has a wider range of dynamic speed control depending on the size of the frequency converter. Typically, the speed range comprises synchronous speed -40% to +30%. The smaller frequency converter makes this concept attractive from an economical point of view.

### 3.3.4 Type D: Variable Speed With Full-Scale Frequency Converter

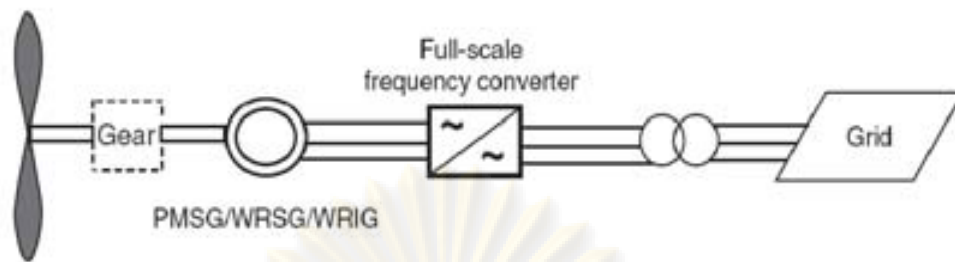


Figure 3.5 Wind turbine type D [10]

This configuration corresponds to the full variable speed wind turbine, with the generator connected to the grid through a full-scale frequency converter. The frequency converter performs the reactive power compensation and the smoother grid connection. The generator can be excited electrically wound rotor synchronous generator (WRSG) or (WRIG) or by a permanent magnet [permanent magnet synchronous generator (PMSG)].

## 3.4 Voltage Control Capability of Wind Turbine

### 3.4.1 Current Wind Turbine Types

The most majority of wind turbines that are currently being installed use one of the three main types of electromechanical conversion system.

The first type is known as Type A. In this type an (asynchronous) squirrel cage induction generator is used to convert the mechanical energy into electricity. Owing to the different operating speeds of the wind turbine rotor and the generator, a gearbox is necessary to match these speeds. The generator slip slightly varies with the amount of generated power and is therefore not entirely constant. However, because these speed variations are in the order of 1 %, this wind turbine type is normally referred to as constant-speed or fixed-speed.

The second type uses a doubly fed induction generator instead of a squirrel cage induction generator, and was introduced as Type C. Similar to the previous type, it needs a gearbox. The stator winding of the generator is coupled to the grid, and the rotor winding to a power electronic converter, usually a back-to-back voltage source converter with current control loops. In this way, the electrical and mechanical rotor frequencies are decoupled, because the power electronic converter compensates the difference between mechanical and electrical frequency by injecting a rotor current with variable frequency. Variable-speed operation thus becomes possible. This means that the mechanical rotor speed can be controlled according to a certain goal function, such as energy yield maximization. The rotor speed is controlled by changing the generator power in such a way that it equals the value derived from the goal function. In this type of conversion system, the control of aerodynamic power is usually performed by pitch control.

The third type is called the 'direct-drive wind turbine' because it does not need a gearbox. It corresponds to Type D. A low-speed multipole synchronous ring generator with the same rotational speed as the wind turbine rotor converts the mechanical energy into electricity. The generator can have a wound rotor or a rotor with permanent magnets. The stator is not coupled directly to the grid but to a power electronic converter. This may consist of a back-to-back voltage source converter or a diode rectifier with a single voltage source converter. The electronic converter makes



it possible to operate the wind turbine at variable speed. Similar to Type C, pitch control limits the mechanical power input. Figure 3.6 presents the three main wind turbine types.

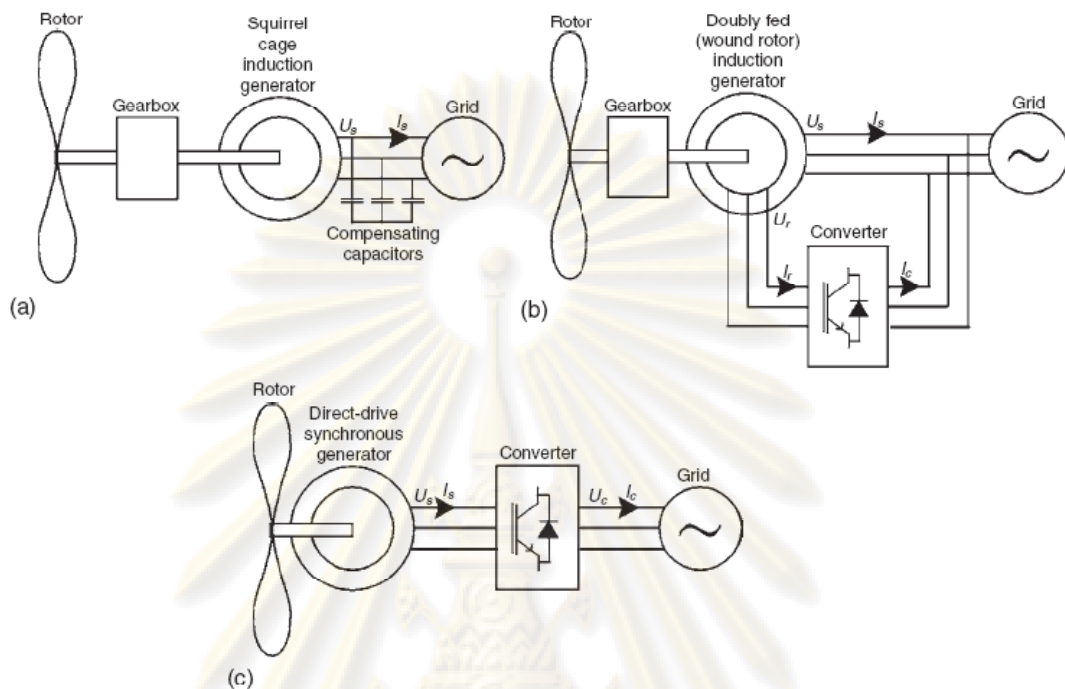


Figure 3.6 Widely used wind turbine types: (a) constant-speed wind turbine (Type A); (b) variable-speed wind turbine with doubly fed induction generator (Type C); and (c) direct-drive variable-speed wind turbine with multipole synchronous generator (Type D) [10]

### 3.4.2 Wind Turbine Voltage Control Capabilities

Node voltages are dependent on branch characteristics and on branch currents. In transmission networks and distribution grids, node voltage and reactive power are correlated and therefore node voltages can be controlled by changing the reactive power generation or consumption of generators. An analysis of the voltage control capabilities of the wind turbine types described in Section 3.4.1 has thus to show what extent they can vary their reactive power output. In the following, we will discuss the voltage control capabilities of each of the wind turbine types described above.

Constant-speed wind turbines (Type A) have squirrel cage induction generators that always consume reactive power. The amount of the reactive power consumption depends on the terminal voltage, active power generation and rotor speed. Figure 3.7 illustrates the relation between terminal voltage, rotor speed, active power generation and reactive power consumption. This figure shows that a squirrel cage induction generator cannot be used for voltage control, because it can only consume and not generate reactive power and because the reactive power exchange with the grid cannot be controlled but is governed by rotor speed, active power generation and terminal voltage.

The fact that a squirrel cage induction generator consumes reactive power can be a disadvantage, particularly in the case of large wind turbines or wind farms and/or weak grids. In such cases, the reactive power consumption may cause severe node voltage drops. Therefore, the reactive power consumption of the generator is in most cases compensated by capacitors, as depicted in Figure 3.6(a). In this way, the

reactive power exchange between the combination of the generator and the capacitors, on the one hand, and the grid, on the other, can be reduced thus improving the power factor of the system as a whole.

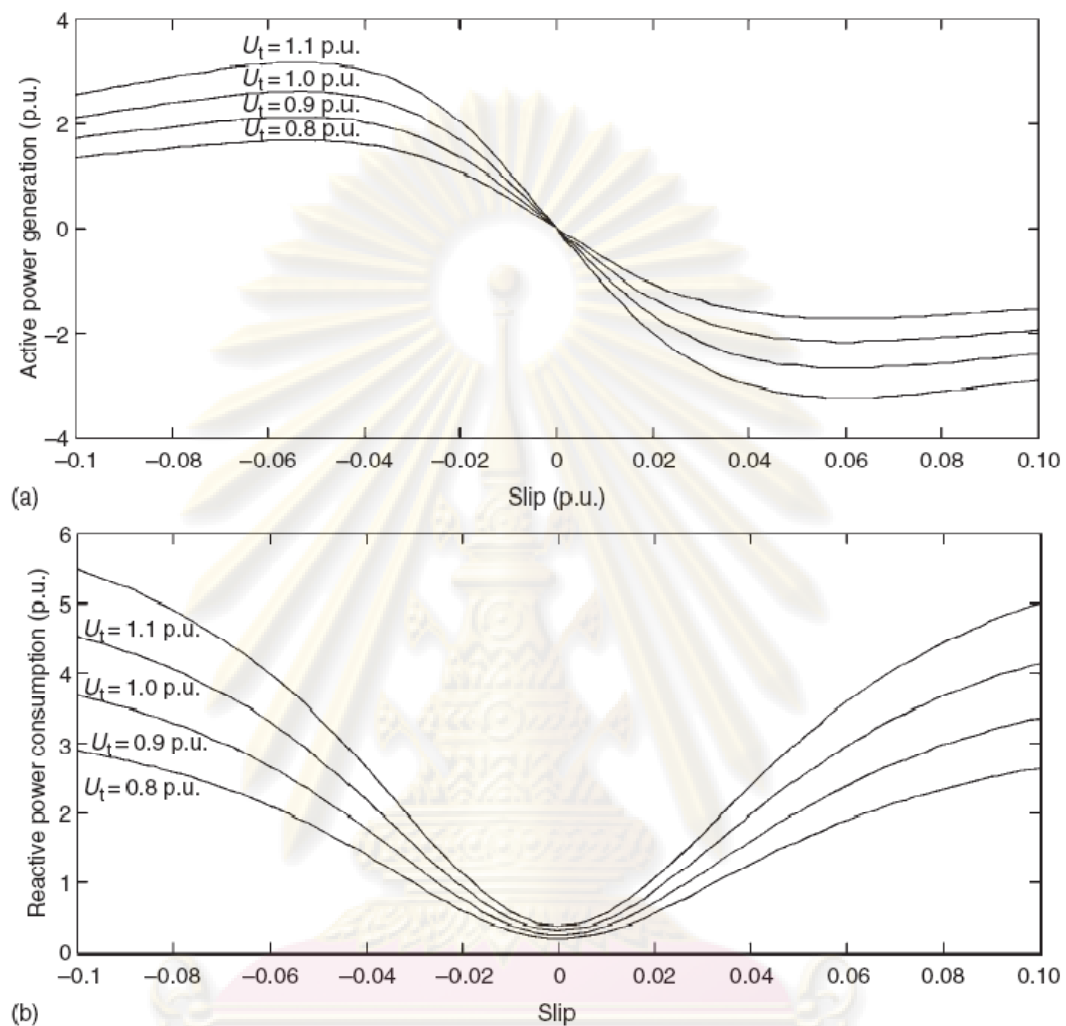


Figure 3.7 Dependence of (a) active and (b) reactive power of a squirrel cage induction generator on the rotor speed, with the terminal voltage,  $U_t$ , as a parameter [10]

A conventional capacitor is an uncontrollable source of reactive power. By adding compensating capacitors, the impact of the wind turbine on the node voltages is reduced. But this is only a qualitative improvement. The voltage control capabilities as such are not enhanced, because there is still a unique relation between rotor speed, terminal voltage and active and reactive power generation. The voltage control capabilities of a constant-speed wind turbine can be enhanced only with use of more advanced solutions instead of conventional capacitors. Such advanced solutions include controllable sources of reactive power, such as switched capacitors or capacitor banks, a static condenser (Statcon) or a static VAR compensator (SVC).

The reactive power generation of a doubly fed induction generator (Type C wind turbine) can be controlled by the rotor current. In this case, there is no unique relation between reactive power and other quantities, such as rotor speed and active power generation. Instead, at a particular rotor speed and the corresponding active power generation a widely varying amount of reactive power can be generated or

consumed. Both generator torque and reactive power generation depend directly on the current that the power electronic converter feeds into the rotor.

In the case of a direct-drive variable-speed wind turbine (Type D), the reactive power exchange with the grid is not determined by the properties of the generator but by the characteristics of the grid side of the power electronic converter. The generator is fully decoupled from the grid. Therefore, the reactive power exchange between the generator itself and the generator side of the converter as well as between the grid side of the converter and the grid are decoupled. This means that the power factor of the generator and the power factor of the grid side of the converter can be controlled independently. And the voltage control of this wind turbine type will not be discussed more detail because it beyond of the scope of this thesis.

### 3.5 Induction Generator

Most of the electrical power in the industry is consumed by the induction machine driving the mechanical load. For this reason, the induction machine represents a well established technology. The primary advantage of the induction machine is the rugged brushless construction and no need for separate DC field power. The disadvantages of both the DC machine and the synchronous machine are eliminated in the induction machine, resulting in low capital cost, low maintenance, and better transient performance. For these reasons, the induction generator is extensively used in small and large wind farms and small hydroelectric power plants. The machine is available in numerous power ratings up to several megawatts capacity, and even larger.

#### 3.5.1 Principle of Operation [12]

The stator magnetic field is rotating at the synchronous speed  $\omega_s$ . This field is conceptually represented by the rotating magnets. The relative speed between the rotating field and the rotor induces the voltage in each rotor turn linking the stator flux  $\phi$ . The magnitude of the induced voltage is given by Faraday's law of electromagnetic induction, namely:

$$e = -\frac{d\phi}{dt} \quad (3.11)$$

This voltage in turn sets up the circulating current in the rotor. The electromagnetic interaction of the rotor current and the stator flux produces the torque. The amplitude of this torque is given by the following:

$$T = k\Phi I_2 \cos\theta \quad (3.12)$$

Where  $k$  = constant of proportionality

$\Phi$  = amplitude of the stator flux wave

$I_2$  = amplitude of induced current in the rotor bars

$\theta$  = phase angle by which the rotor current lags the rotor voltage.

The rotor will accelerate under this torque. If the rotor was on frictionless bearings with no mechanical load attached, it is completely free to rotate with zero resistance. Under this condition, the rotor will attain the same speed as the stator field, namely, the synchronous speed  $\omega_s$ . At this speed, the current induced in the rotor is

zero, no torque is produced. The rotor finds equilibrium at this speed and will continue to run at the synchronous speed.

If the rotor is now attached to a mechanical load such as a fan, it will slow down with the speed  $\omega_r$ . The stator flux, which always rotates at the constant, synchronous speed, will have relative speed with respect to the rotor. As a result, the electromagnetically induced voltage, current, and torque are produced in the rotor. The torque produced must equal that needed to drive the load at that speed. The machine works as the motor in this condition.

If we attach the rotor to a wind turbine and drive it with the speed  $\omega_r$  faster than the synchronous speed, the induced current and the torque in the rotor reverse the direction. The machine now works as the generator, converting the mechanical power of the turbine into electrical power delivered to the load connected to the stator terminals. If the machine was connected to a grid, it would feed power into the grid. Thus, the induction machine can work as the electrical generator only at speeds higher than the synchronous speed. The generator operation, for that reason, is often called the super-synchronous speed operation of the induction machine.

As described above, the induction machine needs no electrical connection between the stator and the rotor. Its operation is entirely based on the electromagnetic induction, hence, the name. The absence of rubbing electrical contacts and simplicity of its construction make the induction generator very robust, reliable, and a low-cost machine. For this reason, it is widely used in numerous applications in the industry.

The working principle of the induction machine can be seen as the transformer. The high voltage coil on the stator is excited and the low voltage coil on the rotor is shorted on itself. The power from one to the other can flow in either direction. The theory of operation of the transformer, therefore, holds true when modified to account for the relative motion between the stator and the rotor. This motion is expressed in terms of the slip of the rotor relative to the synchronously rotating magnetic field.

### 3.5.2 Induction Machine Equivalent [13]

The equivalent of the induction machine is very similar to that for a transformer. Although the rotor currents are at slip frequency, the rotor is incorporated into the circuit in simple way. Recognizing the fact that the stator and the rotor winding have resistances and leakage inductances and that the mutual inductance for modeling the mutual flux links the stator and rotor windings, Figure 3.8 give s the elementary equivalent circuit. The parameters are

$R_s$  : Stator resistance per phase

$L_{ls}$  : Stator leakage inductance

$L_m$  : Mutual inductance

$T_1$  : Stator turns per phase

$E_1$  : Induced emf in the stator per phase

$k_{w1}$  : Effective stator turns per phase

$R_{rr}$  : Rotor resistance per phase  
 $L_{lrr}$  : Rotator leakage inductance

$T_2$  : Rotator turns per phase  
 $E_2$  : Induced emf in the rotor per phase  
 $k_{w2}$  : Effective rotor turns per phase

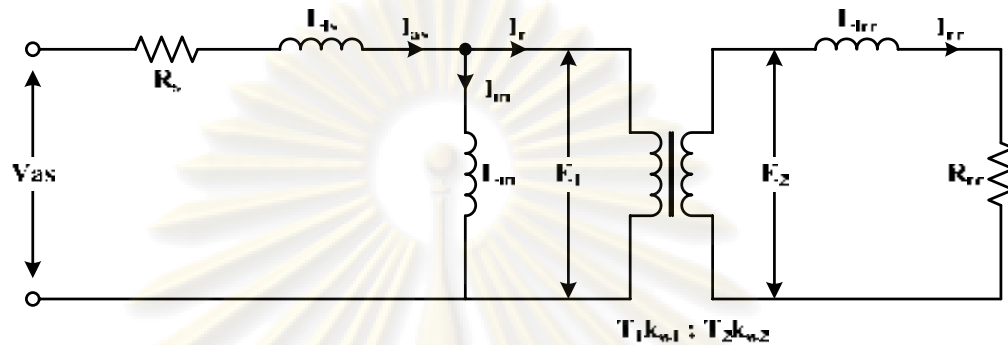


Figure 3.8 Elementary equivalent circuit for induction machine [13]

The relationship between the induced emfs is

$$\frac{E_2}{E_1} = S \frac{k_{w2} T_2}{k_{w1} T_1} = \frac{s}{a} \quad (3.13)$$

Where  $a$  : turns ratio

The rotor current  $I_{rr}$ , then is

$$I_{rr} = \frac{E_2}{R_{rr} + j\omega_s L_{lrr}} = \frac{E_2}{R_{rr} + js\omega_s L_{lrr}} \quad (3.14)$$

Substituting for  $E_2$  from equation (3.13) into (3.14) the rotor current is

$$I_{rr} = \frac{E_1}{\frac{aR_{rr}}{s} + j\omega_s (aL_{lrr})} = \frac{E_1/a}{\frac{R_{rr}}{s} + j\omega_s L_{lrr}} \quad (3.15)$$

Equation (3.15) is incorporated into the equivalent circuit as shown in Figure 3.9. Note that both rotor and stator uniformly have the same frequency, which is that of the stator in equation (3.15). The rotor current reflected into the stator is denoted as  $I_r$  and is given in terms of the rotor current  $I_{rr}$  as

$$I_r = \frac{I_{rr}}{a} \quad (3.16)$$

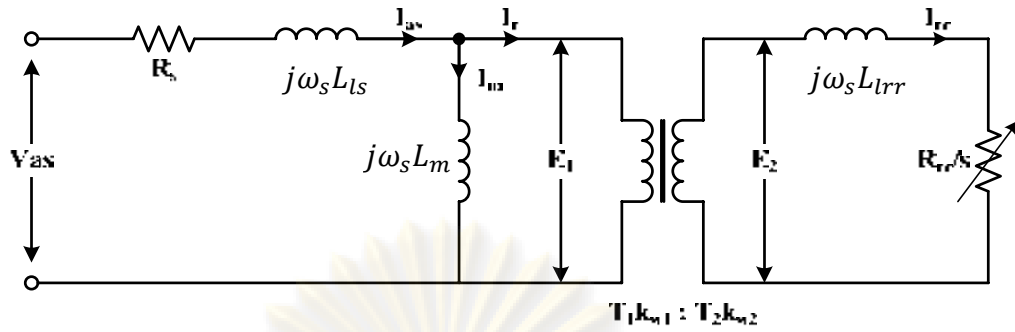


Figure 3.9 Equivalent circuit for an induction machine [13]

Note that the slip does not enter in this; the ratio between the stator and rotor induced emfs viewed at stator frequency does not contain it, and rotor impedance absorbs this slip. Substitution of equation (3.16) into equation (3.15) yields

$$I_r = \frac{E_1}{\frac{(a^2 R_{rr})}{s} + j\omega_s (a^2 L_{lrr})} = \frac{E_1}{\frac{R_r}{s} + j\omega_s L_{lr}} \tag{3.17}$$

Where  $R_r = a^2 R_{rr}$  : Stator-referred rotor resistance  
 $L_{lr} = a^2 L_{lrr}$  : Stator-referred rotor inductance

As the fictitious rotor and stator at the air gap have the same induced emf,  $E_1$ , the physical isolation can be removed to get a connected circuit. The final equivalent circuit, referred to the stator, is shown in Figure 3.10. Magnetization is accounted for by the magnetizing branch of the equivalent circuit, consisting of the magnetizing inductance that is lossless and hence cannot represent core losses. An equivalent resistance can represent the core losses. This core-loss resistance is in parallel the magnetizing inductance, because the core losses are dependent on the flux and hence proportional to the flux linkages and the resulting air gap voltage  $E_1$ . The self-inductances of the stator phase winding,  $L_s$ , and of the rotor phase winding referred to the stator,  $L_r$ , are obtained as the sum of the magnetizing inductance and respective leakage inductances:

$$L_s = L_m + L_{ls} \tag{3.18}$$

$$L_r = L_m + L_{lr} \tag{3.19}$$

The corresponding reactances are obtained by multiplying the inductances by the stator angular frequency.

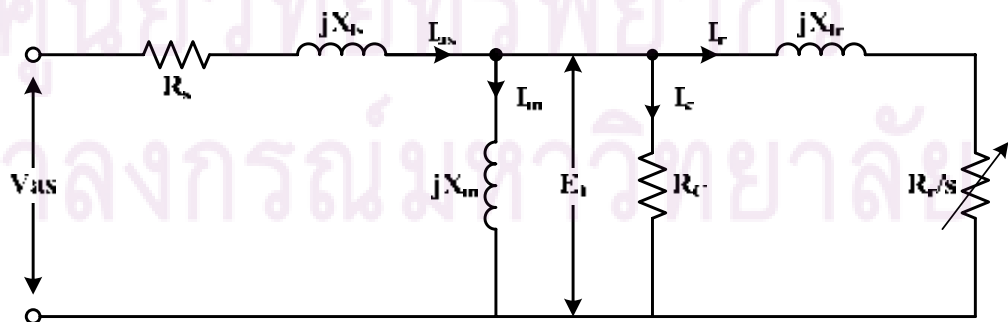


Figure 3.10 Equivalent circuit with rotor at stator frequency [13]

When the machine is energized with no load on the rotor, then the rotor circuit is open-circuited, because the slip is zero. The stator current drawn during this condition known as the no-load current, contributes to the magnetization of the machine and resulting core losses. Then this no-load current is viewed as the sum of the magnetizing and core-loss components of the current and accordingly is written as

$$I_o = I_m + I_c \quad (3.20)$$

The magnetizing current in terms of the air gap voltage and the magnetizing reactance is written as

$$I_m = \frac{E_1}{jX_m} \quad (3.21)$$

And the core-loss component of the stator current is written as

$$I_c = \frac{E_1}{R_c} \quad (3.22)$$

The rotor phase current is given by

$$I_r = \frac{E_1}{\frac{R_r}{s} + jX_{lr}} \quad (3.23)$$

The stator phase current is given by

$$I_{as} = I_r + I_o \quad (3.24)$$

In terms of the induced emf, stator current, and stator parameters, the applied stator phase voltage is expressed as

$$V_{as} = E_1 + (R_s + jX_{ls})I_{as} \quad (3.25)$$

### 3.5.3 Steady State Performance Equations of an Induction Machine

The key variables in the machine are the air gap power, mechanical and shaft output power, and electromagnetic torque. These are derived from the equivalent circuit of the induction machine as follows. The real power transmitted from the stator,  $P_i$  to the air gap,  $P_a$  is the difference between total input power to the stator windings and copper losses in the stator and is given as

$$P_a = P_i - 3I_s^2 R_s \quad (3.26)$$

Neglecting the core losses, the air gap power is equal to the total power dissipated in  $R_r/s$  in the three phases of the machine, there is no other element to consume power in the rotor equivalent circuit. It is given as

$$P_a = 3I_r^2 \frac{R_r}{s} \quad (3.27)$$

Which could be written alternatively as

$$P_a = \underbrace{3I_r^2 R_r}_{\substack{s.P_a \\ \text{rotor copper} \\ \text{losses power}}} + \underbrace{3I_r^2 R_r \frac{(1-s)}{s}}_{\substack{(1-s).P_a \\ \text{power converted} \\ \text{to mechanical form}}} \quad (3.28)$$

The mechanical power,  $P_m$  is obtained as

$$P_m = 3I_r^2 R_r \frac{(1-s)}{s} = (1-s).P_a \quad (3.29)$$

Alternately, in terms of the electromagnetic torque and rotor speed, the mechanical power output is equal to their product:

$$P_m = T_e \omega_{rm} \quad (3.30)$$

Where  $T_e$  is the internal or electromagnetic torque, derived from equations (3.29) and (3.30) as

$$T_e = \frac{3I_r^2 R_r (1-s)}{s \omega_r} \quad (3.31)$$

Substituting for the rotor speed in terms of the slip and stator frequency, given by

$$\omega_{rm} = \frac{\omega_r}{P/2} = \frac{\omega_s(1-s)}{P/2} \quad (3.32)$$

into (3.29), the electromagnetic or air gap torque is obtained as

$$T_e = 3 \left( \frac{P}{2} \right) \frac{I_r^2 R_r}{s \omega_s} \quad (3.33)$$

Without taking into account of the windage and friction losses of the rotor, the shaft power of the machine is equal to the mechanical of the machine and defined as

$$P_{shaft} = P_m \quad (3.34)$$

### 3.5.4 Steady State Performance

A set or sample torque-vs.-slip characteristic for constant input voltage is shown in Figures 3.11 and Figures 3.12.

The torque-vs.-slip characteristics are shown for slip varying from 0 to 1. The slip is chosen in place of rotor speed because it is nondimensional and so is applicable to any motor frequency. Near the synchronous speed, i.e., at low slips, the torque is linear and is proportional to slip; beyond the maximum torque (also known as breakdown torque), the torque is approximately inversely proportional to slip, as is seen from the Figure 3.11. At standstill, the slip equals unity, and, at this operating point, the torque produced is known as standstill torque. To accelerate a load, this standstill torque has to be greater than the load torque. It is preferable to operate near low slips to have higher efficiency. This is due to the fact that the rotor copper losses are directly proportional to slip and are equal to the slip power, and, hence, at low slips, the rotor copper losses are small.



The positive-slope region of the torque-slip characteristics provides stable operation. Consider the machine operating at 1 p.u. with a low slip, and let the load torque be increased to 1.5 p.u. The rotor slows down and thereby develops a larger slip, which increases the electromagnetic torque capable of meeting the load torque. The new steady state is reached at 1.5 p.u. torque after a transient period with oscillations in torque. If the operating point at 1 p.u. torque at a slip of 0.85 is considered, the load torque disturbance will lead to increasing slip, resulting in less and less torque generation, thereby diverging more and more from the new load torque leading to a final pullout of the machine and reaching standstill. As this discussion is addressed to the steady-state characteristics of the machine, the two regions are named statically stable and unstable, as indicated in Figure 3.11.

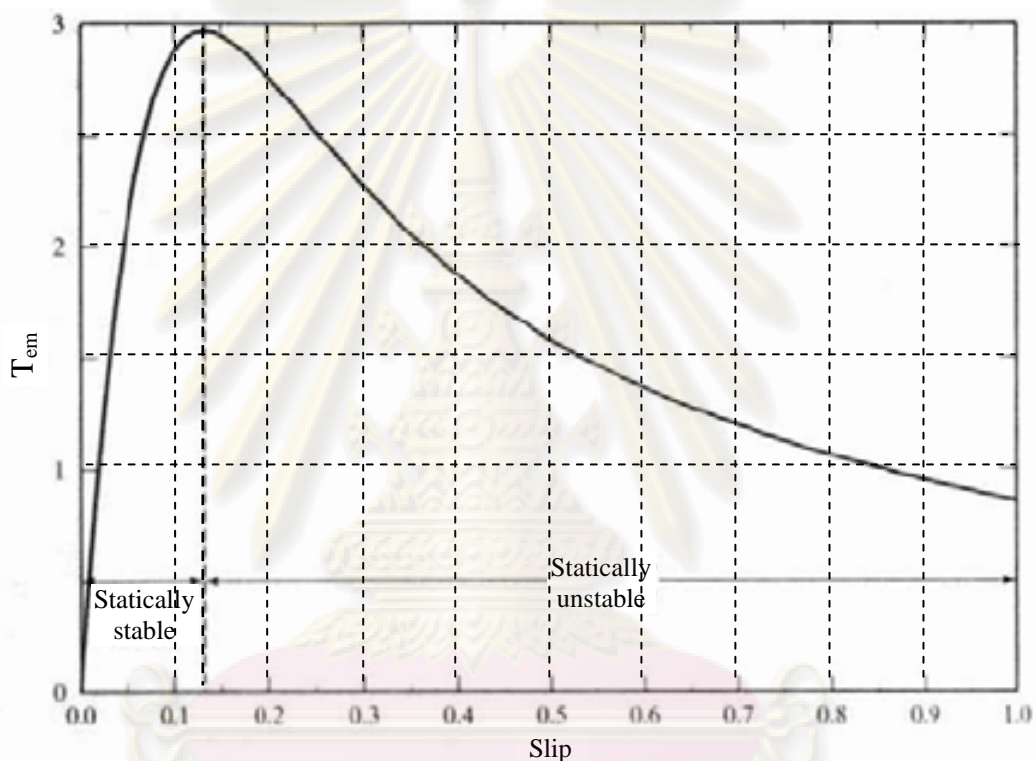


Figure 3.11 Induction machine speed-torque characteristic [13]

ศูนย์วิทยทรัพยากร  
จุฬาลงกรณ์มหาวิทยาลัย

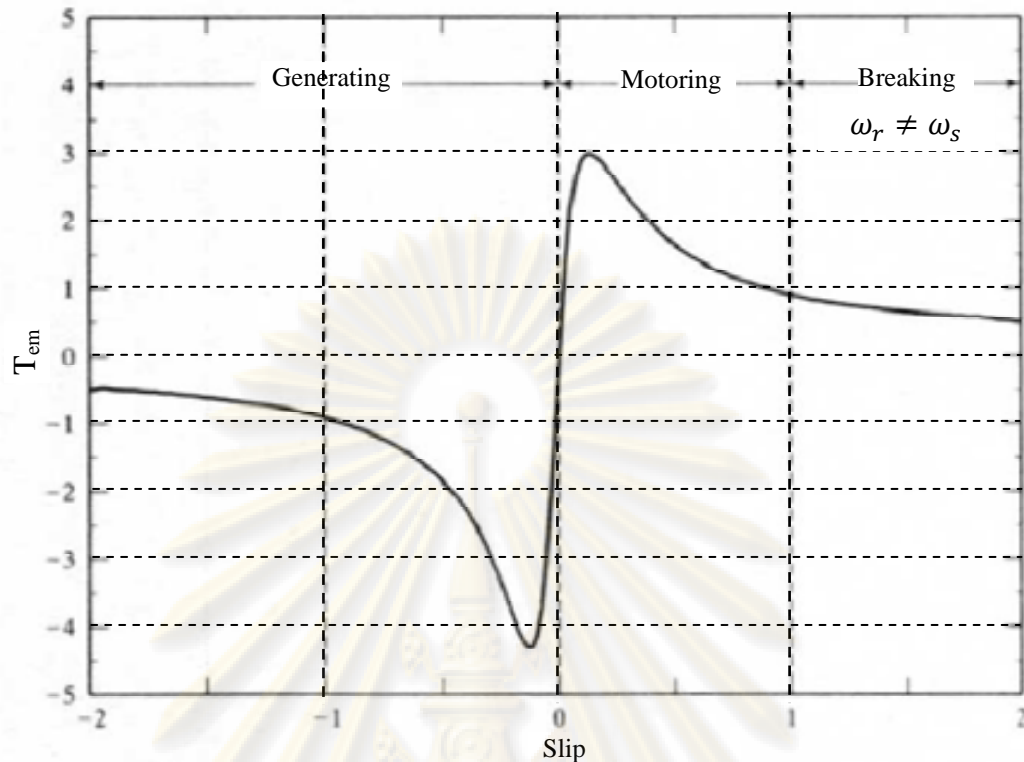


Figure 3.12 Generation and braking characteristics of the induction machine [13]

Figure 3.12 shows the torque vs. slip for a wide range of slip, from -2 to 2, with the stator supplied with rated voltages and frequency. Consider the motor as spinning in the direction opposite to that of a phase sequence abc. Assume that a set of stator voltages with a phase sequence abc is applied at supply frequency. This creates a stator flux linkage counter to the direction of rotor speed, resulting in a braking action. This also creates a slip greater than one: the rotor speed is negative with respect to synchronous speed. This braking action brings rotor speed to standstill in time.

Consider the rotor electrical speed to be greater than the synchronous speed, resulting in a negative slip. A negative slip changes the generation of positive (motoring) to negative (generating) torque as the induced emf phase is reversed. Hence, for negative slip, the torque-vs.-slip characteristic is similar to the motoring characteristic discussed earlier, except that the breakdown torque is much higher with negative-slip operation. This is due to the fact that the mutual flux linkages are strengthened by the generator action of the induction machine. The reversal of rotor current reduces the motor impedance voltage drop, resulting in a boost of magnetizing current and hence in an increase of mutual flux linkages and torque.

จุฬาลงกรณ์มหาวิทยาลัย

# CHAPTER IV

## SYSTEM MODELED

### 4.1 Microgrid System Model

Fig.4. 1 shows a single line diagram of a 13.8 kV microgrid system connected to a 120 kV utility main grid, represented by an infinite-bus equivalent, through a radial distribution line to be used as a test system here. The system includes a wind-turbine unit with a variable speed doubly-fed induction generator, a synchronous generator equipped with governor action, and combination of fixed-impedance and constant-power load models connected to the microgrid at three different load points.

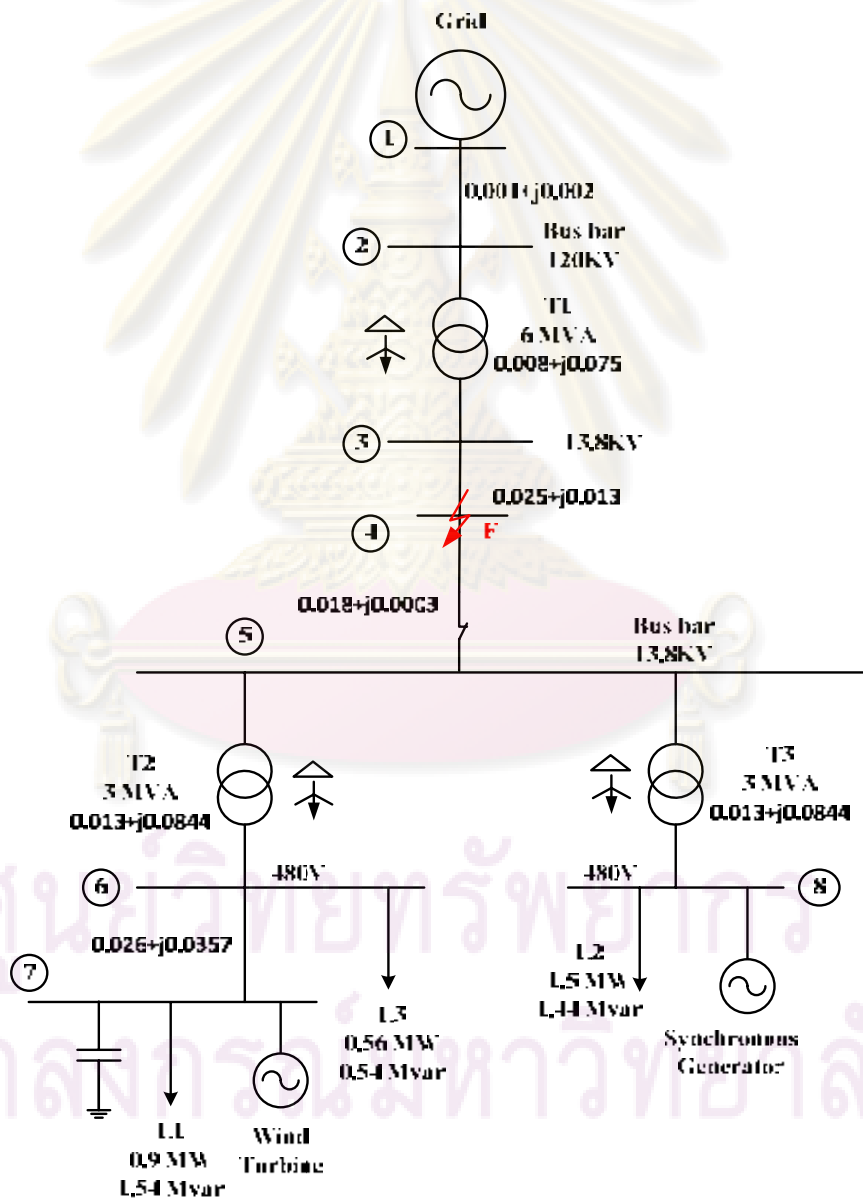


Figure 4.1 Single line diagram of the studied microgrid system

## 4.2 Wind Power System Model

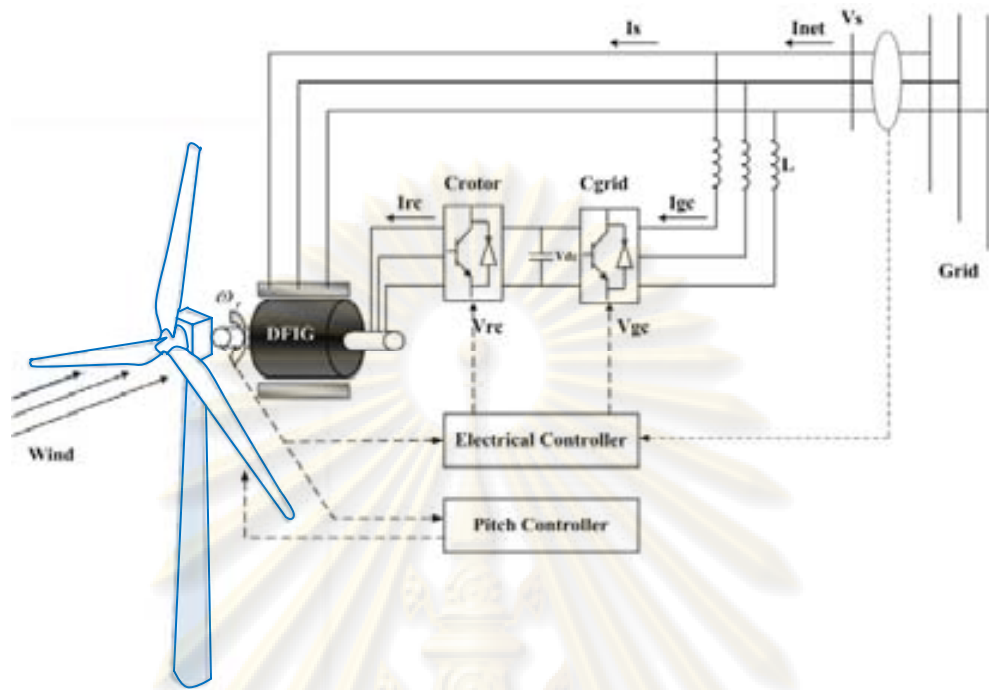


Figure 4.2 Wind power system

Figure 4.2 represents the block diagram of the wind power system model that includes wind speed, wind turbine, induction generator (IG) whose stator winding directly connected to the main grid, converter block integrated at rotor-side of IG and controller block that encompasses both electrical and mechanical using pitch controller.

### 4.2.1 Wind Speed Model

Wind turbine installation should be done within the suitable windy site. The data on wind speeds and directions are needed in order to obtain a proper match between the characteristics of the wind turbine and those of the site. Since the wind speed and direction are varied continuously, estimation of power generation required some statistic. In the case the total data of wind speeds against time is not available, but the average wind speed may be known. In this case the wind speeds distribution can be obtained approximately from the magnitude of average wind speed, by using a standard statistical distribution function. The more general distribution function used to obtain an approximation for wind speed distribution of the site knowing its average wind speed is Weibull distribution, given by

$$f(v) = \left(\frac{k}{c}\right) \left(\frac{v_{wind}}{c}\right)^{k-1} \exp\left[-\left(\frac{v_{wind}}{c}\right)^k\right] \quad (4.1)$$

Where  $c$  is a scale factor taken equal to mean wind speed,  
 $k$  is a shape factor, ranging between 1.8 and 2.3.

Fig.4.3 is a simulation of wind speed with average wind speed  $c=6\text{m/s}$  and shape factor  $k=1.8$ . And Figure 4.4 shows the Weibull distribution of the wind at each wind speed.

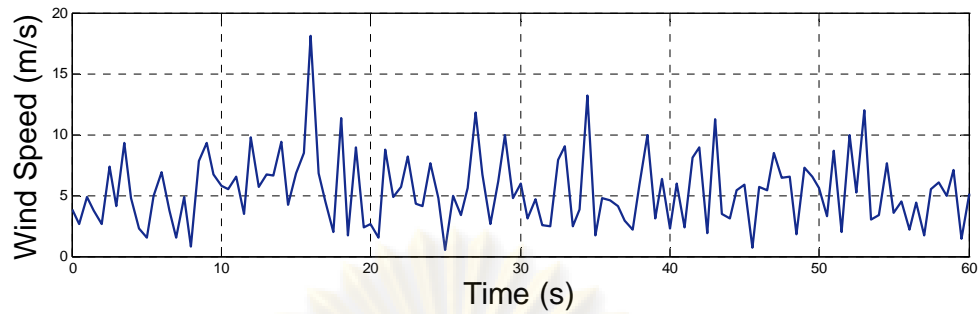


Figure 4.3 Wind speed simulation

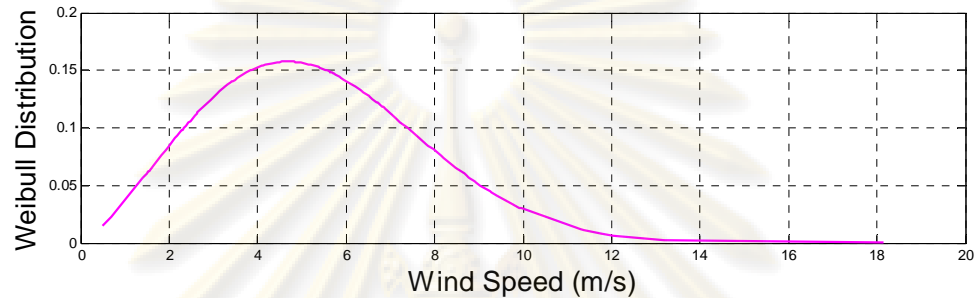


Figure 4.4 Weibull distribution at each wind speed

#### 4.2.2 Rotor Model

The model is based on the steady-state power characteristics of the turbine. The stiffness of drive train is infinite and fraction factor and the inertia of the turbine must be combined with those of generator couple to turbine. The mechanical power is given by following equation.

$$P_{mech} = C_p(\lambda, \beta) \frac{\rho A}{2} V_{wind}^3 \quad (4.2)$$

Equation (4.2) can be normalized so in the p.u. system we have

$$P_{mech-pu} = k_p C_{p-pu}(\lambda, \beta) V_{wind-pu}^3 \quad (4.3)$$

The numerical approximated curves of  $C_p(\lambda, \beta)$  based on equations (3.9) and (3.10), for different values of the pitch angle, are illustrated in Figure 4.5. The mechanical power  $P_m$  as a function of generator speed, for different wind speeds and for blade pitch angle  $\beta = 0^\circ$  is depicted in Figure 4.6. Here, the base wind speed is equal to 6m/s, maximum power at base wind speed equal 0.73 p.u. ( $k_p = 0.73$ ), and base rotational speed equal 1.2 p.u., respectively.

จุฬาลงกรณ์มหาวิทยาลัย

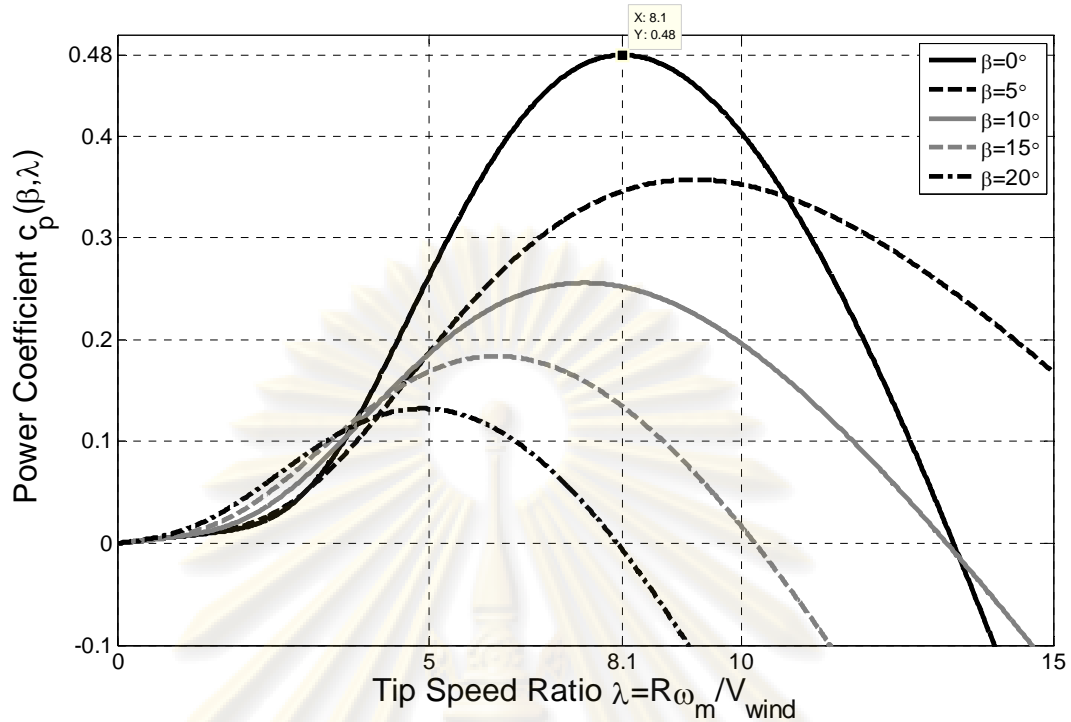


Figure 4.5 Performance coefficient of wind turbine

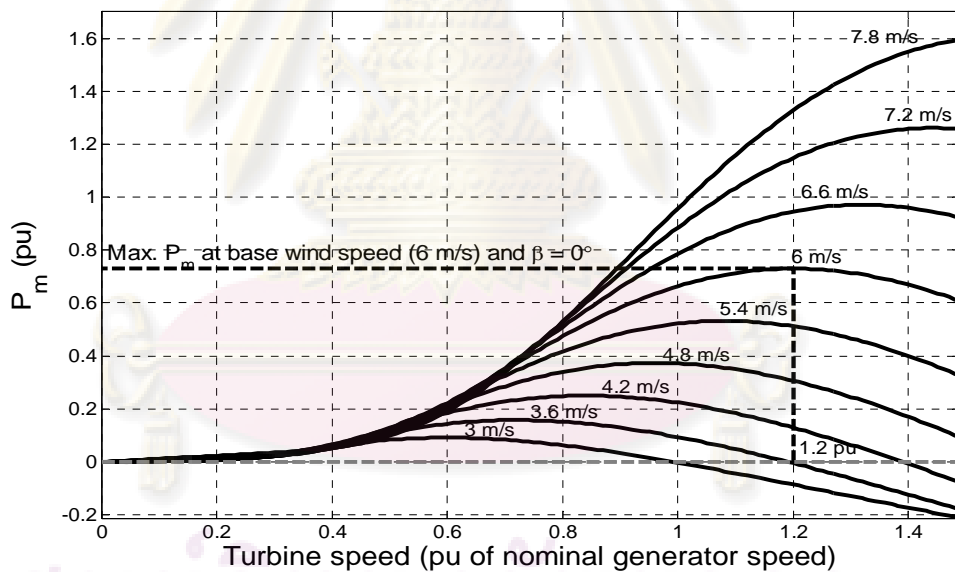


Figure 4.6 Turbine characteristic

The simulink block diagram of the turbine is illustrated in Figure 4.7. The three inputs needed are

- Generator speed  $\omega_r$  in p.u. of the nominal speed of generator
- Pitch angle  $\beta$  in degree and
- Wind speed in m/s

The tip speed ratio  $\lambda$  in p.u. of  $\lambda_{nom}$  is obtained by division of rotational speed in p.u. of the base rotational speed and the wind speed in p.u. of base wind speed. The output is

- Mechanical torque  $T_m$  applied to the generator shaft in p.u. nominal generator torque.

The table 4.1 is the nominal values to be used for the rotor model

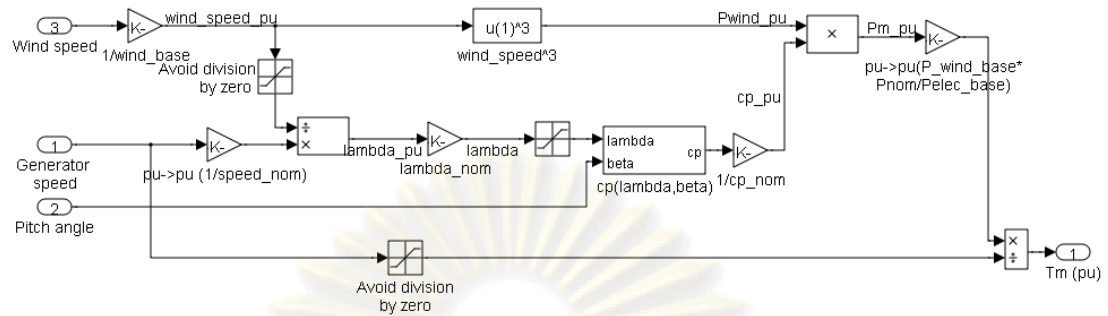


Figure 4.7 Block diagram of rotor model

Table 4. 1 Nominal values of wind turbine rotor

Name	Value
Base mechanical power [Mw]	2
Base electrical power [MVA]	2.22
Base wind speed (wind_base) [m/s]	6
Base rotational speed or rotational speed at maximum power for the base wind speed (speed_nom) [p.u.]	1.2
Nominal tip speed ratio $\lambda_{nom}$	8.1
Nominal power coefficient $Cp_{nom}$	4.8

### 4.2.3 Doubly-Fed Induction Generator Model

The dynamic voltage equations of a three-phase symmetrical doubly fed induction generator in terms of equivalent dq-base system, with respect to the synchronously rotating reference frame, are given as follows:

$$v_{ds}^e = R_s i_{ds}^e + \frac{d\lambda_{ds}^e}{dt} - \omega_s \lambda_{qs}^e \quad (4.4)$$

$$v_{qs}^e = R_s i_{qs}^e + \frac{d\lambda_{qs}^e}{dt} + \omega_s \lambda_{ds}^e \quad (4.5)$$

$$v_{dr}^e = R_r i_{dr}^e + \frac{d\lambda_{dr}^e}{dt} - (\omega_s - \omega_r) \lambda_{qr}^e \quad (4.6)$$

$$v_{qr}^e = R_r i_{qr}^e + \frac{d\lambda_{qr}^e}{dt} + (\omega_s - \omega_r) \lambda_{dr}^e \quad (4.7)$$

The flux linkages above can be calculated by using the following equations:

$$\lambda_{ds}^e = L_s i_{ds}^e + L_m i_{dr}^e \quad (4.8)$$

$$\lambda_{qs}^e = L_s i_{qs}^e + L_m i_{qr}^e \quad (4.9)$$

$$\lambda_{dr}^e = L_r i_{dr}^e + L_m i_{ds}^e \quad (4.10)$$

$$\lambda_{qr}^e = L_r i_{qr}^e + L_m i_{qs}^e \quad (4.11)$$

The electromagnetic torque is defined as:

$$T_e = \frac{3p}{2} (\lambda_{ds}^e i_{qs}^e - \lambda_{qs}^e i_{ds}^e) \quad (4.12)$$

The active power is given by:

$$P_s = \frac{3}{2} (v_{ds}^e i_{ds}^e + v_{qs}^e i_{qs}^e) \quad (4.13)$$

The reactive power is defined as:

$$Q_s = \frac{3}{2} (v_{qs}^e i_{ds}^e - v_{ds}^e i_{qs}^e) \quad (4.14)$$

The mechanical system of the DFIG is given by:

$$J \frac{d\omega_{rm}}{dt} = T_e - T_m \quad (4.15)$$

### • Per-Unit System

A per-unit quantity  $\bar{Q}$  is defined as the ratio of an actual quantity  $Q_A$  to an appropriately chosen base value  $Q_B$  so that

$$\bar{Q} = Q_A / Q_B \quad (4.16)$$

If  $Q_A$  and  $Q_B$  are the same order of magnitude,  $\bar{Q}$  takes on a value close to unity. So while  $Q_A$  and  $Q_B$  vary widely in absolute values depending on the size or rating of the device to which they relate and have dimensions such as Volt, Ampere, Ohm, Weber, Newton-meter,  $\bar{Q}$  is a dimensionless relative quantity that lies in a narrow numerical range. In the context of electric machines, the following advantages to the use of per-unit (p.u.) parameters and p.u. equations can be cited:

1. Per-unit parameters do not vary appreciably over a wide range of machine ratings, thereby providing a better characterization and comparison of differing designs.
2. A p.u. system simplifies the analysis of machine systems because it eliminates the consideration of such cumbersome factors as numbers of poles and phases, winding turns ratios; in effect, it allows to view the machine on the basis of an equivalent two-phase, two-pole configuration with coupled windings having 1:1 turns ratios.
3. When dealing with an interconnected system of machines of different ratings, a common overall system normalization provides an effective way to account for the interconnections.

### • Machine rating

The rating of an electric machine invariably serves as the basis for determining the normalizing factors required to define the p.u. system. Typically, the rating (as it normally appears on the nameplate) provides most of the following information:

- f of poles =  $p$
- number of phases =  $m$  (usually 3)



- speed =  $n_B$  (rpm)
- rated voltage =  $V_r$  (usually on a line-to-line rms basis) (V)
- power factor =  $pf_B$
- efficiency =  $\eta_B$
- electrical power output  $P_e$  (Watts) for a generator;  $P_B = P_e / pf_B$  (VA)
- mechanical power output  $P_m$  (hp) for a motor;  $P_B = 746 \times P_m$  (W)

• **Base Values**

- Base frequency  $\omega_B = 2\pi f_B$  [rad/s]
- Base Power =  $P_B$
- Base voltage = peak phase voltage =  $V_B = \sqrt{\frac{2}{3}} V_r$  [V]
- Base peak current =  $I_B = \frac{2P_B}{3V_B}$  [A]
- Base impedance =  $Z_B = \frac{V_B}{I_B}$  [ $\Omega$ ]
- Base flux linkage =  $\lambda_B = \frac{V_B}{\omega_B}$
- Base inductance =  $L_B = \frac{\lambda_B}{I_B} = \frac{Z_B}{\omega_B}$
- Base synchronous speed  $\omega_{mB} = \frac{2\omega_B}{p}$
- Base torque =  $\frac{P_B}{\omega_{mB}} = \frac{pP_B}{2\omega_B}$

Dividing (4.4)-(4.7) by the base values  $V_B = Z_B I_B = \omega_B \lambda_B$  we get the p.u. equations

$$\bar{v}_{ds}^e = \bar{R}_s \bar{i}_{ds}^e + \frac{1}{\omega_B} \frac{d\bar{\lambda}_{ds}^e}{dt} - \bar{\omega}_s \bar{\lambda}_{qs}^e \quad (4.17)$$

$$\bar{v}_{qs}^e = \bar{R}_s \bar{i}_{qs}^e + \frac{1}{\omega_B} \frac{d\bar{\lambda}_{qs}^e}{dt} + \bar{\omega}_s \bar{\lambda}_{ds}^e \quad (4.18)$$

$$\bar{v}_{dr}^e = \bar{R}_r \bar{i}_{dr}^e + \frac{1}{\omega_B} \frac{d\bar{\lambda}_{dr}^e}{dt} - (\bar{\omega}_s - \bar{\omega}_r) \bar{\lambda}_{qr}^e \quad (4.19)$$

$$\bar{v}_{qr}^e = \bar{R}_r \bar{i}_{qr}^e + \frac{1}{\omega_B} \frac{d\bar{\lambda}_{qr}^e}{dt} + (\bar{\omega}_s - \bar{\omega}_r) \bar{\lambda}_{dr}^e \quad (4.20)$$

Dividing (4.8)-(4.11) by base values  $\lambda_B = L_B I_B$  yield

$$\bar{\lambda}_{ds}^e = \bar{L}_s \bar{i}_{ds}^e + \bar{L}_m \bar{i}_{dr}^e \quad (4.21)$$

$$\bar{\lambda}_{qs}^e = \bar{L}_s \bar{i}_{qs}^e + \bar{L}_m \bar{i}_{qr}^e \quad (4.22)$$

$$\bar{\lambda}_{dr}^e = \bar{L}_r \bar{i}_{dr}^e + \bar{L}_m \bar{i}_{ds}^e \quad (4.23)$$

$$\bar{\lambda}_{qr}^e = \bar{L}_r \bar{i}_{qr}^e + \bar{L}_m \bar{i}_{qs}^e \quad (4.24)$$

Dividing (4.12) by  $T_B = \frac{P_B}{\omega_{mB}} = \frac{p}{2} \frac{3}{2} \frac{V_B I_B}{\omega_B} = \frac{p}{2} \frac{3}{2} \lambda_B I_B = \frac{p}{2} \frac{3}{2} L_B I_B I_B$  we get

$$\bar{T}_e = (\bar{\lambda}_{ds}^e \bar{i}_{qs}^e - \bar{\lambda}_{qs}^e \bar{i}_{ds}^e) \quad (4.25)$$

Dividing (4.13) and (4.14) by  $P_B = \frac{3}{2} V_B I_B$  we get

$$\bar{P}_s = (\bar{v}_{ds}^e \bar{i}_{ds}^e + \bar{v}_{qs}^e \bar{i}_{qs}^e) \quad (4.26)$$

The reactive power is defined as:

$$\bar{Q}_s = (\bar{v}_{qs}^e \bar{i}_{ds}^e - \bar{v}_{ds}^e \bar{i}_{qs}^e) \quad (4.27)$$

And divide (4.15) by  $T_B = \frac{P_B}{\omega_{mB}} = \frac{p}{2} \frac{3}{2} \frac{V_B I_B}{\omega_B} = \frac{p}{2} \frac{3}{2} \lambda_B I_B = \frac{p}{2} \frac{3}{2} L_B I_B I_B$  we get

$$\begin{aligned} J \frac{\omega_{mB}}{P_B} \frac{d\omega_{rm}}{dt} &= \bar{T}_e - \bar{T}_m \\ \frac{J}{P_B} \omega_{mB} \frac{d}{dt} \left( \frac{p}{2} \omega_r \right) &= \bar{T}_e - \bar{T}_m \\ \frac{J}{P_B} \frac{p}{2} \omega_{mB}^2 \frac{d}{dt} \left( \frac{\omega_r}{\omega_{mB}} \right) &= \bar{T}_e - \bar{T}_m \\ \frac{J}{P_B} \frac{p}{2} \omega_{mB}^2 \frac{d}{dt} \left( \frac{\omega_r}{\frac{p}{2} \omega_B} \right) &= \bar{T}_e - \bar{T}_m \\ \frac{J}{P_B} \omega_{mB}^2 \frac{d\bar{\omega}_r}{dt} &= \bar{T}_e - \bar{T}_m \\ 2H \frac{d\bar{\omega}_r}{dt} &= \bar{T}_e - \bar{T}_m \end{aligned} \quad (4.28)$$

With  $H = \frac{1}{2} \frac{J}{P_B} \omega_{mB}^2$  [s]

#### 4.2.4 Converter Model

Converters are model with dual PWM voltage-fed, current-regulated converter, connected back to back as switching power electronic devices in the purpose of providing the required voltage outputs for the generated or absorbed power at rotor-side of doubly-fed induction generator [14].

In order to understand the concept of inverter PWM, first the discussion of PWM with full-bridge dc-dc converter is highlighted and the inverter circuits will be clarified thereafter. In PWM of full-bridge dc-dc converter, there exists the control signal  $v_{control}$  (constant or slowly varying in time) was compared with a repetitive switching-frequency triangular wave form in order to generate switching signals. And the controlling the switch duty ratios allowed the average dc voltage output to be controlled.

In the full-bridge converter shown in Figure 4.7, the input is fixed-magnitude dc voltage  $V_d$ . The output of the converter is a dc voltage  $V_0$ , which can be controlled in magnitude as well as polarity. In the bipolar voltage switching type, switches

$(T_{A^+}, T_{B^-})$  and  $(T_{B^+}, T_{A^-})$  are treated as switch pairs (two switches in a pair are simultaneously turned on and off). The switching signals are generated by comparing switching-frequency triangular waveforms  $v_{tri}$  with control voltage  $v_{control}$ . When  $v_{control} > v_{tri}$ ,  $T_{A^+}$  and  $T_{B^-}$  are turned on.

The switch duty ratios can be obtained from the waveforms in Figure 4.8 as follows by arbitrary choosing a time origin as shown in the figure:

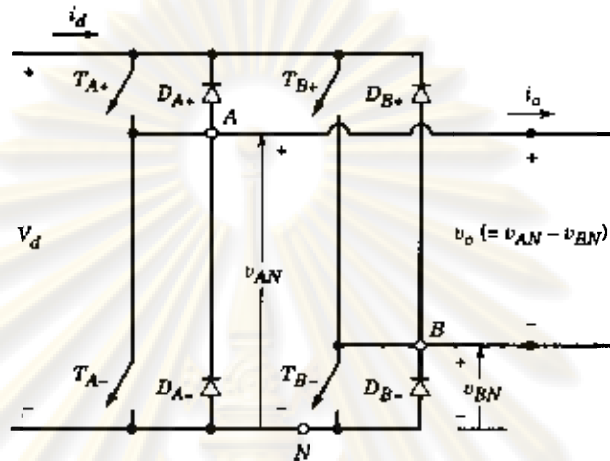


Figure 4.8 Full-bridge dc-dc converter [6]

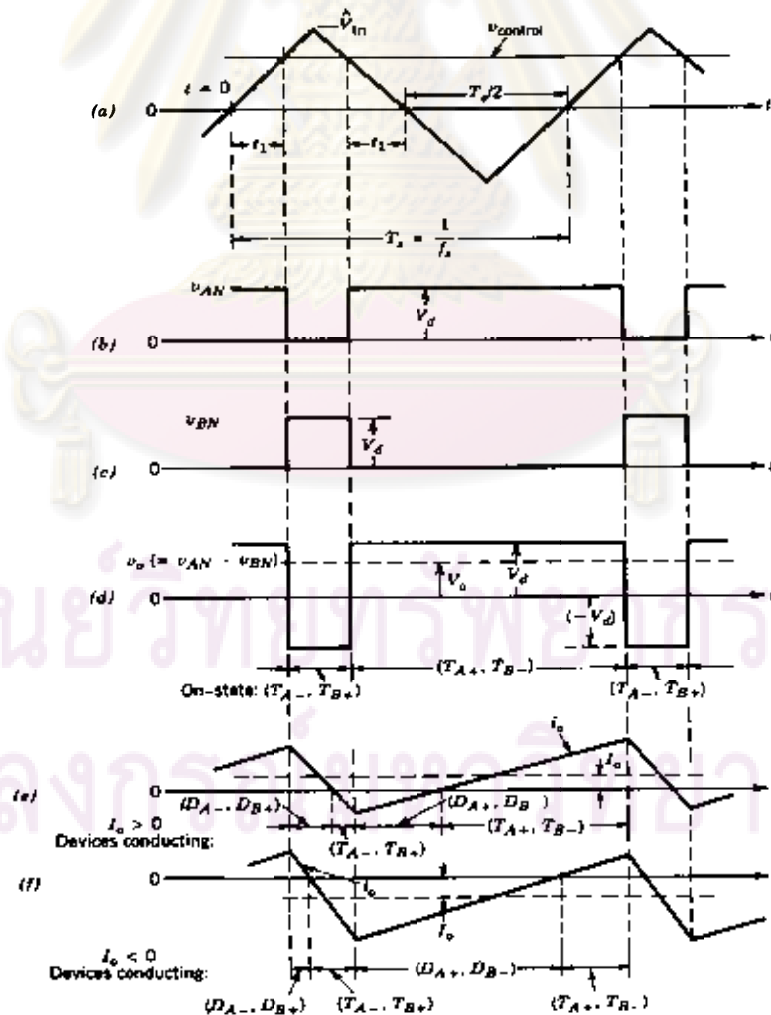


Figure 4.9 PWM with bipolar voltage switching [6]

$$v_{tri} = \hat{V}_{tri} \frac{t}{T_s/4} \quad 0 < t < \frac{1}{4}T_s \quad (4.29)$$

At  $t = t_1$  in Figure 4.8, and  $v_{tri} = v_{control}$ . From equation (4.29)

$$t_1 = \frac{v_{control} T_s}{\hat{V}_{tri} 4} \quad (4.30)$$

From Figure 4.8, we also find that the on duration of switch pair 1 ( $T_{A^+}, T_{B^-}$ ) is

$$t_{on} = 2t_1 + \frac{1}{2}T_s \quad (4.31)$$

Therefore, their duty ratio defined as:

$$D_1 = \frac{t_{on}}{T_s} = \frac{1}{2} \left( 1 + \frac{v_{control}}{\hat{V}_{tri}} \right) \quad (4.32)$$

And the duty ratio  $D_2$  of the switch pair 2 ( $T_{B^+}, T_{A^-}$ ) is

$$D_2 = 1 - D_1 \quad (4.33)$$

By using these duty ratio, from Figure 4.8 we can obtain  $V_{AN}, V_{BN}$ , and  $V_0$ :

$$V_0 = V_{AN} - V_{BN} = D_1 V_d - D_2 V_d = (2D_1 - 1)V_d \quad (4.34)$$

Substituting  $D_1$  from (4.32) into (4.34) yields

$$V_0 = \frac{V_d}{\hat{V}_{tri}} v_{control} \quad (4.35)$$

The basic of switching-mode for dc-to-ac inverter is derived from the one-leg inverter as seen in Figure 4.9 and it will assume that the midpoint "o" of the dc input voltage is available. Unlike PWM of full-bridge dc-dc converter, in the case of inverter circuit, the PWM is bit more complex, since we would like the invert output to be sinusoidal with magnitude and frequency controllable. In order to produce a sinusoidal output voltage waveform at a desired frequency, a sinusoidal control signal at a desired frequency is compared with a triangle wave form as shown in Figure 4.10. The output voltage  $v_{Ao}$  fluctuates between two values ( $\frac{1}{2}V_d$  and  $-\frac{1}{2}V_d$ ).

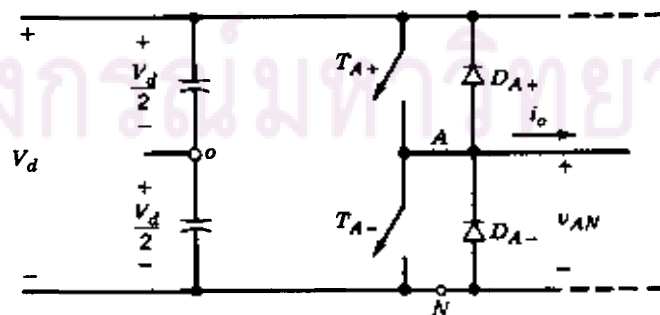


Figure 4.10 One-leg switch-mode inverter [6]

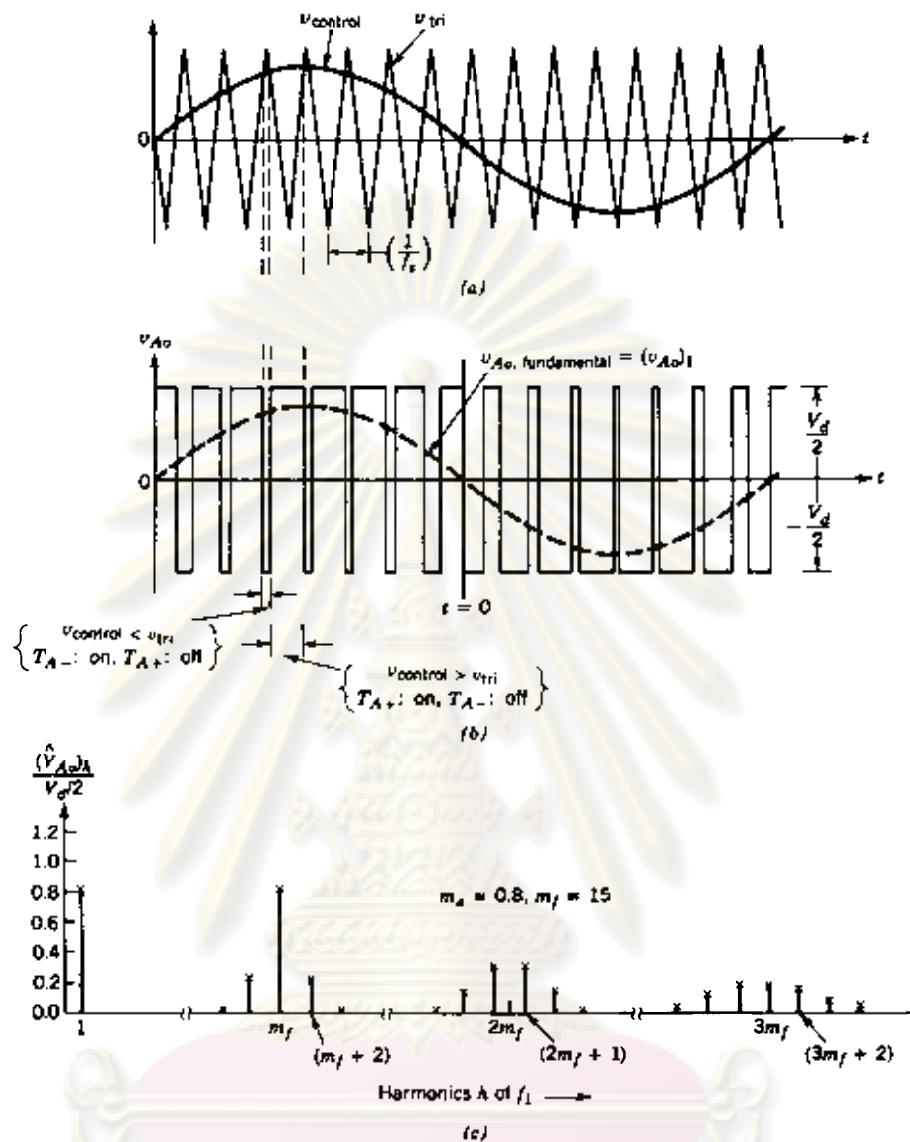


Figure 4.11 Pulse-width modulation (PWM) [6]

Considering a constant  $v_{control}$  as shown in Figure 4.11 and from the aforementioned PWM in a full-bridge dc-dc converter, the output voltage averaged over one switching time period  $T_s = 1/f_s$  is given as follows:

$$V_{Ao} = \frac{v_{control}}{\hat{V}_{tri}} \frac{V_d}{2} \quad (4.36)$$

Assuming that  $v_{control}$  varies very little during a switching time period, that is,  $m_f = \frac{f_s}{f_1}$  is large, as shown in Figure 4.11b, therefore, assuming  $v_{control}$  to be constant over a switching time period, (4.36) indicate how the “instantaneous average” value of  $v_{Ao}$  (averaged over one switching time period  $T_s$ ) varies from one switching time period to the next. This “instantaneous average” is the same as fundamental-frequency component of  $v_{Ao}$ .

The foregoing argument shows why  $v_{control}$  is chosen to be sinusoidal to provide a sinusoidal output voltage.

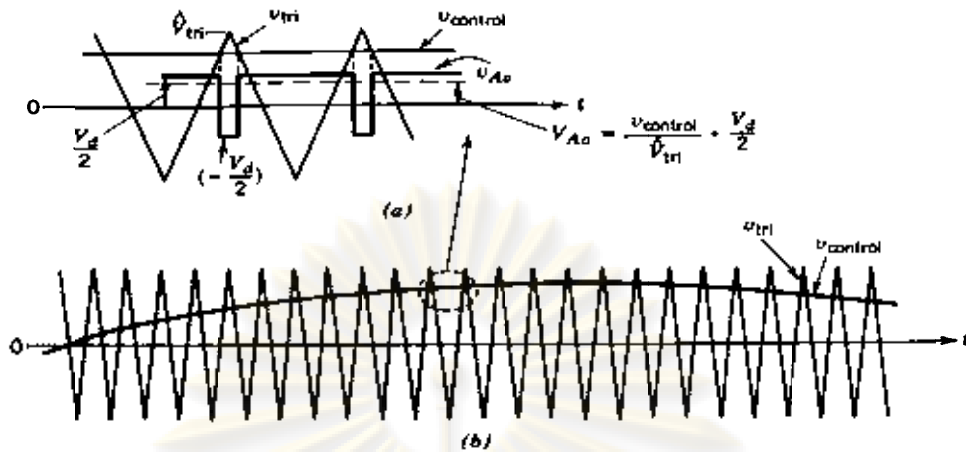


Figure 4.12 Sinusoidal PWM

And let the control voltage vary sinusoidally at the frequency  $f_1 = \omega_1/2\pi$ , which is the desired (or fundamental) frequency of the inverter output:

$$v_{control} = \hat{V}_{control} \sin \omega_1 t \quad \hat{V}_{control} \leq \hat{V}_{tri} \quad (4.37)$$

Using (4.36) and (4.37), the fundamental-frequency component  $(v_{Ao})_1$  varies sinusoidally and in phase with  $v_{control}$  as a function of time, result in

$$(v_{Ao})_1 = \frac{\hat{V}_{control}}{\hat{V}_{tri}} \sin \omega_1 t \frac{V_d}{2} = m_a \sin \omega_1 t \frac{V_d}{2} \quad (4.38)$$

Therefore,

$$(\hat{V}_{Ao})_1 = m_a \frac{V_d}{2} \quad (4.39)$$

#### 4.2.5 Rotor-Side PWM Controller Model

The control for rotor-side PWM provides the decoupled control of the active and reactive power (or voltage) of the DFIG measured at the grid terminals. The control approach is performed in a synchronously rotating  $d-q$  axis frame, with the  $d$ -axis oriented along the stator-flux vector position. With such orientation of the  $d$ -axis,

$$\lambda_{qs}^e = 0 \quad (4.40)$$

Applying this condition to equations (4.17)-(4.18) and (4.21)-(4.22) result in:

$$v_{ds}^e = R_s i_{ds}^e + \frac{d\lambda_{ds}^e}{dt} \quad (4.41)$$

$$v_{qs}^e = R_s i_{qs}^e + \omega_e \lambda_{ds}^e \quad (4.42)$$

$$\lambda_{ds}^e = L_s i_{ds}^e + L_m i_{dr}^e \quad (4.43)$$

$$0 = L_s i_{qs}^e + L_m i_{qr}^e \quad (4.44)$$

Since the stator is connected to the grid and the influence of stator resistant is small, the stator flux can be considered to be constant, decided by the magnitude and frequency of the grid voltage [14]. Thus, for stator field orientation and  $R_s \approx 0$ ,

$$\lambda_{ds}^e = \lambda_s \quad (4.45)$$

Which is a constant. This makes (4.41) and (4.42) become:

$$v_{ds}^e = 0 \quad (4.46)$$

$$v_{qs}^e = \omega_e \lambda_s \quad (4.47)$$

From equation (4.26) and (4.45), the active power at the terminal of stator winding becomes:

$$P_s = \omega_e \lambda_s i_{qs}^e \quad (4.48)$$

Using equation (4.44),

$$P_s = -\frac{L_m}{L_s} \omega_e \lambda_s i_{qr}^e \quad (4.49)$$

Using equation (4.27) in (4.47), the reactive power at the stator terminals becomes:

$$Q_s = \omega_e \lambda_s i_{ds}^e \quad (4.50)$$

Which using equation (4.43), becomes

$$Q_s = \frac{\omega_e \lambda_s}{L_s} (\lambda_s - L_m i_{dr}^e) \quad (4.51)$$

Using (4.43) and (4.44), equation (4.23) and (4.24) become

$$\lambda_{dr}^e = \frac{L_m}{L_s} \lambda_{ds}^e \sigma L_r i_{dr}^e \quad (4.52)$$

$$\lambda_{qr}^e = \sigma L_r i_{qr}^e \quad (4.53)$$

With

$$\sigma = \left(1 - \frac{L_m^2}{L_r L_s}\right) \quad (4.54)$$

Substituting (4.52) and (4.53) in (4.19) and (4.20) we get voltage of the rotor related to currents as following:

$$v_{dr}^e = R_r i_{dr}^e + \sigma L_r \frac{di_{dr}^e}{dt} - (\omega_e - \omega_r) L_r i_{qr}^e - (\omega_e - \omega_r) L_m i_{qs}^e \quad (4.55)$$

$$v_{qr}^e = R_r i_{qr}^e + \sigma L_r \frac{di_{qr}^e}{dt} + (\omega_e - \omega_r) L_r i_{dr}^e + (\omega_e - \omega_r) L_m i_{ds}^e \quad (4.56)$$

#### 4.2.5.1 Power Control

From equation (4.49), we see that the stator active power is proportional to the rotor current component  $i_{qr}^e$  and can be regulated by using  $v_{qr}^e$ .

The power is controlled in order to follow a pre-defined power-speed characteristic, named tracking characteristic. Such a characteristic is illustrated in the Figure 4.13 called turbine characteristics and tracking characteristic, by the ABCD curve superimposed to the mechanical power characteristics of the turbine obtained at different wind speeds. The actual speed of the turbine  $\omega_r$  is measured and the corresponding mechanical power of the tracking characteristic is used as the reference power for the power control loop. The tracking characteristic is defined by four points: A, B, C and D. From zero speed to speed of point A the reference power is zero. Between point A and point B the tracking characteristic is a straight line, the speed of point B must be greater than the speed of point A. Between point B and point C the tracking characteristic is the locus of the maximum power of the turbine (maxima of the turbine power vs turbine speed curves). The tracking characteristic is a straight line from point C and point D. The power at point D is one per unit (1 p.u.) and the speed of the point D must be greater than the speed of point C. Beyond point D, the reference power is a constant equal to one per unit (1 p.u.).

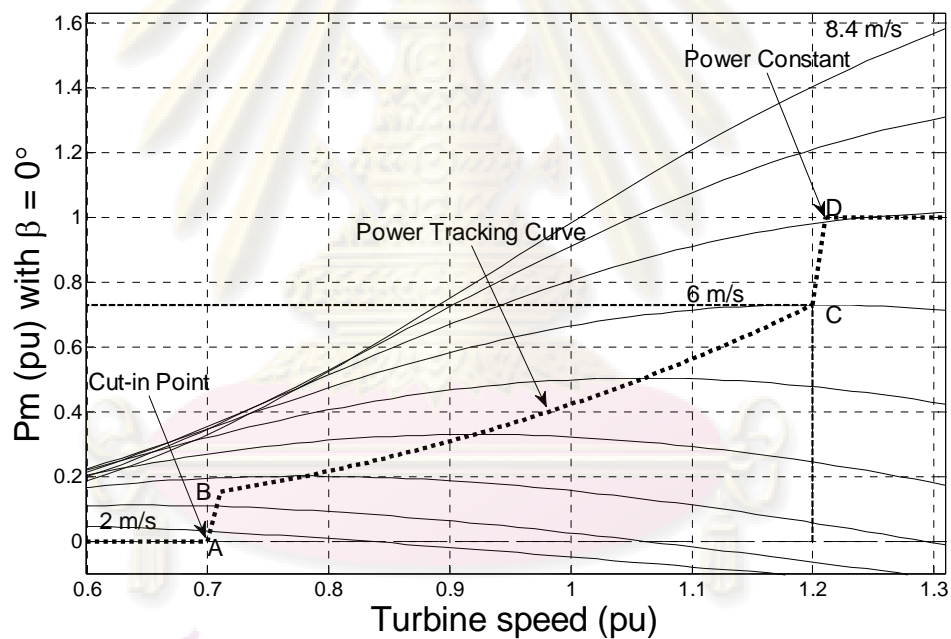


Figure 4.13 Turbine characteristic and optimal power tracking curves

The actual electrical output power, measured at the grid terminals of the wind turbine, is added to the total power losses (mechanical and electrical) and is compared with the reference power obtained from the tracking characteristic. A Proportional-Integral (PI) regulator is used to reduce the power error to zero. The output of this regulator is the reference rotor current  $I_{qr}^*$  that must be injected in the rotor by converter  $C_{rotor}$ . This is the current component that produces the electromagnetic torque  $T_e$ . The actual  $I_{qr}$  component of positive-sequence current is compared to  $I_{qr}^*$  and the error is reduced to zero by a current regulator (PI). The output of this current controller is the voltage  $V_{qr}^*$  generated by rotor-side converter.



#### 4.2.5.2 Var Regulator

When the wind turbine is operated in var regulation mode the reactive power at grid terminals is kept constant by a var regulator. From (4.51) we see that the stator reactive power is proportional to the rotor current component  $i_{dr}^e$  and can be regulated by using  $v_{dr}^e$ .

#### 4.2.5.3 Voltage Regulator

When the wind turbine is operated in voltage regulation mode, it implements the following V-I characteristic.

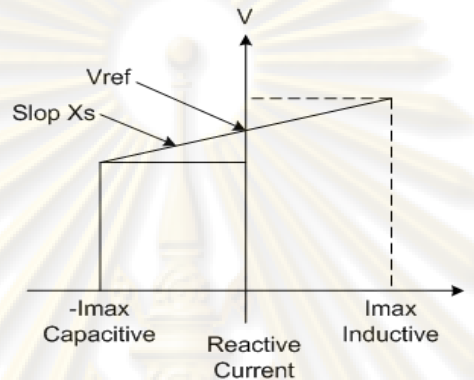


Figure 4.14 V-I characteristic

As long as the reactive current stays within the maximum current values ( $-I_{max}$ ,  $I_{max}$ ) imposed by the converter rating, the voltage is regulated at the reference voltage  $V_{ref}$ . However, a voltage droop is normally used (usually between 1% and 4% at maximum reactive power output), and the V-I characteristic has the slope indicated in the figure called wind turbine V-I characteristic shown in Figure 4.13. In the voltage regulation mode, the V-I characteristic is described by the following equation:

$$V = V_{ref} + X_s \cdot I \quad (4.57)$$

Where $V$	Positive sequence voltage (p.u.)
$I$	Reactive current (p.u./Pnom) ( $I > 0$ indicates an inductive current)
$X_s$	Slope or droop reactance

The output of the voltage regulator or the var regulator is the reference d-axis current  $I_{dr}^*$  that must be injected in the rotor by converter  $C_{rotor}$ . The same current regulator as for the power control is used to regulate the actual  $I_{dr}^e$  component of positive-sequence current to its reference value. The output of this regulator is the d-axis voltage  $V_{dr}^*$  generated by rotor-side converter. Figure 4.15 shows the block diagram of the DFIG's rotor-side PWM control.

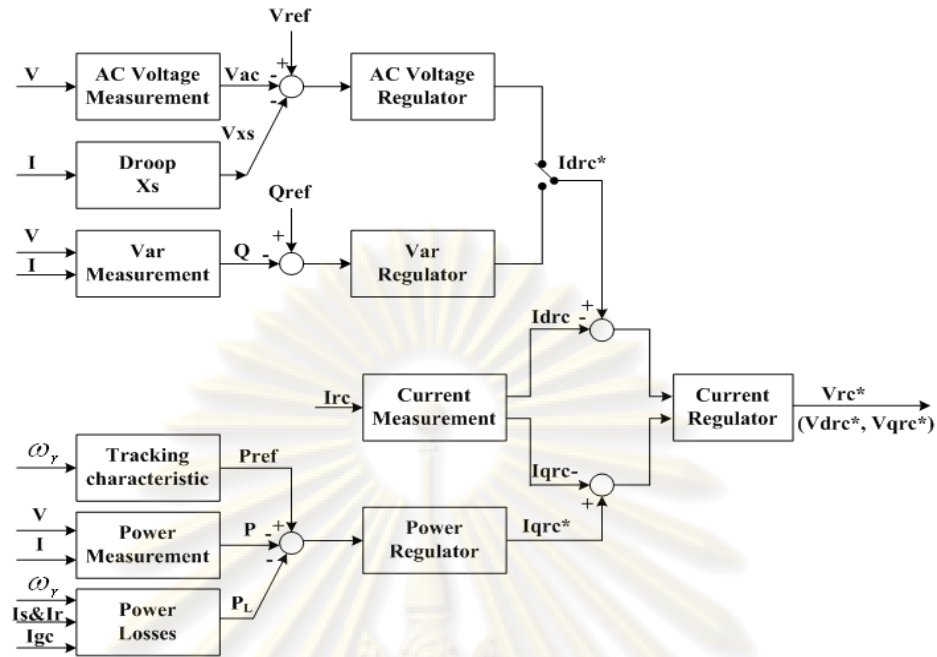


Figure 4.15 Block diagram of rotor-side converter control

### 4.2.6 Grid-Side PWM Control Model

The objective of the grid-side converter is to keep the DC-link voltage constant regardless of the magnitude and direction of the rotor power. A vector-control approach is used, with a reference frame oriented along the stator (or supply) voltage vector position, enabling independent control of the active and reactive power flowing between the supply and the grid-side converter. The PWM converter is current regulated, with the direct axis current  $i_{dgc}^e$  used to regulate the DC-link voltage and the quadrature axis current component  $i_{qgc}^e$  used to regulate the reactive power. Figure 4.16 shows the schematic of the grid-side converter. The voltage balance across the inductors is

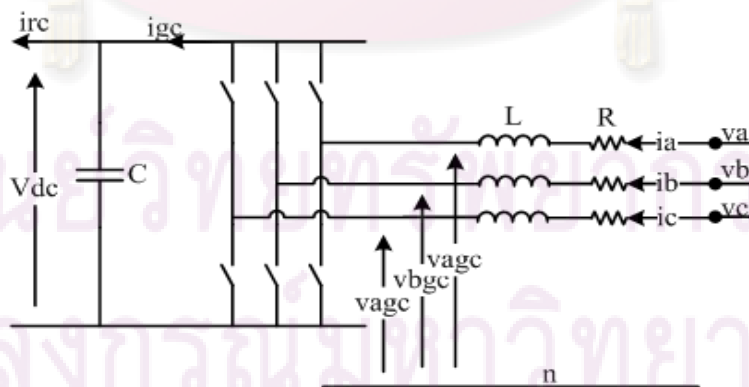


Figure 4.16 Schematic of grid-side converter

$$\begin{bmatrix} v_a \\ v_b \\ v_c \end{bmatrix} = R \begin{bmatrix} i_a \\ i_b \\ i_c \end{bmatrix} + L \frac{d}{dt} \begin{bmatrix} i_a \\ i_b \\ i_c \end{bmatrix} + \begin{bmatrix} v_{avg} \\ v_{bgc} \\ v_{cgc} \end{bmatrix} \tag{4.58}$$

In  $d$ - $q$  synchronously reference frame, the equation (4.58) becomes

$$\left. \begin{aligned} v_{ds}^e &= Ri_{dgc}^e + L \frac{di_{dgc}^e}{dt} - \omega_e Li_{qgc}^e + v_{dgc}^e \\ v_{qs}^e &= Ri_{dgc}^e + L \frac{di_{dgc}^e}{dt} + \omega_e Li_{dgc}^e + v_{qgc}^e \end{aligned} \right\} \quad (4.59)$$

The active and reactive power flow of grid-side converter is

$$\left. \begin{aligned} P_{gc} &= v_{ds}^e i_{dgc}^e + v_{qs}^e i_{qgc}^e \\ Q_{gc} &= v_{qs}^e i_{dgc}^e - v_{ds}^e i_{qgc}^e \end{aligned} \right\} \quad (4.60)$$

With the  $d$ -axis of the reference frame along the stator-voltage position,  $v_{qs}^e$  is zero and since the amplitude of the supply voltage is constant so that  $v_{ds}^e$  is constant. From (4.60), the active and the reactive power will be proportional to  $i_{dgc}^e$  and  $i_{qgc}^e$  respectively as in 4.61.

$$\left. \begin{aligned} P_{gc} &= v_{ds}^e i_{dgc}^e \\ Q_{gc} &= -v_{ds}^e i_{qgc}^e \end{aligned} \right\} \quad (4.61)$$

By neglecting harmonics due to switching and losses in the inductor resistance and converter, we obtain:

$$\left. \begin{aligned} P_r &= V_{dc} i_{rc} \\ P_{gc} &= V_{dc} i_{gc} = v_{ds}^e i_{dgc}^e \end{aligned} \right\} \quad (4.62)$$

The dynamic model of DC link is provided by

$$C \frac{dV_{dc}}{dt} = i_{gc} - i_{rc} = \frac{1}{V_{dc}} (P_{gc} - P_r) = \frac{1}{V_{dc}} (v_{ds}^e i_{dgc}^e - P_r) \quad (4.63)$$

From equation (4.63), it is seen that the DC-link voltage can be controlled via  $i_{dgc}^e$ . The control scheme thus utilises current control loops for  $i_{dgc}^e$  and  $i_{qgc}^e$ , with the  $i_{dgc}^e$  demand being derived from the DC-link voltage error through a standard PI controller. The  $i_{qgc}^e$  demand determines the displacement factor on the supply-side of the inductors. Figure 4.17 illustrates the control block of the grid-side PWM control.

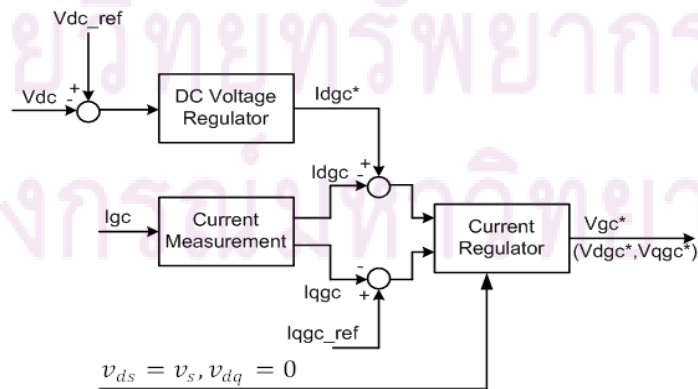


Figure 4.17 Block diagram of grid-side converter control

### 4.2.7 Pitch Angle Controller Model

The pitch angle controller is active only in high wind speeds. In such circumstances, the rotor speed can no longer be controlled by increasing the generated power, as this would lead to overloading the generator and/or the converter. Therefore the blade pitch angle is changed in order to limit the aerodynamic efficiency of the rotor. This prevents the rotor speed from becoming too high, which would result in mechanical damage. The optimal pitch angle is approximately zero below the nominal wind speed. From the nominal wind speed onwards, the optimal angle increases steadily with increasing wind speed, as can be seen in Figure 4.13. Equations (3.9) and (3.10) are used to calculate the impact of the pitch angle,  $\beta$ , on the performance coefficient. The resulting value can be inserted in Equation (4.2) in order to calculate the mechanical power extracted from the wind.

It should be taken into account that the pitch angle cannot change immediately, but only at a finite rate, which may be quite low because of the size of the rotor blades of modern wind turbines. Blade drives are usually as small as possible in order to save money. The maximum rate of change of the pitch angle is in the order of 3–10 degrees per second, depending on the size of the wind turbine.

Figure 4.18 depicts the pitch angle controller. This controller is a proportional (P) controller. Using this controller type implies that the rotor speed is allowed to exceed its nominal value by an amount that depends on the value chosen for the constant  $K_p$ .

However, we use a proportional controller because:

- A slight overspeeding of the rotor above its nominal value can be tolerated and does not pose any problems to the wind turbine construction;
- The system is never in steady state because of the varying wind speed. The advantage of an integral controller, which can achieve zero steady state error, would therefore be hardly noticeable

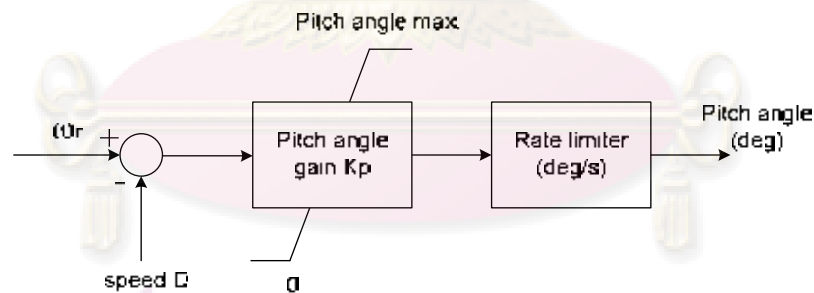


Figure 4.18 Pitch angle control model

## 4.3 Synchronous Machine Model

### 4.3.1 Generator Model

The model of the synchronous machine is well documented in the literature. One of the various models is represented in this thesis with the use of simplified model with one damping winding on the  $q$ -axis.

In the case that one damping winding is included on the  $q$ -axis, from page 86-87 of [15] the set of electrical equations are simplified from the full model and redefined as following:

In  $d$ -axis:

- Voltage equations

$$e_d = -R_a i_d - \omega \psi_q \quad (4.64)$$

$$e_q = -R_a i_q + \omega \psi_d \quad (4.65)$$

$$e_{fd} = R_{fd} i_{fd} + \frac{1}{\omega_b} \frac{d\psi_{fd}}{dt} \quad (4.66)$$

$$0 = R_{kq} i_{kq} + \frac{1}{\omega_b} \frac{d\psi_{kq}}{dt} \quad (4.67)$$

- Flux linkage equation

$$\psi_d = - \underbrace{(L_{ad} + L_l)}_{L_d} i_d + L_{ad} i_{fd} \quad (4.68)$$

$$\psi_q = - \underbrace{(L_{aq} + L_l)}_{L_q} i_q + L_{aq} i_{kq} \quad (4.69)$$

$$\psi_{fd} = -L_{ad} i_d + \underbrace{(L_{ad} + L_{fd})}_{L_{ffd}} i_{fd} \quad (4.70)$$

$$\psi_{kq} = -L_{aq} i_q + \underbrace{(L_{aq} + L_{kq})}_{L_{kkq}} i_{kq} \quad (4.71)$$

From (4.68)-(4.71)

$$\psi_d = \psi_{ad} - L_l i_d \quad (4.72)$$

$$\psi_q = \psi_{aq} - L_l i_q \quad (4.73)$$

$$\psi_{fd} = \psi_{ad} + L_{fd} i_{fd} \quad (4.74)$$

$$\psi_{kq} = \psi_{aq} + L_l i_{kq} \quad (4.75)$$

With

$$\psi_{ad} = -L_{ad} i_d + L_{ad} i_{fd} \quad (4.76)$$

$$\psi_{aq} = -L_{aq} i_q + L_{aq} i_{kq} \quad (4.77)$$

From (4.75) and (4.73) we have

$$\begin{aligned} \psi_{ad} &= -L_{ad} i_d + L_{ad} i_{fd} \\ \psi_{ad} &= -L_{ad} i_d + L_{ad} \frac{1}{L_{fd}} (\psi_{fd} - \psi_{ad}) \\ \psi_{ad} &= L'_{ad} \left( -i_d + \frac{\psi_{fd}}{L_{fd}} \right) \end{aligned} \quad (4.78)$$

With

$$L'_{ad} = \frac{1}{\frac{1}{L_{ad}} + \frac{1}{L_{fd}}} \quad (4.79)$$

From (4.77) and (4.75) we have

$$\begin{aligned} \psi_{aq} &= -L_{aq} i_q + L_{aq} i_{kq} \\ \psi_{aq} &= -L_{aq} i_q + L_{aq} \frac{1}{L_{kq}} (\psi_{kq} - \psi_{aq}) \end{aligned}$$

$$\psi_{aq} = L'_{aq} \left( -i_q + \frac{\psi_{kq}}{L_{kq}} \right) \quad (4.80)$$

With

$$L'_{aq} = \frac{1}{\frac{1}{L_{aq}} + \frac{1}{L_{kq}}} \quad (4.81)$$

From (4.64) and (4.73)

$$\begin{aligned} e_d &= -R_a i_d - \omega \psi_q \\ &= -R_a i_d - \omega (\psi_{aq} - L_l i_q) \\ &= -R_a i_d - \omega \left( L'_{aq} \left( -i_q + \frac{\psi_{kq}}{L_{kq}} \right) - L_l i_q \right) \\ &= -R_a i_d + \underbrace{\omega (L'_{aq} - L_l)}_{X'_q} i_q - \underbrace{\omega L'_{aq} \frac{\psi_{kq}}{L_{kq}}}_{E'_d} \\ e_d &= -R_a i_d + X'_q i_q + E'_d \end{aligned} \quad (4.82)$$

With

$$E'_d = -\omega L'_{aq} \frac{\psi_{kq}}{L_{kq}} = -\omega \frac{1}{\frac{1}{L_{aq}} + \frac{1}{L_{kq}}} \frac{\psi_{kq}}{L_{kq}} = -\omega \frac{L_{aq}}{L_{aq} + L_{kq}} \psi_{kq} = -\omega \frac{L_{aq}}{L_{kkq}} \psi_{kq} \quad (4.83)$$

From (4.65) and (4.72)

$$\begin{aligned} e_q &= -R_a i_q + \omega \psi_d \\ &= -R_a i_q + \omega (\psi_{ad} - L_l i_d) \\ &= -R_a i_q + \omega \left( L'_{ad} \left( -i_d + \frac{\psi_{fd}}{L_{fd}} \right) - L_l i_d \right) \\ &= -R_a i_q - \underbrace{\omega (L'_{ad} + L_l)}_{X'_d} i_d + \underbrace{\omega L'_{ad} \frac{\psi_{fd}}{L_{fd}}}_{E'_q} \\ e_q &= -R_a i_q + X'_d + E'_q \end{aligned} \quad (4.84)$$

With

$$E'_q = \omega L'_{ad} \frac{\psi_{fd}}{L_{fd}} = \omega \frac{1}{\frac{1}{L_{ad}} + \frac{1}{L_{fd}}} \frac{\psi_{fd}}{L_{fd}} = \omega \frac{L_{ad}}{L_{ad} + L_{fd}} \psi_{fd} = \omega \frac{L_{ad}}{L_{ffd}} \psi_{fd} \quad (4.85)$$

From (4.66)

$$\frac{1}{\omega_b} \frac{d\psi_{fd}}{dt} = e_{fd} - R_{fd} i_{fd}$$

Multiplying both sides by  $\frac{L_{ad}}{L_{ffd}}$

$$\frac{1}{\omega_b} \frac{d}{dt} \left( \frac{L_{ad}}{L_{ffd}} \psi_{fd} \right) = \frac{L_{ad}}{L_{ffd}} e_{fd} - \frac{L_{ad}}{L_{ffd}} R_{fd} i_{fd}$$

$$\frac{1}{\omega_b} \frac{d}{dt} (E'_q) = \frac{L_{ad}}{R_{fd} L_{ffd}} e_{fd} - \frac{R_{fd}}{L_{ffd}} L_{ad} i_{fd} \quad (4.86)$$

And multiplying (4.70) by  $\frac{L_{ad}}{L_{ffd}}$

$$\begin{aligned}\frac{L_{ad}}{L_{ffd}}\psi_{fd} &= -\frac{L_{ad}^2}{L_{ffd}}i_d + L_{ad}i_{fd} \\ E'_q &= -\frac{L_{ad}^2}{L_{ffd}}i_d + L_{ad}i_{fd} \quad \text{or} \\ L_{ad}i_{fd} &= E'_q + \frac{L_{ad}^2}{L_{ffd}}i_d\end{aligned}\quad (4.87)$$

Replace (4.87) in (4.86)

$$\frac{1}{\omega_b} \frac{dE'_q}{dt} = \frac{R_{fd}}{L_{ffd}} \frac{L_{ad}}{R_{fd}} e_{fd} - \frac{R_{fd}}{L_{ffd}} \left( E'_q + \frac{L_{ad}^2}{L_{ffd}} i_d \right) \quad (4.88)$$

And we have

$$\begin{aligned}L'_d &= L'_{ad} + L_l \\ L'_d &= \frac{1}{\frac{1}{L_{ad}} + \frac{1}{L_{fd}}} + L_l \\ L'_d &= \frac{L_{ad}L_{fd}}{L_{ad}+L_{fd}} + L_d - L_{ad} \\ L'_d &= -\frac{L_{ad}^2}{L_{ad}+L_{fd}} + L_d \\ -\frac{L_{ad}^2}{L_{ad}+L_{fd}} &= L'_d - L_d\end{aligned}\quad (4.89)$$

Replace (4.89) in (4.88)

$$\begin{aligned}\frac{1}{\omega_b} \frac{dE'_q}{dt} &= \frac{R_{fd}}{L_{ffd}} \frac{L_{ad}}{R_{fd}} e_{fd} - \frac{R_{fd}}{L_{ffd}} (E'_q - (L'_d - L_d)i_d) \\ &= \frac{1}{T'_{do}} E_{fd} - \frac{1}{T'_{do}} (E'_q - (L'_d - L_d)i_d) \\ \frac{1}{\omega_b} \frac{dE'_q}{dt} &= \frac{1}{T'_{do}} E_{fd} - \frac{1}{T'_{do}} (E'_q - (L'_d - L_d)i_d) \\ \frac{1}{\omega_b} \frac{dE'_q}{dt} &= \frac{1}{T'_{do}} (-E'_q - (L'_d - L_d)i_d + E_{fd})\end{aligned}\quad (4.90)$$

The same for q-axis from (4.67)

$$\frac{1}{\omega_b} \frac{d\psi_{kq}}{dt} = -R_{kq}i_{kq}$$

Multiplying both sides by  $-\frac{L_{aq}}{L_{kkq}}$

$$\begin{aligned}\frac{1}{\omega_b} \frac{d}{dt} \left( -\frac{L_{aq}}{L_{kkq}} \psi_{kq} \right) &= R_{kq} \frac{L_{aq}}{L_{kkq}} i_{kq} \\ \frac{1}{\omega_b} \frac{d}{dt} (E'_d) &= R_{kq} \frac{L_{aq}}{L_{kkq}} i_{kq}\end{aligned}\quad (4.91)$$

And multiplying (4.71) by  $-\frac{L_{aq}}{L_{kkq}}$

$$-\frac{L_{aq}}{L_{kkq}} \psi_{kq} = \frac{L_{aq}^2}{L_{kkq}} i_q - L_{aq} i_{kq}$$

$$E'_d = \frac{L_{aq}^2}{L_{kkq}} i_q - L_{aq} i_{kq} \quad \text{or}$$

$$L_{aq} i_{kq} = \frac{L_{aq}^2}{L_{kkq}} i_q - E'_d \quad (4.92)$$

Replace (4.92) in (4.91)

$$\frac{1}{\omega_b} \frac{d}{dt} (E'_d) = \frac{R_{kq}}{L_{kkq}} \left( \frac{L_{aq}^2}{L_{kkq}} i_q - E'_d \right) \quad (4.93)$$

And we have

$$\begin{aligned} L'_q &= L_{aq} + L_{kq} \\ L'_q &= \frac{1}{\frac{1}{L_{aq}} + \frac{1}{L_{kq}}} + (L_q - L_{aq}) \\ L'_q &= L_q + \left( \frac{L_{aq} L_{kq}}{L_{aq} + L_{kq}} - L_{aq} \right) \\ L'_q &= L_q - \frac{L_{aq}^2}{L_{aq} + L_{kq}} \\ L'_q &= L_q - \frac{L_{aq}^2}{L_{kkq}} \\ \frac{L_{aq}^2}{L_{kkq}} &= L_q - L'_q \end{aligned} \quad (4.94)$$

Replace (4.94) in (4.93)

$$\begin{aligned} \frac{1}{\omega_b} \frac{d}{dt} (E'_d) &= \frac{R_{kq}}{\frac{L_{kkq}}{\frac{1}{T'_{q0}}}} \left( (L_q - L'_q) i_q - E'_d \right) \\ \frac{1}{\omega_b} \frac{d}{dt} (E'_d) &= \frac{1}{T'_{q0}} (-E'_d + (L_q - L'_q) i_q) \end{aligned} \quad (4.95)$$

From (4.82), (4.84), (4.90) and (4.95) we obtained the electrical equation of synchronous generator and in form of matrices

$$\begin{bmatrix} e_d \\ e_q \end{bmatrix} = \underbrace{\begin{bmatrix} -R_a & X'_q \\ -X'_d & -R_a \end{bmatrix}}_{[ReqM]} \begin{bmatrix} i_d \\ i_q \end{bmatrix} + \begin{bmatrix} E'_d \\ E'_q \end{bmatrix} \quad (4.96)$$

$$\frac{1}{\omega_b} \begin{bmatrix} E'_d \\ E'_q \end{bmatrix} = \underbrace{\begin{bmatrix} \frac{1}{T'_{q0}} & 0 \\ 0 & \frac{1}{T'_{d0}} \end{bmatrix}}_{[TeqM]} \begin{bmatrix} E'_d \\ E'_q \end{bmatrix} + \underbrace{\begin{bmatrix} 0 & \frac{L_q - L'_q}{T'_{q0}} \\ -\frac{L_d - L'_d}{T'_{d0}} & 0 \end{bmatrix}}_{[LeqM]} \begin{bmatrix} i_d \\ i_q \end{bmatrix} + \begin{bmatrix} 0 \\ \frac{1}{T'_{d0}} \end{bmatrix} E_{fd} \quad (4.97)$$



- Electromagnetic torque can be expressed as following

$$T_{em} = \psi_d i_q - \psi_q i_d$$

$$T_{em} = (E'_q - L'_d i_d) i_q - (-E'_d - L'_q i_q) i_d$$

$$T_{em} = E'_q i_q + E'_d i_d + (L'_q - L'_d) i_d i_q \quad (4.98)$$

- Synchronous Generator Equation of Motion

$$\frac{d\Delta\omega_r}{dt} = \frac{1}{2H} (T_m - T_e - K_D \Delta\omega_r) \quad (4.99)$$

$$\frac{d\delta}{dt} = \omega_b \Delta\omega_r \quad (4.100)$$

### 4.3.2 Governor Model

The governor is modeled by a droop characteristic specified by the constant  $R$ , which is negative of slope shown in Figure 4.18, whose unit is in per unit or percent based on the machine rated [16].

$$R = -\frac{\Delta\omega(pu.)}{\Delta P_m(pu.)}, \text{ or } \Delta P_m(pu.) = -\frac{1}{R} \Delta\omega_s(pu.) \quad (4.101)$$

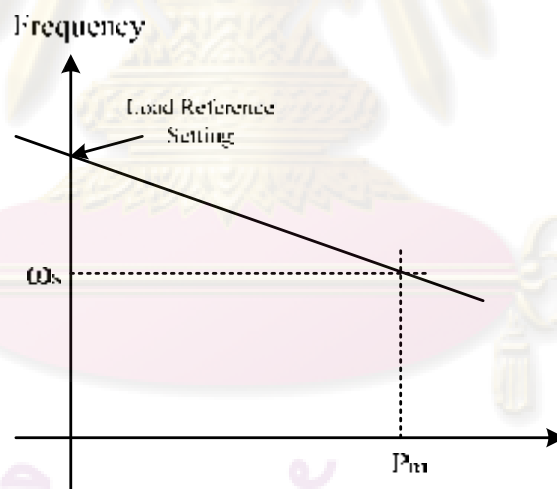


Figure 4.19 Droop characteristic

### 4.4 Load Model

The load models are traditionally classified into two broad categories: static models and dynamic models [15]. The models of load represented in this section are included both static model as a constant impedance and dynamic load model. Equation (4.102) is the equation describe the dynamic load model and Figure 4.20 represents the constant energy dynamic model of the load.

$$T_r \frac{dG}{dt} = P_o - GV^2 \quad (4.102)$$

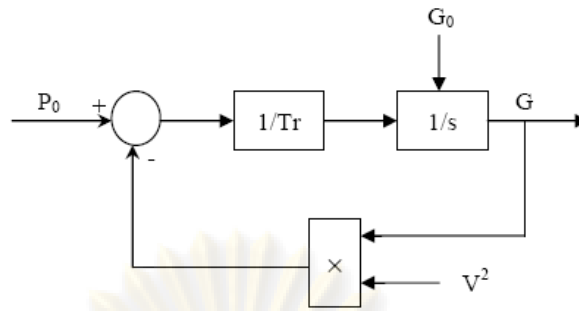


Figure 4.20 Constant power dynamic load model

#### 4.5 Network Model

The model of network can be expressed either in power-balance form or current-balance form. The latter form is more popular with industry software package [17] and will be used here. Equation (4.103) and (4.104) is the nodal set of equations.

$$I_{bus} = Y_{bus} \cdot V_{bus} \quad (4.103)$$

Or

$$\begin{bmatrix} I_1 \\ \vdots \\ I_i \\ \vdots \\ I_n \end{bmatrix} = \begin{bmatrix} Y_{11} & \cdots & Y_{1i} & \cdots & Y_{1n} \\ \vdots & & \vdots & & \vdots \\ Y_{i1} & \cdots & Y_{ii} & \cdots & Y_{in} \\ \vdots & & \vdots & & \vdots \\ Y_{n1} & \cdots & Y_{ni} & \cdots & Y_{nn} \end{bmatrix} \begin{bmatrix} V_1 \\ \vdots \\ V_i \\ \vdots \\ V_n \end{bmatrix} \quad (4.104)$$

Where  $Y_{bus}$  is  $n \times n$  bus admittance matrix of  $n$  buses network,  $I_{bus}$  is the net injected current vector and  $V_{bus}$  is bus voltage vector. From the network equation (4.104), since there are different dynamic models of generation respect to their type of inputs and outputs, for instant, some dynamic model of generator that is modeled as voltage input and current as an output to network and all load buses that also have the current as the input to the network, hence they have to be gyrated between input and output of equation (4.104).

And the corresponding algorithm of gyrated process for example row  $i$  to be gyrated is as following

From (4.104) can be written as

$$i_1 = Y_{11}V_1 + \cdots + Y_{1i}V_i + \cdots + Y_{1n}V_n \quad (4.105)$$

...

$$i_i = Y_{i1}V_1 + \cdots + Y_{ii}V_i + \cdots + Y_{in}V_n \quad (4.106)$$

...

$$i_n = Y_{n1}V_1 + \cdots + Y_{ni}V_i + \cdots + Y_{nn}V_n \quad (4.107)$$

From (4.105) we can find  $V_i$  as

$$V_i = -\frac{Y_{i1}}{Y_{ii}} V_1 - \dots + \frac{1}{Y_{ii}} i_i - \dots - \frac{Y_{in}}{Y_{ii}} V_n \quad (4.108)$$

By substituting  $V_i$  to all currents expression (4.105)-(4.108) we get the new equations of the current as

$$i_1 = Y_{11}V_1 + \dots + Y_{1i} \left( -\frac{Y_{i1}}{Y_{ii}} V_1 - \dots + \frac{1}{Y_{ii}} i_i - \dots - \frac{Y_{in}}{Y_{ii}} V_n \right) + \dots + Y_{1n}V_n \quad \text{or}$$

$$i_1 = \left( Y_{11} - \frac{Y_{1i}Y_{i1}}{Y_{ii}} \right) V_1 + \dots + \frac{Y_{1i}}{Y_{ii}} i_i + \dots + \left( Y_{1n} - \frac{Y_{1i}Y_{in}}{Y_{ii}} \right) V_n \quad (4.109)$$

...

$$V_i = -\frac{Y_{i1}}{Y_{ii}} V_1 - \dots + \frac{1}{Y_{ii}} i_i - \dots - \frac{Y_{in}}{Y_{ii}} V_n \quad (4.110)$$

...

$$i_n = Y_{n1}V_1 + \dots + Y_{ni} \left( -\frac{Y_{i1}}{Y_{ii}} V_1 - \dots + \frac{1}{Y_{ii}} i_i - \dots - \frac{Y_{in}}{Y_{ii}} V_n \right) + \dots + Y_{nn}V_n \quad \text{or}$$

$$i_n = \left( Y_{n1} - \frac{Y_{ni}Y_{i1}}{Y_{ii}} \right) V_1 + \dots + \frac{Y_{ni}}{Y_{ii}} i_i + \dots + \left( Y_{nn} - \frac{Y_{ni}Y_{in}}{Y_{ii}} \right) V_n \quad (4.111)$$

In matrices form we get

$$\begin{bmatrix} I_1 \\ \vdots \\ V_i \\ \vdots \\ I_n \end{bmatrix} = \begin{bmatrix} Y_{11} - \frac{Y_{1i}Y_{i1}}{Y_{ii}} & \dots & \frac{Y_{1i}}{Y_{ii}} & \dots & Y_{1n} - \frac{Y_{1i}Y_{in}}{Y_{ii}} \\ \vdots & \vdots & \vdots & \vdots & \vdots \\ -\frac{Y_{i1}}{Y_{ii}} & \dots & \frac{1}{Y_{ii}} & \dots & -\frac{Y_{in}}{Y_{ii}} \\ \vdots & \vdots & \vdots & \vdots & \vdots \\ Y_{n1} - \frac{Y_{ni}Y_{i1}}{Y_{ii}} & \dots & \frac{Y_{ni}}{Y_{ii}} & \dots & Y_{nn} - \frac{Y_{ni}Y_{in}}{Y_{ii}} \end{bmatrix} \begin{bmatrix} V_1 \\ \vdots \\ I_i \\ \vdots \\ V_n \end{bmatrix} \quad (4.112)$$

Or

$$\begin{bmatrix} I_1 \\ \vdots \\ V_i \\ \vdots \\ I_n \end{bmatrix} = \underbrace{\begin{bmatrix} H_{11} & \dots & H_{1i} & \dots & H_{1n} \\ \vdots & \vdots & \vdots & \vdots & \vdots \\ H_{i1} & \dots & H_{ii} & \dots & H_{in} \\ \vdots & \vdots & \vdots & \vdots & \vdots \\ H_{n1} & \dots & H_{ni} & \dots & H_{nn} \end{bmatrix}}_{[H_{mod}]} \begin{bmatrix} V_1 \\ \vdots \\ I_i \\ \vdots \\ V_n \end{bmatrix} \quad (4.113)$$

- **Break Algebraic Loop for Synchronous Generator**

From the network equations (4.113), the expression of terminal current at bus  $t$  where the synchronous generator is connected to is the current at  $t^{th}$  row and given as

$$I_t = H_{t1}V_1 + \dots + H_{ti}I_i + \dots + H_{tt}V_t + \dots + H_{tn}V_n \quad (4.114)$$

Or in complex form

$$\begin{aligned} I_{dt}^s + jI_{qt}^s = & (\text{Real}(H_{t1}) + j\text{Im}(H_{t1}))(V_{d1}^s + jV_{q1}^s) + \dots \\ & + (\text{Real}(H_{ti}) + j\text{Im}(H_{ti}))(I_{di}^s + jI_{qi}^s) + \dots \\ & + (\text{Real}(H_{tt}) + j\text{Im}(H_{tt}))(V_{dt}^s + jV_{qt}^s) + \dots \\ & + (\text{Real}(H_{tn}) + j\text{Im}(H_{tn}))(V_{dn}^s + jV_{qn}^s) \end{aligned}$$

$$\begin{aligned} I_{dt}^s + jI_{qt}^s = & (\text{Real}(H_{t1})V_{d1}^s - \text{Im}(H_{t1})V_{q1}^s) + j(\text{Real}(H_{t1})V_{q1}^s + \text{Im}(H_{t1})V_{d1}^s) + \dots \\ & + (\text{Real}(H_{ti})I_{di}^s - \text{Im}(H_{ti})I_{qi}^s) + j(\text{Real}(H_{ti})I_{qi}^s + \text{Im}(H_{ti})I_{di}^s) + \dots \\ & + (\text{Real}(H_{tt})V_{dt}^s - \text{Im}(H_{tt})V_{qt}^s) + j(\text{Real}(H_{tt})V_{qt}^s + \text{Im}(H_{tt})V_{dt}^s) + \dots \\ & + (\text{Real}(H_{tn})V_{dn}^s - \text{Im}(H_{tn})V_{qn}^s) + j(\text{Real}(H_{tn})V_{qn}^s + \text{Im}(H_{tn})V_{dn}^s) \end{aligned}$$

Where superscript “s” defines as synchronous reference frame

In matrices form

$$\begin{bmatrix} I_{dt}^s \\ I_{qt}^s \end{bmatrix} = [H_{t1}] \begin{bmatrix} V_{d1}^s \\ V_{q1}^s \end{bmatrix} + \dots + [H_{ti}] \begin{bmatrix} I_{di}^s \\ I_{qi}^s \end{bmatrix} + \dots + [H_{tt}] \begin{bmatrix} V_{dt}^s \\ V_{qt}^s \end{bmatrix} + \dots + [H_{tn}] \begin{bmatrix} V_{dn}^s \\ V_{qn}^s \end{bmatrix} \quad (4.115)$$

Where

$$[H_{\alpha\beta}] = \begin{bmatrix} \text{Real}(H_{\alpha\beta}) & -\text{Im}(H_{\alpha\beta}) \\ \text{Im}(H_{\alpha\beta}) & \text{Real}(H_{\alpha\beta}) \end{bmatrix} \quad (4.116)$$

And  $V_t$  is the terminal voltage where synchronous generator connected to bus  $t$  so we

$$\text{have} \begin{bmatrix} V_{dt}^s \\ V_{qt}^s \end{bmatrix} = \begin{bmatrix} e_{dt}^s \\ e_{qt}^s \end{bmatrix}.$$

From (4.96) the terminal voltage of synchronous generator in rotor reference frame is redefined here

$$\begin{bmatrix} e_{dt}^r \\ e_{qt}^r \end{bmatrix} = [R_{eq}M] \begin{bmatrix} i_{dt}^r \\ i_{qt}^r \end{bmatrix} + \begin{bmatrix} E_d'^r \\ E_q'^r \end{bmatrix} \quad (4.117)$$

Multiplying both sides by  $[T]^{-1}$

$$[T]^{-1} \begin{bmatrix} e_{dt}^r \\ e_{qt}^r \end{bmatrix} = [T]^{-1} \left( [R_{eq}M] \begin{bmatrix} i_{dt}^r \\ i_{qt}^r \end{bmatrix} + \begin{bmatrix} E_d'^r \\ E_q'^r \end{bmatrix} \right) \quad (4.118)$$

Or

$$\begin{bmatrix} e_{dt}^s \\ e_{qt}^s \end{bmatrix} = [T]^{-1} \left( [R_{eq}M][T] \begin{bmatrix} i_{dt}^s \\ i_{qt}^s \end{bmatrix} + [T] \begin{bmatrix} E_d'^s \\ E_q'^s \end{bmatrix} \right) \quad (4.119)$$

Replacing (4.119) in (4.115)

$$\begin{aligned} \begin{bmatrix} I_{dt}^s \\ I_{qt}^s \end{bmatrix} &= [H_{t1}] \begin{bmatrix} V_{d1}^s \\ V_{q1}^s \end{bmatrix} + \dots [H_{ti}] \begin{bmatrix} I_{di}^s \\ I_{qi}^s \end{bmatrix} + \dots [H_{tn}] [T]^{-1} \left( [R_{eq}M][T] \begin{bmatrix} i_{dt}^s \\ i_{qt}^s \end{bmatrix} + [T] \begin{bmatrix} E_d'^s \\ E_q'^s \end{bmatrix} \right) + \\ &\quad \dots + [H_{tn}] \begin{bmatrix} V_{dn}^s \\ V_{qn}^s \end{bmatrix} \\ \underbrace{\left( I - [H_{tn}][T]^{-1}[R_{eq}M][T] \right)}_{[A]} \begin{bmatrix} I_{dt}^s \\ I_{qt}^s \end{bmatrix} &= [H_{t1}] \begin{bmatrix} V_{d1}^s \\ V_{q1}^s \end{bmatrix} + \dots [H_{ti}] \begin{bmatrix} I_{di}^s \\ I_{qi}^s \end{bmatrix} + \dots + [H_{tn}] \begin{bmatrix} E_{dt}'^s \\ E_{qt}'^s \end{bmatrix} + \\ &\quad \dots + [H_{tn}] \begin{bmatrix} V_{dn}^s \\ V_{qn}^s \end{bmatrix} \\ \begin{bmatrix} I_{dt}^s \\ I_{qt}^s \end{bmatrix} &= \underbrace{[A]^{-1} \left( [H_{t1}] \begin{bmatrix} V_{d1}^s \\ V_{q1}^s \end{bmatrix} + \dots [H_{ti}] \begin{bmatrix} I_{di}^s \\ I_{qi}^s \end{bmatrix} + \dots + [H_{tn}] \begin{bmatrix} E_{dt}'^s \\ E_{qt}'^s \end{bmatrix} + \dots + [H_{tn}] \begin{bmatrix} V_{dn}^s \\ V_{qn}^s \end{bmatrix} \right)}_{[B]} \\ \begin{bmatrix} I_{dt}^s \\ I_{qt}^s \end{bmatrix} &= [A]^{-1}[B] \quad (4.120) \end{aligned}$$

Where  $[T] = \begin{bmatrix} \cos \theta & \sin \theta \\ -\sin \theta & \cos \theta \end{bmatrix}$ , is a transformation matrix from rotor reference frame to synchronous reference frame and  $\theta$  is an angle that d-axis rotor reference frame lead d-axis of synchronous reference frame.

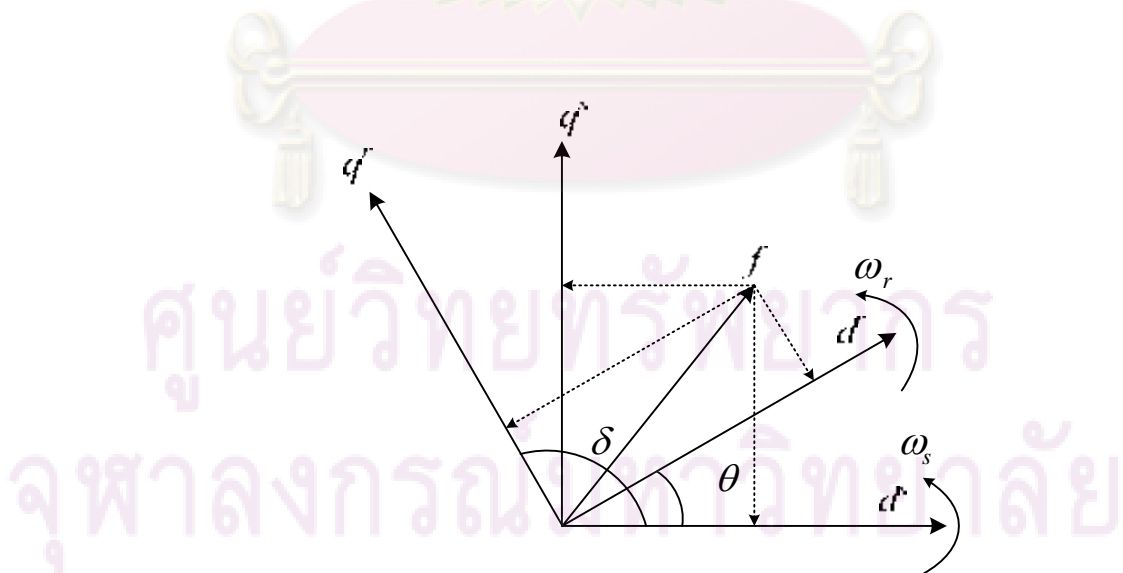


Figure 4.21 Transformation reference frame

And we see that the matrix  $[B]$  is the  $t^{th}$  row output from  $[H_{mod}]$  when the input of the  $[H_{mod}]$  is state  $\begin{bmatrix} E'_{dt} \\ E'_{qt} \end{bmatrix}$ .

And as the synchronous generator is modeled in rotor reference frame so we have to transform the current expression obtained from network in synchronous reference frame to the rotor reference frame.

$$\begin{bmatrix} I_{dt}^r \\ I_{qt}^r \end{bmatrix} = [T] \begin{bmatrix} I_{dt}^s \\ I_{qt}^s \end{bmatrix} \quad (4. 121)$$



ศูนย์วิทยทรัพยากร  
จุฬาลงกรณ์มหาวิทยาลัย

# CHAPTER V

## TEST RESULTS AND DISCUSSION

Several case studies have been conducted to examine responses of dynamic model and the operation of the 13.8 kV system in Figure 4.1. Firstly, the impact of a local compensator on WT-SCIG is investigated, following which validity of the induction generator operation as it is the main component used in the wind power generation. Next, two cases of disturbances applied to the microgrid including small disturbance caused by natural wind speed fluctuation and large disturbance that results from the fault occurring at bus 4 are examined. The two types of clearing fault are also contributed to the case study, it consists of a temporary fault and a permanent fault. In the case of the temporary fault, the fault is cleared followed by the reconnecting of the microgrid to the main grid. For the permanent fault, the fault is cleared by removing the line between the bus 4 and bus 5, leading to the islanding operation mode of the microgrid. The case study also investigated the impact of three control schemes with the comparison among case of fix-speed wind turbine with squirrel cage induction generator (SCIG), VAR-controlled wind turbine and voltage-controlled wind turbine with doubly-fed induction generator (DFIG). Furthermore, observation of the impact of different types of load model encompassing constant impedance and constant power has been .

### 5.1 Validation of System Model

#### 5.1.1 WT-SCIG without Local VAR Compensation

In this case only wind turbine with squirrel cage induction generator (WT-SCIG) source is inside the microgrid and Figure 5.1 illustrates the simulink block of the system.

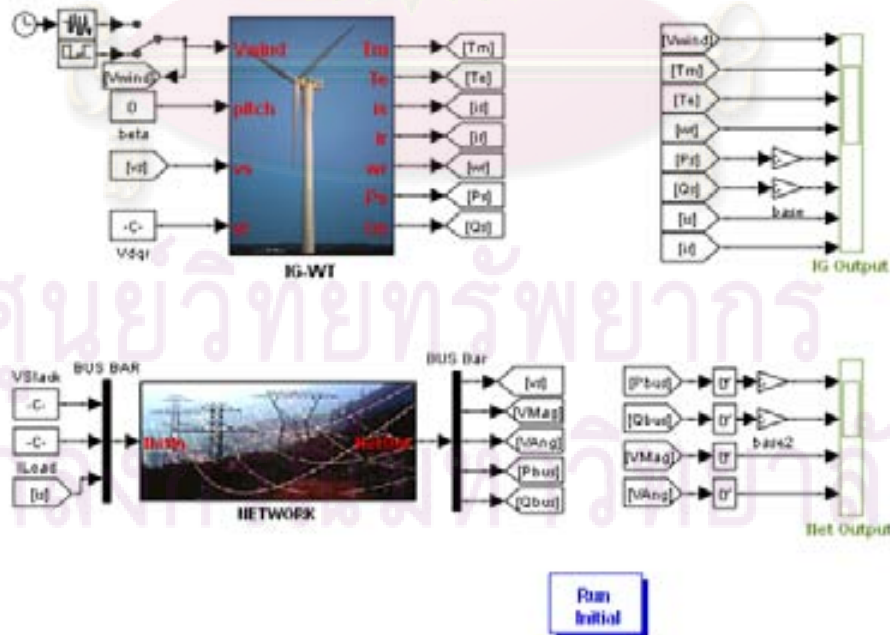


Figure 5.1 Simulink block of microgrid with WT-SCIG

From the result of load flow in the table 5.1, we see that at bus 7 which is a PV bus, it needs to generate active power 2 MW and reactive power about 2.308 MVar in order to combine with the power main grid to balance the demand and the losses in the system as seen from table 5.2. However, as this bus is connected to the wind turbine with squirrel cage induction generator that always absorbs reactive power, the system will operate with this condition unless there is a reactive source to compensate the reactive consumed by load and SCIG. In the case that there is no compensating source of reactive power, the SCIG directly absorbs the reactive power from the main grid that can lead to the decrease of voltage in the system as shown in the Figure 5.2. And from the figure we also seen that the active power of SCIG is reduced closely to zero, it is the fact that, in the case of SCIG, there is a relation between terminal voltage, rotor speed, active power generation and reactive power consumption [10].

Table 5.1 Load flow initialization without local VAr compensation

Bus No.	Voltage		Load		Generation		Injected
	Mag.	Angle (deg.)	MW	MVAr	MW	MVAr	MVAr
1	1.050	0.000	-	-	1.094	1.596	-
2	1.048	-0.014	-	-	-	-	-
3	0.994	-1.727	-	-	-	-	-
4	0.973	-1.116	-	-	-	-	-
5	0.964	-0.394	-	-	-	-	-
6	0.975	0.731	0.560	0.540	-	-	-
7	1.000	1.250	0.900	1.540	2.000	2.308	0.000
8	0.892	-3.613	1.500	1.440	0.000	0.000	-
<b>Total</b>			<b>2.960</b>	<b>3.520</b>	<b>3.094</b>	<b>3.904</b>	<b>0.000</b>

Table 5.2 Line flow and losses without local VAr compensation

Line		Power at bus and line flow			Line losses	
From bus	To bus	MW	MVAr	MVA	MW	MVAr
1		1.094	1.596	1.935		
	2	1.094	1.596	1.935	0.002	0.003
2		0.000	0.000	0.000		
	1	-1.093	-1.593	1.932	0.002	0.003
	3	1.093	1.593	1.932	0.012	0.115
3		0.000	0.000	0.000		
	2	-1.080	-1.478	1.831	0.012	0.115
	4	1.080	1.478	1.831	0.038	0.020
4		0.000	0.000	0.000		
	3	-1.042	-1.459	1.793	0.038	0.020
	5	1.042	1.459	1.793	0.028	0.000
5		0.000	0.000	0.000		
	4	-1.015	-1.459	1.777	0.028	0.000
	6	-0.517	-0.187	0.550	0.002	0.012
	8	1.532	1.646	2.248	0.032	0.206
6		-0.560	-0.540	0.778		
	5	0.519	0.199	0.556	0.002	0.012
	7	-1.079	-0.739	1.308	0.021	0.029
7		1.100	0.768	1.342		
	6	1.100	0.768	1.342	0.021	0.029



8		-1.500	-1.440	2.079		
	5	-1.500	-1.440	2.079	0.032	0.206
<b>Total losses</b>					<b>0.134</b>	<b>0.385</b>

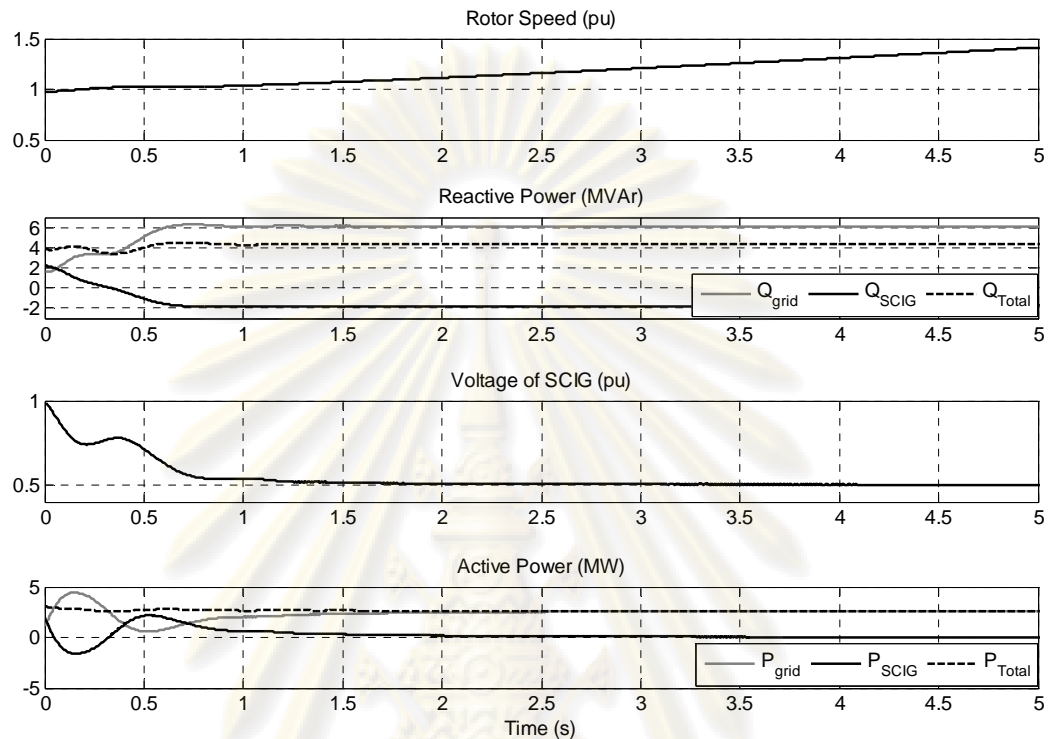


Figure 5.2 Dynamic responses of SCIG without local VAR compensation

### 5.1.2 WT-SCIG with Local VAR Compensation

Table 5.3 Load flow initialization with local VAR compensation

Bus No.	Voltage		Load		Generation		Injected
	Mag.	Angle (deg.)	MW	MVAr	MW	MVAr	MVAr
1	1.050	0.000	-	-	1.094	1.596	-
2	1.048	-0.014	-	-	-	-	-
3	0.994	-1.727	-	-	-	-	-
4	0.973	-1.116	-	-	-	-	-
5	0.964	-0.394	-	-	-	-	-
6	0.975	0.731	0.560	0.540	-	-	-
7	1.000	1.250	0.900	1.540	2.000	-1.422	3.730
8	0.892	-3.613	1.500	1.440	0.000	0.000	-
<b>Total</b>			<b>2.960</b>	<b>3.520</b>	<b>3.094</b>	<b>0.174</b>	<b>3.730</b>

Table 5.4 Line flow and losses with local VAR compensation

Line		Power at bus and line flow			Line losses	
From bus	To bus	MW	MVAr	MVA	MW	MVAr
1		1.094	1.596	1.935		
	2	1.094	1.596	1.935	0.002	0.003
2		0.000	0.000	0.000		
	1	-1.093	-1.593	1.932	0.002	0.003

	3	1.093	1.593	1.932	0.012	0.115
3		0.000	0.000	0.000		
	2	-1.080	-1.478	1.831	0.012	0.115
	4	1.080	1.478	1.831	0.038	0.020
4		0.000	0.000	0.000		
	3	-1.042	-1.459	1.793	0.038	0.020
	5	1.042	1.459	1.793	0.028	0.000
5		0.000	0.000	0.000		
	4	-1.015	-1.459	1.777	0.028	0.000
	6	-0.517	-0.187	0.550	0.002	0.012
	8	1.532	1.646	2.248	0.032	0.206
6		-0.560	-0.540	0.778		
	5	0.519	0.199	0.556	0.002	0.012
	7	-1.079	-0.739	1.308	0.021	0.029
7		1.100	0.768	1.342		
	6	1.100	0.768	1.342	0.021	0.029
8		-1.500	-1.440	2.079		
	5	-1.500	-1.440	2.079	0.032	0.206
<b>Total losses</b>					<b>0.134</b>	<b>0.385</b>

We know that, at the operating point obtained from the load flow, the SCIG absorbed about 1.422 MVar. So we need the source that can generate the reactive  $2.308 + 1.422 = 3.73$  MVar by using compensating capacitor in order to avoid the direct absorbing reactive power from the grid that can lead to voltage instability as the previous case. the values of power supplied, consumed and lost of the system are provided in table 5.3 and table 5.4, respectively . This case study investigates dynamic responses of the WT-SCIG due to the step change of wind speed.

From the Figure 5.4, we see that the WT-SCIG operate at rated value with the wind speed around 8 m/s. At time 5 sec, the wind speed steps down to zero this means that there is no mechanical torque apply to the turbine and there is no induced current in the rotor circuit, so the rotor free rotates with the synchronous speed  $\omega_r = 1 pu$ .

And from the Figure 5.3 that shows the mechanical torque of the modeled wind turbine, it shows that in some range of turbine's rotor speed and wind speed it can give the negative torque. As we know that in the case of SCIG with the negative torque, it will operate as motor mode so that in this case by applying step change of wind speed, as seen in the Figure 5.4, to 2 m/s at time 10 sec. The mechanical torque also steps down from positive to negative and the SCIG operates as a motor by absorbing active power form the grid as we can see from the figure that there is also changing sign from positive to negative of active power and it leads to the more increase of active power from the grid. And the SCIG also operates at speed less than the synchronous speed (or positive slip) as a motor.

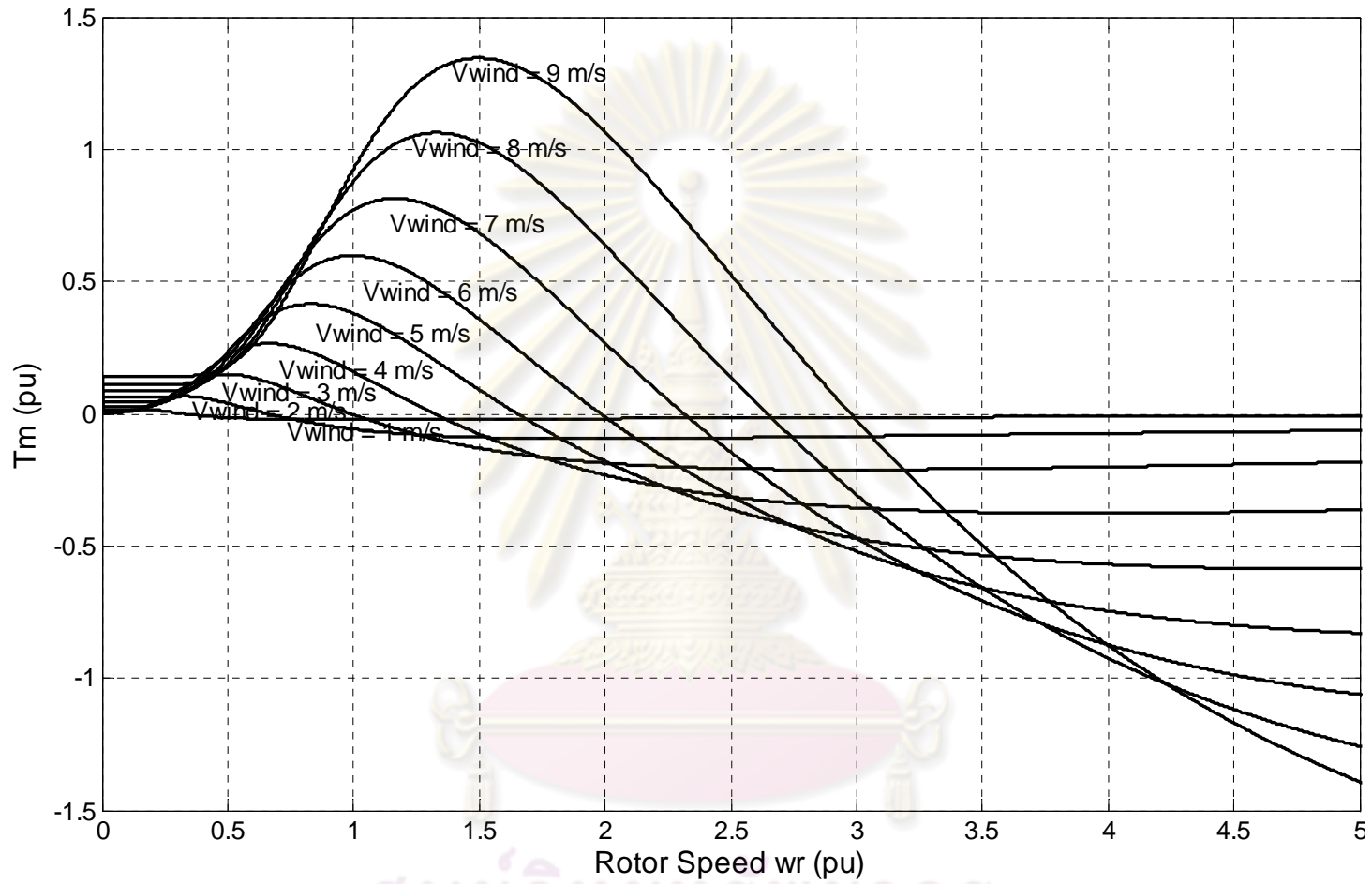


Figure 5.3 Mechanical torque of wind turbine

ศูนย์วิจัยทรัพยากร  
จุฬาลงกรณ์มหาวิทยาลัย

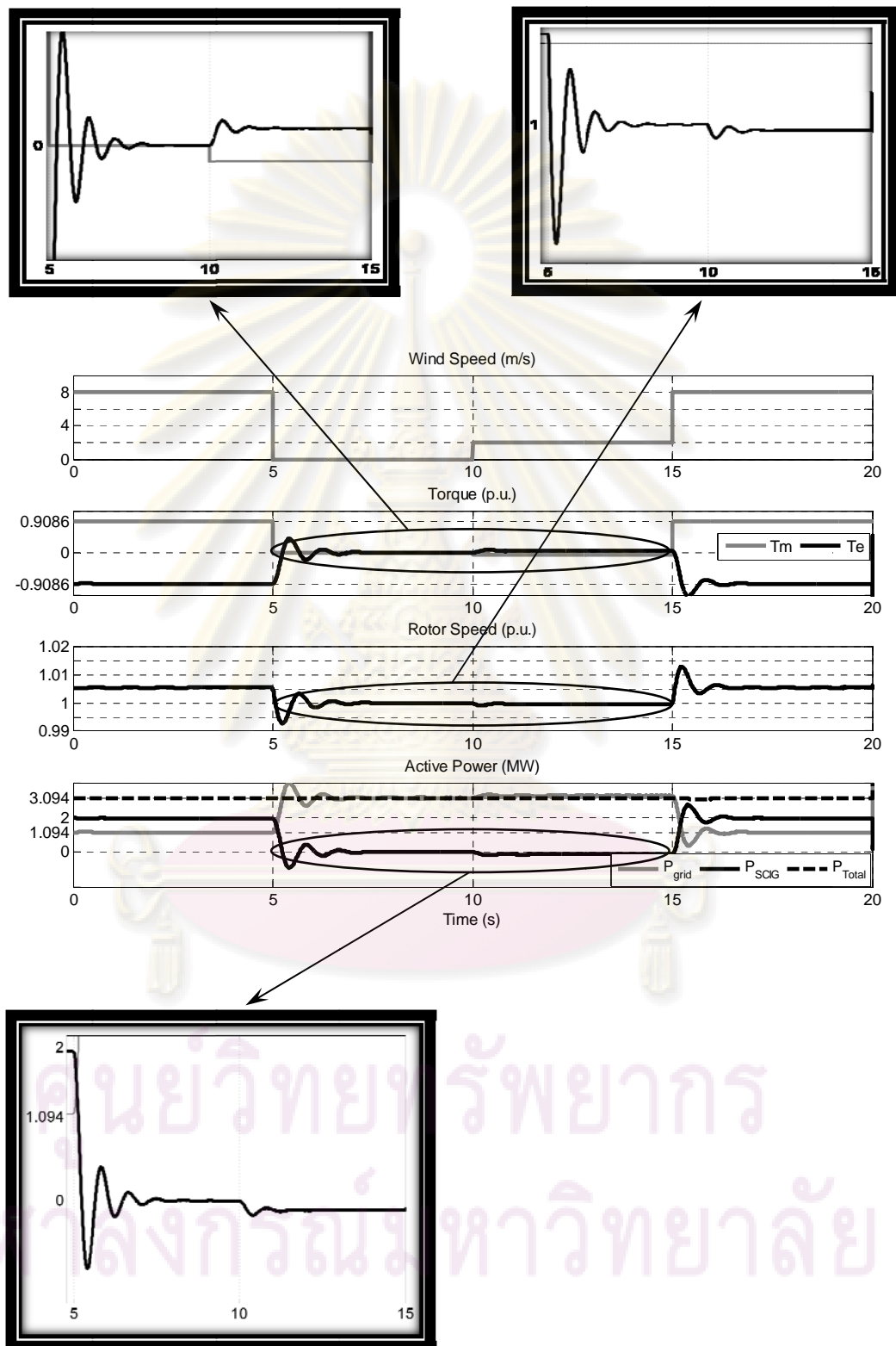


Figure 5.4 Dynamic responses of SCIG with var compensate

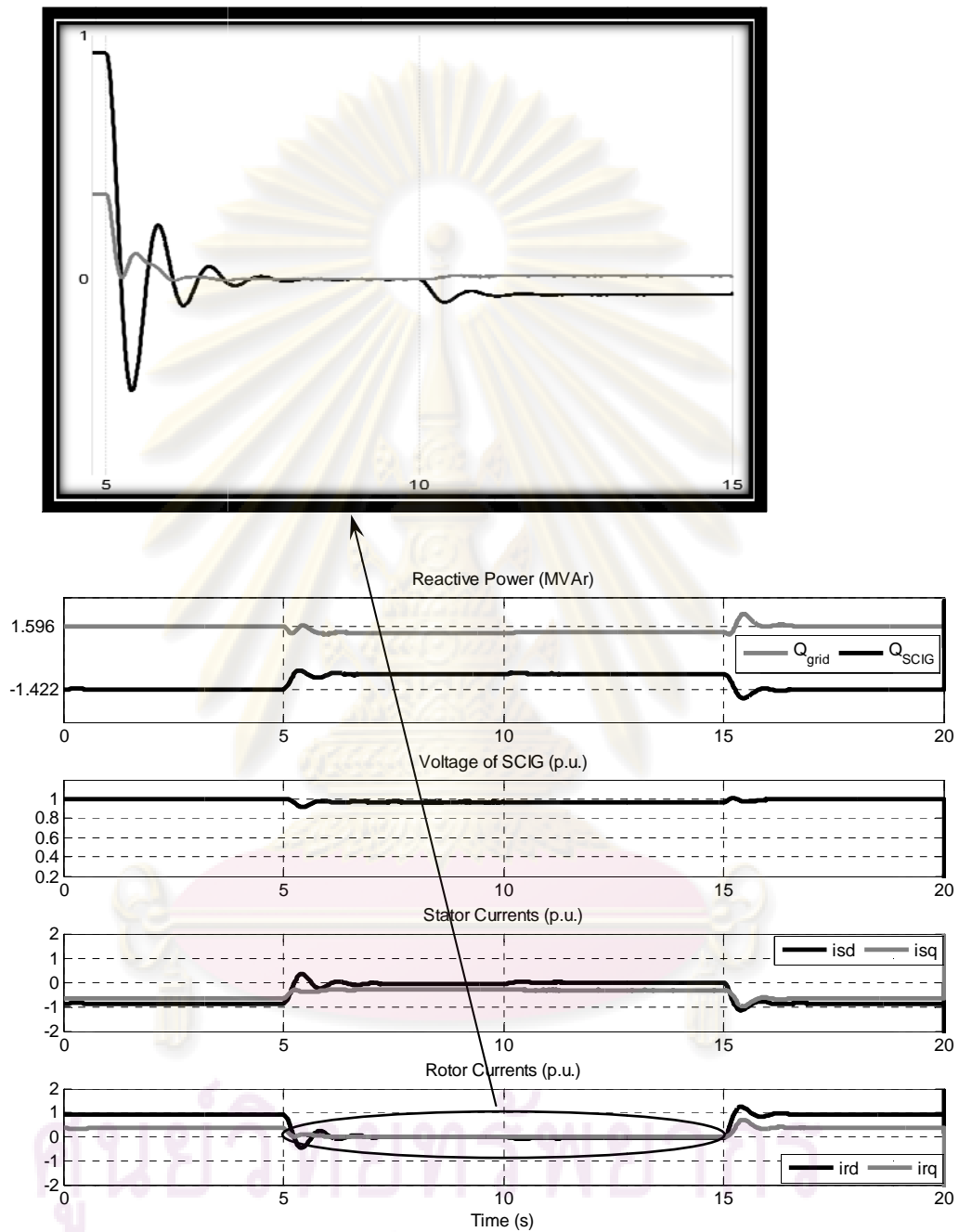


Figure 5.4 Dynamic responses of SCIG with var compensation (cont.)

## 5.2 Dynamic Responses under Local Capacitor Switching

In this case study, there exists WT-SCIG combined with the synchronous generator (SG) inside the microgrid and all loads are modeled as constant impedance. Figure 5.5 illustrated the simulink block of the system when SG is included.

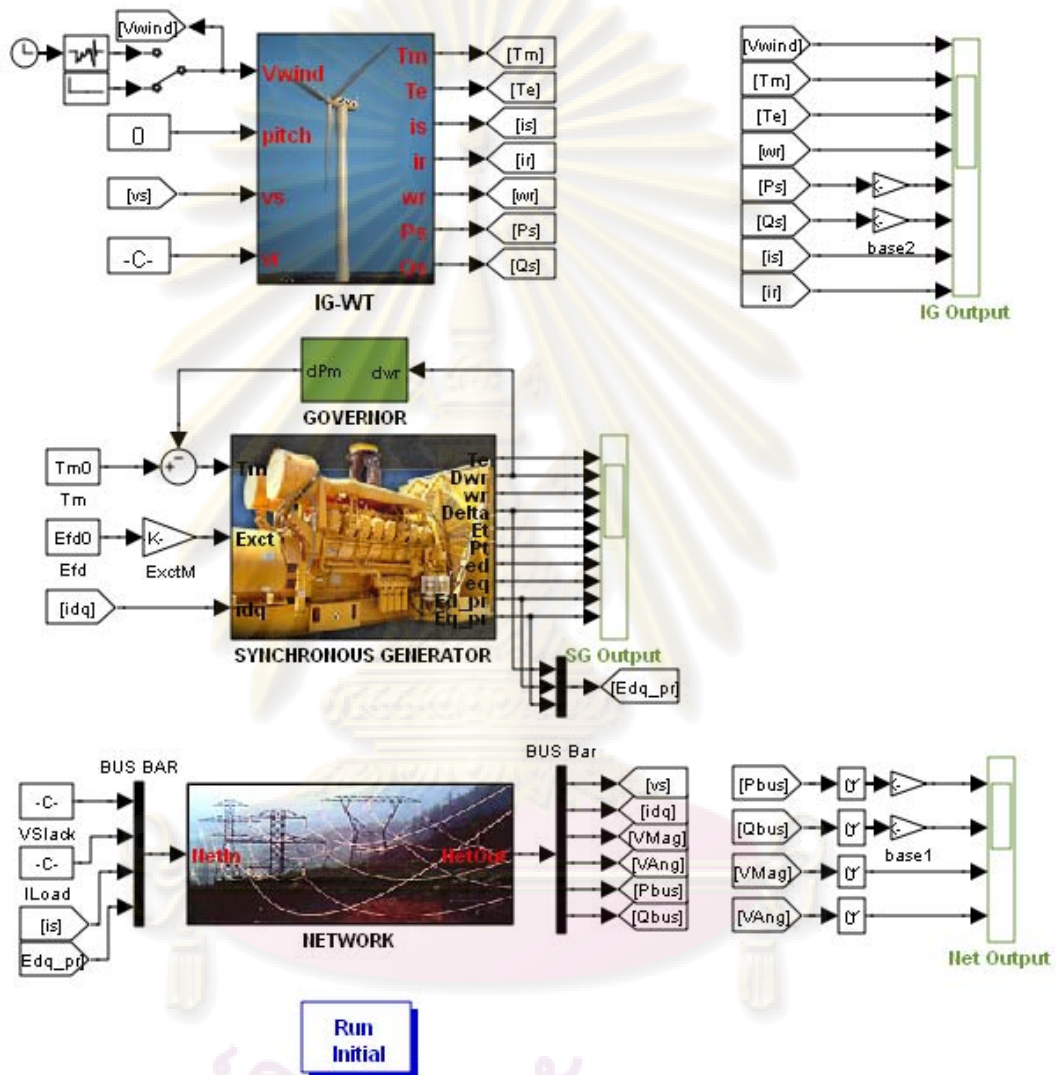


Figure 5.5 Simulink block of microgrid with WT-SCIG and SG

Again, from the result of load flow in the table 5.5, we see that at bus 7 which is a PV bus it needs to generate active power 2 MW and reactive power about 1.426 MVar in order to combine with the power main grid to balance the demand and the losses in the system as seen from table 5.6. So in order to operate the system at this condition, we need the compensation of reactive power about  $1.422 + 1.426 = 2.848$  MVar. And table 5.7 shows the load flow when we include var compensator to the system.

Table 5.5 Load flow initialization without local VAr compensation

Bus No.	Voltage		Load		Generation		Injected
	Mag.	Angle (deg.)	MW	MVAr	MW	MVAr	MVAr
1	1.050	0.000	-	-	0.001	0.988	-
2	1.049	0.023	-	-	-	-	-
3	1.017	0.212	-	-	-	-	-
4	1.012	0.813	-	-	-	-	-
5	1.012	1.244	-	-	-	-	-
6	0.989	2.607	0.560	0.540	-	-	-
7	1.000	3.717	0.900	1.540	2.000	1.426	0.000
8	1.000	0.253	1.500	1.440	1.000	1.201	-
<b>Total</b>			<b>2.960</b>	<b>3.520</b>	<b>3.001</b>	<b>3.616</b>	<b>0.000</b>

Table 5.6 Line flow and losses without local VAr compensation

Line		Power at bus and line flow			Line losses	
From bus	To bus	MW	MVAr	MVA	MW	MVAr
1		0.001	0.988	0.988		
	2	0.001	0.988	0.988	0.000	0.001
2		0.000	0.000	0.000		
	1	-0.001	-0.988	0.988	0.000	0.001
	3	0.001	0.988	0.988	0.003	0.030
3		0.000	0.000	0.000		
	2	0.002	-0.958	0.958	0.003	0.030
	4	-0.002	0.958	0.958	0.010	0.005
4		0.000	0.000	0.000		
	3	0.012	-0.952	0.952	0.010	0.005
	5	-0.012	0.952	0.952	0.007	0.000
5		0.000	0.000	0.000		
	4	0.020	-0.952	0.952	0.007	0.000
	6	-0.521	0.702	0.875	0.004	0.028
	8	0.502	0.250	0.561	0.002	0.012
6		-0.560	-0.540	0.778		
	5	0.526	-0.674	0.855	0.004	0.028
	7	-1.086	0.134	1.094	0.014	0.020
7		1.100	-0.114	1.106		
	6	1.100	-0.114	1.106	0.014	0.020
8		-0.500	-0.239	0.554		
	5	-0.500	-0.239	0.554	0.002	0.012
<b>Total losses</b>					<b>0.041</b>	<b>0.096</b>

Table 5.7 Load flow initialization with local VAr compensation

Bus No.	Voltage		Load		Generation		Injected
	Mag.	Angle (deg.)	MW	MVAr	MW	MVAr	MVAr
1	1.050	0.000	-	-	0.001	0.988	-
2	1.049	0.023	-	-	-	-	-
3	1.017	0.212	-	-	-	-	-
4	1.012	0.813	-	-	-	-	-
5	1.012	1.244	-	-	-	-	-
6	0.989	2.607	0.560	0.540	-	-	-
7	1.000	3.717	0.900	1.540	2.000	-1.422	2.848
8	1.000	0.253	1.500	1.440	1.000	1.201	0.000
<b>Total</b>			<b>2.960</b>	<b>3.520</b>	<b>3.001</b>	<b>0.768</b>	<b>2.848</b>

Table 5.8 Line flow and losses with local VAr compensation

Line		Power at bus and line flow			Line losses	
From bus	To bus	MW	MVAr	MVA	MW	MVAr
1		0.001	0.988	0.988		
	2	0.001	0.988	0.988	0.000	0.001
2		0.000	0.000	0.000		
	1	-0.001	-0.988	0.988	0.000	0.001
	3	0.001	0.988	0.988	0.003	0.030
3		0.000	0.000	0.000		
	2	0.002	-0.958	0.958	0.003	0.030
	4	-0.002	0.958	0.958	0.010	0.005
4		0.000	0.000	0.000		
	3	0.012	-0.952	0.952	0.010	0.005
	5	-0.012	0.952	0.952	0.007	0.000
5		0.000	0.000	0.000		
	4	0.020	-0.952	0.952	0.007	0.000
	6	-0.521	0.702	0.875	0.004	0.028
	8	0.502	0.250	0.561	0.002	0.012
6		-0.560	-0.540	0.778		
	5	0.526	-0.674	0.855	0.004	0.028
	7	-1.086	0.134	1.094	0.014	0.020
7		1.100	-0.114	1.106		
	6	1.100	-0.114	1.106	0.014	0.020
8		-0.500	-0.239	0.554		
	5	-0.500	-0.239	0.554	0.002	0.012
<b>Total losses</b>					<b>0.041</b>	<b>0.096</b>

The investigation on the impact of local compensator is performed. The microgrid is first operated at normal operation and at time  $t = 5$  sec, there is a switching off local capacitor. The Figure 5.6 shows the responses of the microgrid during absence of compensation, the *gray curves* represent the responses in the case there is a switching off a local capacitor at time  $t = 5$  sec and it is reconnected to the system after 1 sec and the *black curves* represent the responses in the case there is a switching of local capacitor and it is not reconnected to the system.



The result indicates that during the switching off local capacitor, there is a large amount of reactive power absorbed from the main grid. This leads to the large drop of voltages. Unless there is reactive compensator, the rotor of the SCIG continues to increase so that more and more reactive power is absorbed by SCIG and brings to the voltage instability (black curve). The voltage is restored to the normal operation after reconnection of local compensator (gray curve). However, the frequency of the microgrid is subjected to long time oscillation even the reconnection of local compensator before it reaches the steady state.

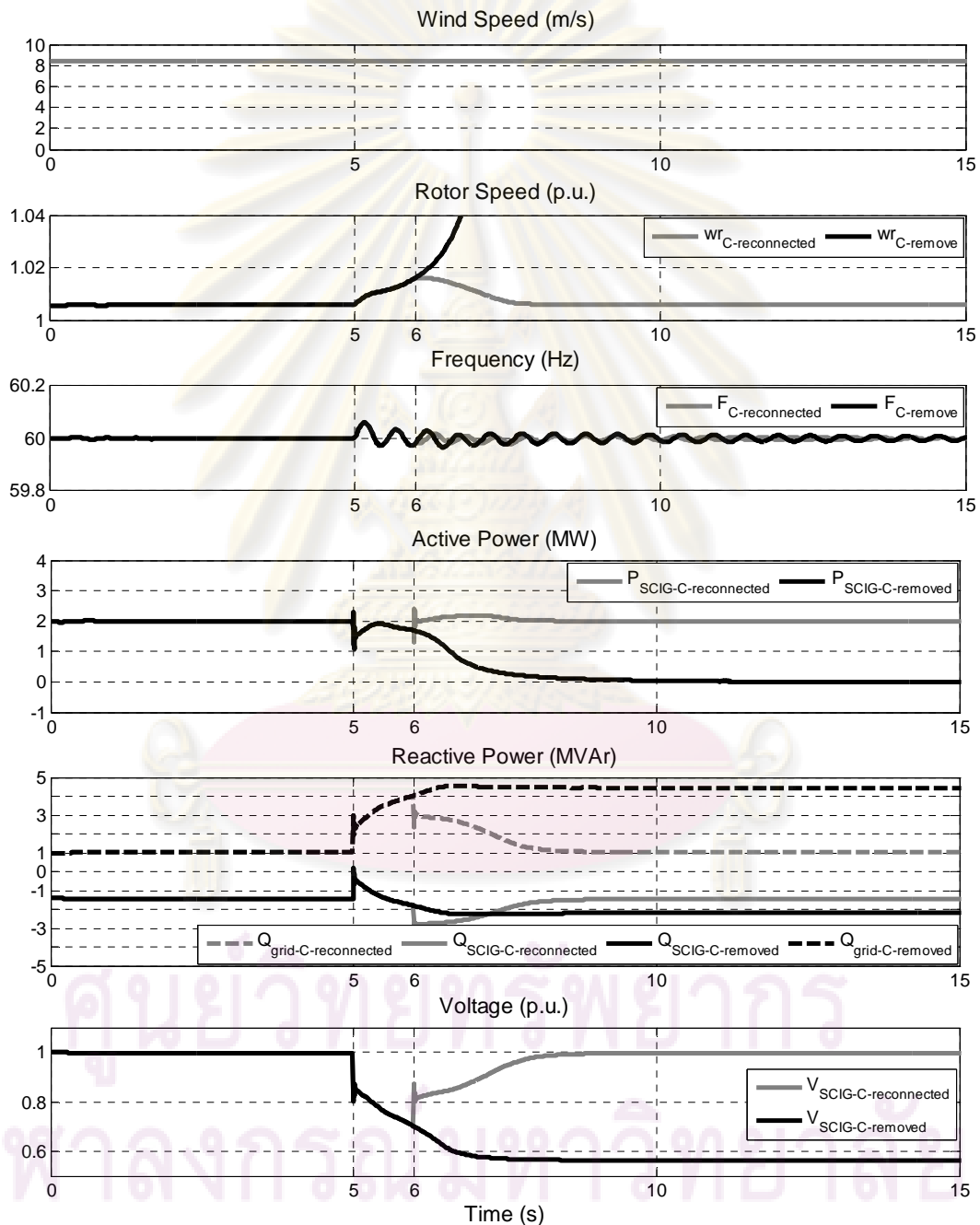


Figure 5.6 Impact of local compensator on stability of MG

### 5.3 Dynamic Responses Under Small Disturbance

In this section the dynamic responses of the microgrid during the small disturbance caused by the wind fluctuation are conducted with comparison of these dynamic responses among the three different control modes of the wind power: fix-speed wind turbine with the wind turbine driving the SCIG, and the other two control modes including VAR and voltage control of a variable-speed wind turbine with wind turbine driving the DFIG. In this case, the system is also included the dynamic load model with constant power at bus 6. The Figure 5.7 illustrates the simulink block of the microgrid with the presence of DFIG and the constant power load model.

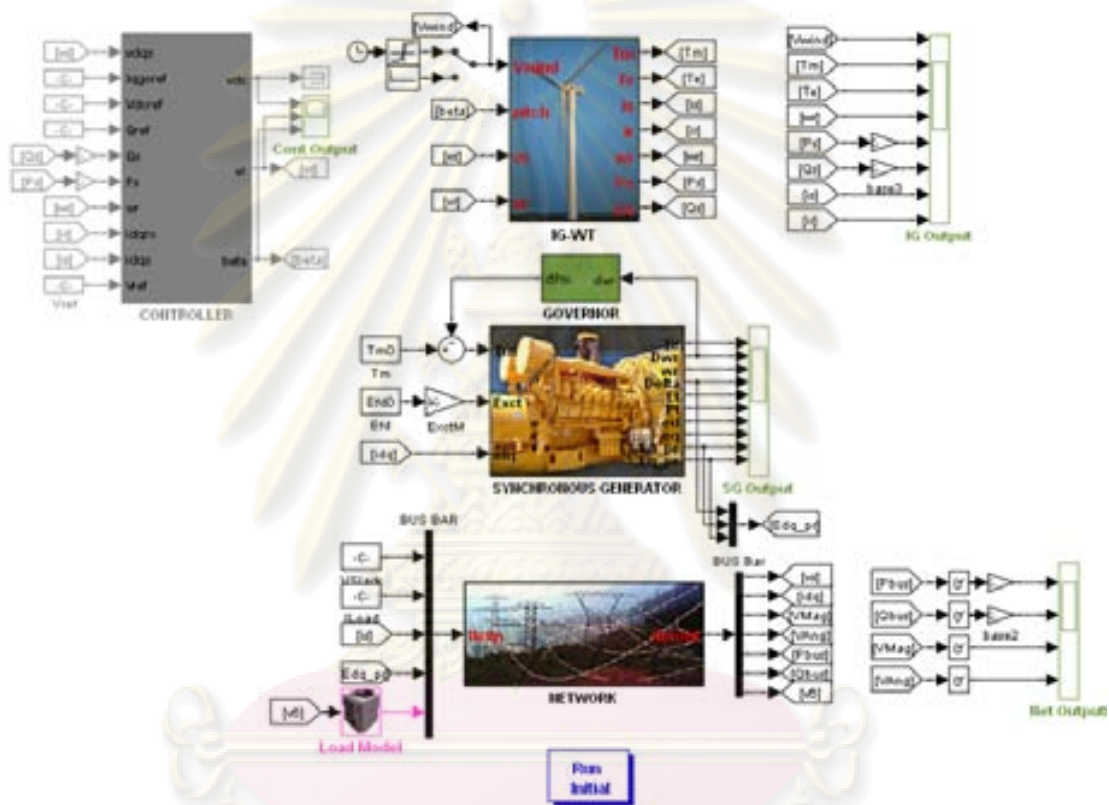


Figure 5.7 Simulink block of MG with DFIG and a constant power load model

Figure 5.8 shows the simulated results of wind speed with respect to time, the corresponding generated power from wind turbine, the terminal voltage at bus 7, and the frequency of the microgrid, for three different control modes, respectively. The stabilizing power generated of sources corresponding to power fluctuations from wind can be examined in the Figure 5.9.

It can be seen from the results the effectiveness of variable-speed control of WT-DFIG which results in significantly reduced output power fluctuations, and the corresponding small frequency variation comparing to the fix-speed wind turbine driving the SCIG.

The fact that fix-speed wind turbine contributes to more power oscillation than that in the case of variable-speed wind turbine is that: with fix-speed wind turbine, the wind turbine is designed to achieve maximum efficiency of mechanical power at only

one particular wind speed, mostly at average wind speed at the windy site, and the wind turbine rotor speed is fixed and determined by the frequency of supply grid, gear ratio and generator design, so that all the fluctuations in wind speed are transmitted as fluctuations in mechanical torque and then as fluctuations in the electrical grid. However, with the variable-speed wind turbine, it has become possible to adapt accelerating or decelerating rotational speed of wind turbine to the change of wind speed. This way, the tip speed ratio is kept constant at a predefined value corresponding to the maximum power coefficient that leads to faire constant in generator torque and the same constant in power generation.

Additionally, the results confirm performances of the VAR and the voltage control, and as verified by Figure 5.9, the independence between active and reactive power controls, respectively. As it is seen that the active power outputs is the same in case of VAR or voltage control.

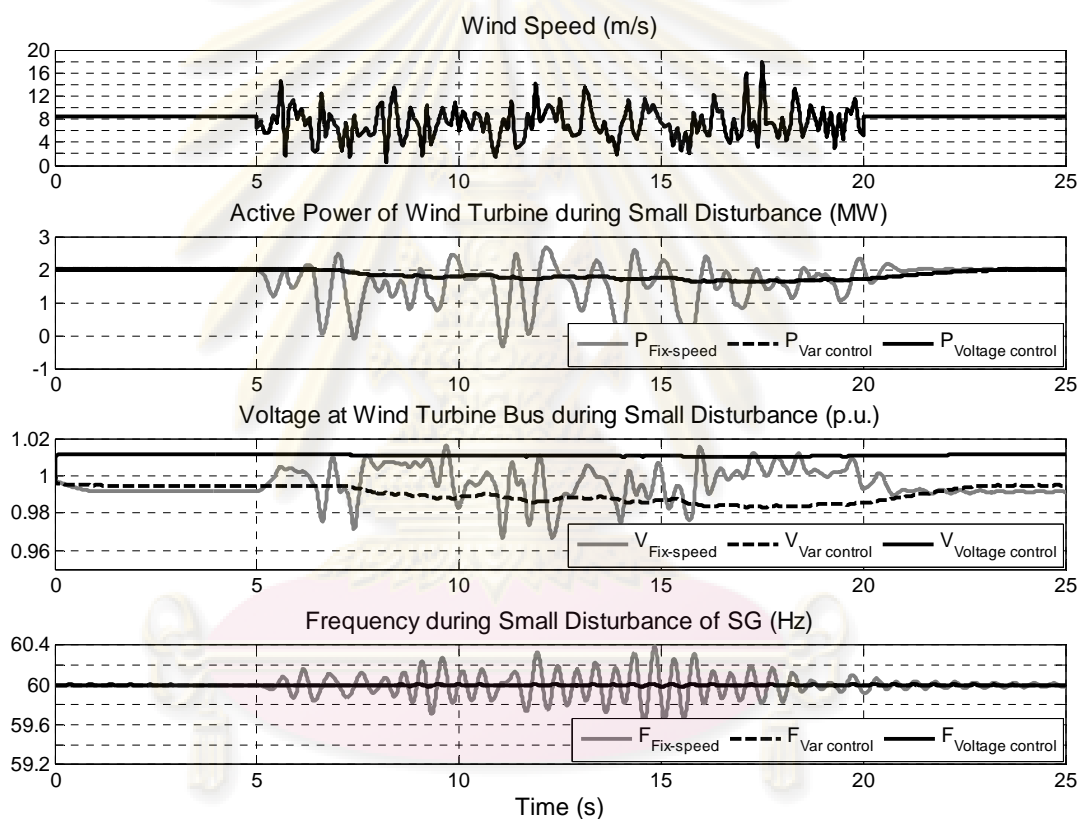


Figure 5.8 Dynamic performances under small disturbance

ศูนย์วิทยทรัพยากร  
จุฬาลงกรณ์มหาวิทยาลัย

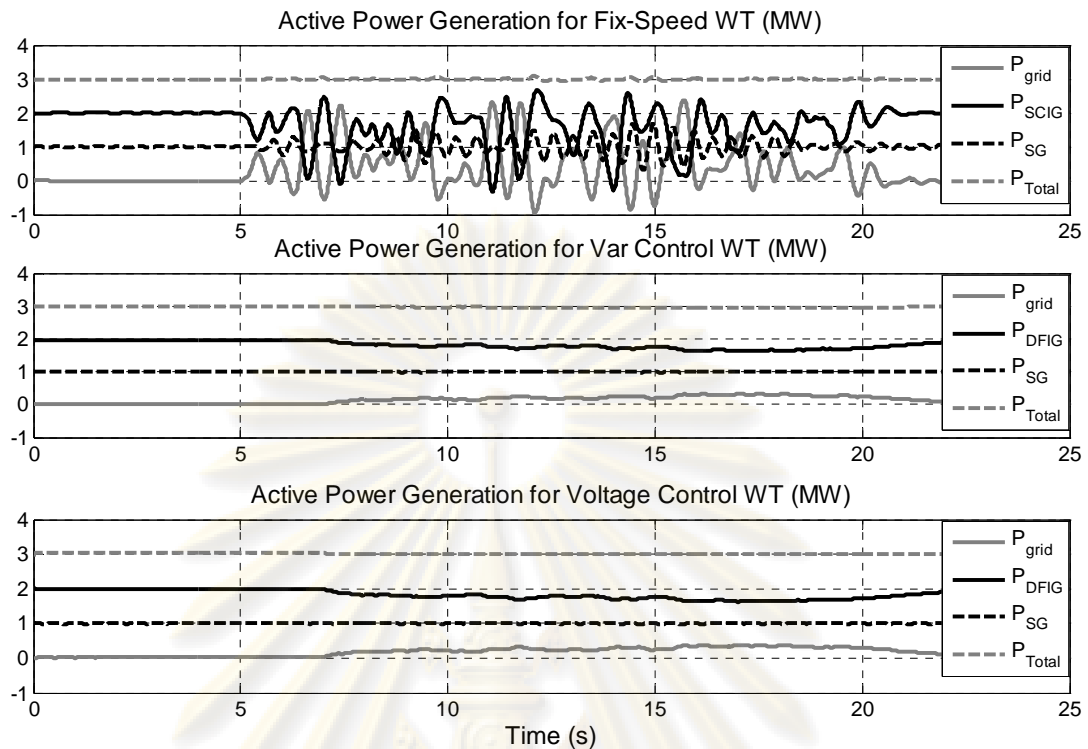


Figure 5.9 Active power fluctuations

#### 5.4 Dynamic Responses Under Temporary Fault

In this case, short-circuit fault is applied at bus 4 at time  $t=10$  sec, and temporarily sustains for 150 msec. After clearing fault, the MG is reconnected to the main grid. The respective test results are shown in Figure 5.10. It is noted that during the fault, there are a large drops of voltages as well as the powers generated from the wind turbine and synchronous generator. However, the MG can operate stably after fault is cleared, mainly due to interaction between governor action of the SG and stabilizing tie-flow from the main grid. It is seen that there is swing of the frequency in all the three control modes. This maybe comes from a small size of synchronous generator's inertia and constant power load model resulting in weak damping of the system during the disturbance. And it is also seen that in the case of the voltage control wind turbine, the system subjected to the weakest damping leading to the highest oscillation as seen in the figure. And the voltage drops recover quite fast in all the three cases.

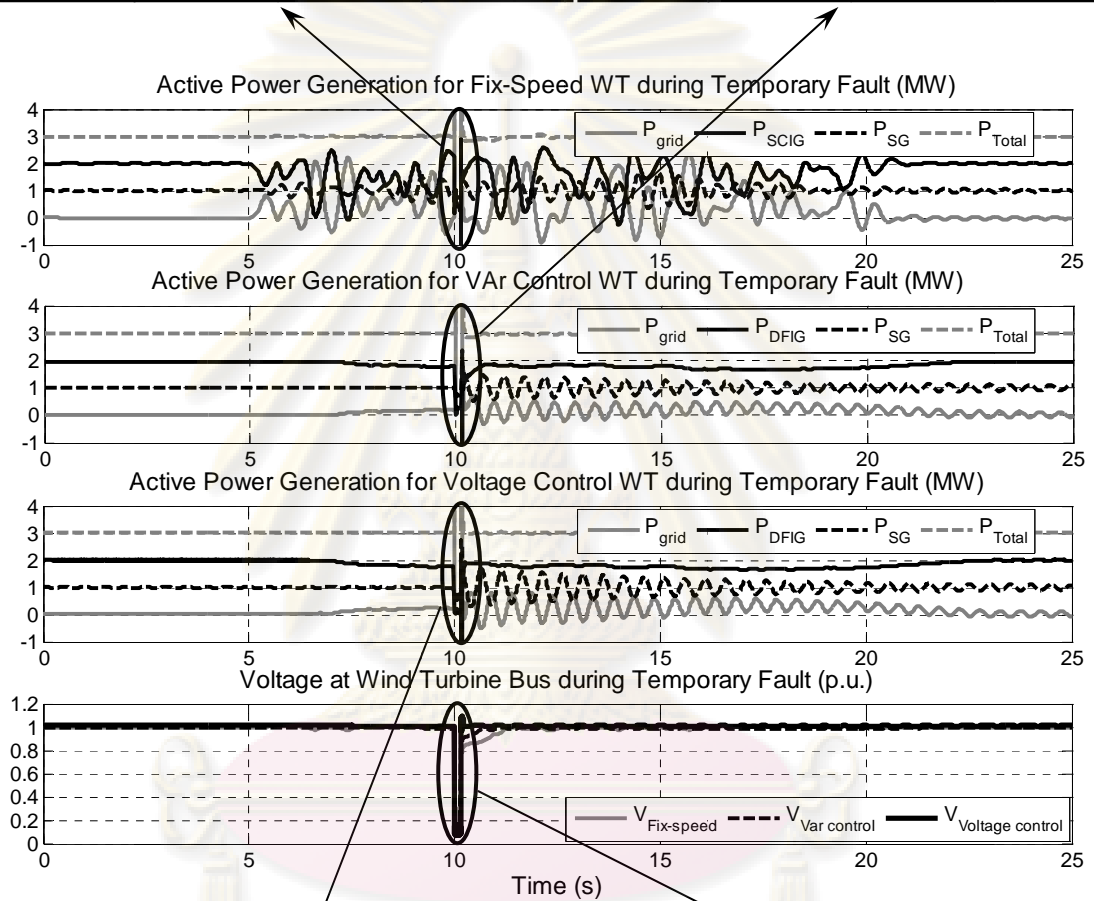
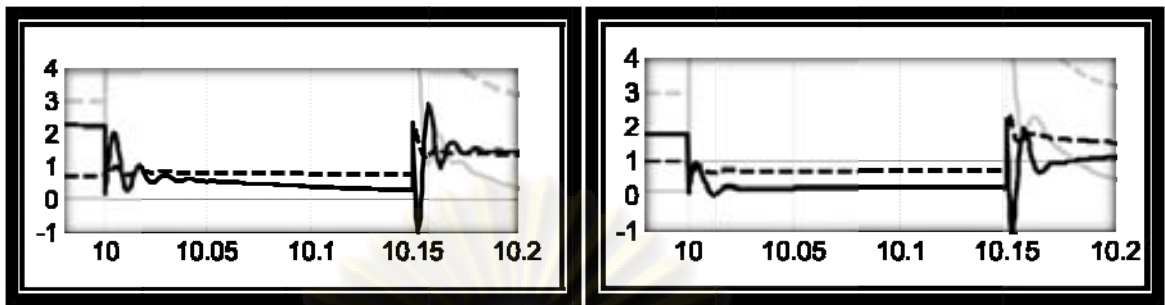
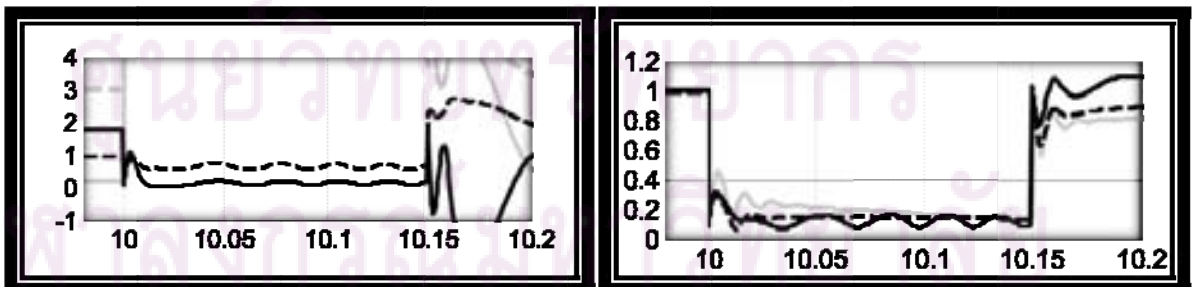


Figure 5.10 Dynamic performances under temporary fault



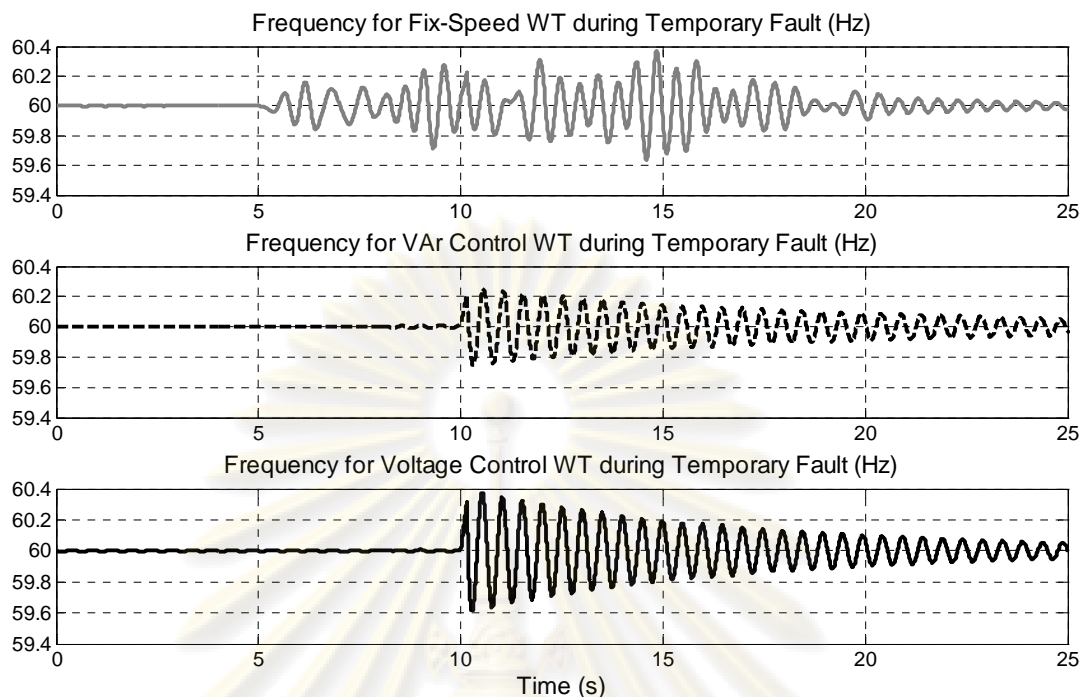


Figure 5.10 Dynamic performances under temporary fault

### 5.5 Dynamic Responses Under Permanent Fault

For this case, the fault has been cleared after 150 msec by opening the line between bus 4 and 5. The MG is then driven into the islanding mode of operation. Test results shown in Figure 5.11 show the active powers of the generation sources, voltage at wind turbine bus and the frequency of the synchronous generator with the three different control modes respectively in the different subplots. It reveals that after fault is cleared, there is no supply from the main grid so that the islanding operation of the microgrid has only sources from the wind turbine and the synchronous generator.

It is seen that during occurring of fault changing topologies of the system, the electrical power generation from the wind turbine and synchronous generator is reduced resulting in increase of frequency due to unbalance of electrical and mechanical torque and there is large drop of voltage with all three control modes (fix-speed, VAr and voltage control wind turbine).

In the case of fix-speed wind turbine when the fault is cleared, the wind turbine still sustains to operate for period of time and there is a balance from the synchronous generator. However, the frequency of synchronous generator still continues to increase until at time around 17 sec when the power from the wind turbine become zero due to the large drop of voltage. As the result, the whole microgrid depends only on the supply from the synchronous generator that tries to generate more power supply to load leading to large drop in frequency.

Likely, in the case of VAr control wind turbine with the PF = 0.8 lagging, the wind turbine cannot operate immediately after clearing fault due to sudden drop of voltage. Hence, again, the whole microgrid depends only on the supply from the synchronous generator that tries to generate more power supply to load leading to large drop in frequency.

In contrast, the wind turbine in the case of voltage control mode can operate stably because capability of voltage control wind turbine can restore the voltage to

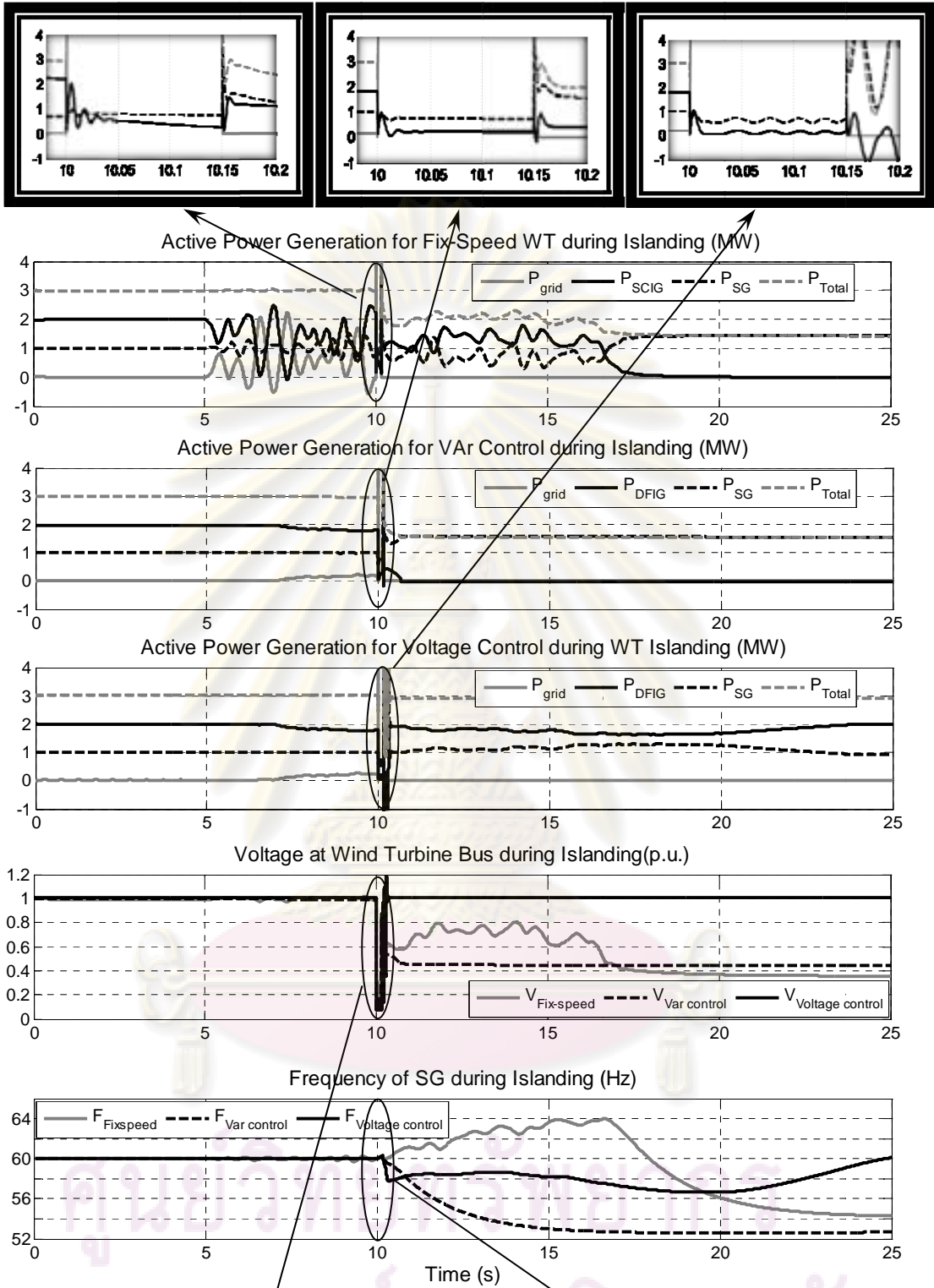
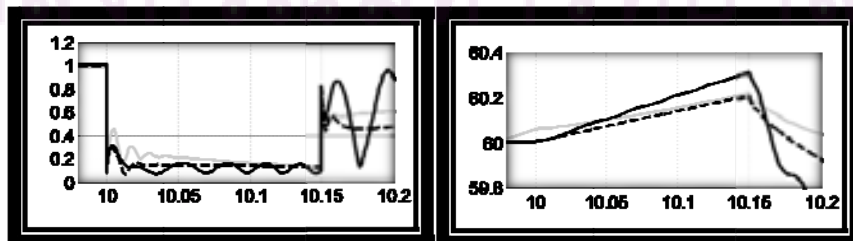


Figure 5.11 Dynamic performances under permanent fault



normal operation after the clearing fault. However, the microgrid still subjected to the variation of frequency resulting from the variation of power generation from the wind turbine.

### 5.6 Impact of Load Model

The case study here compares between the microgrid frequency of the existing system that includes only a constant power load model to that of the MG system that includes all the loads as constant power load model. The comparison is done only in the case of variable-speed wind turbine with voltage control during the both temporary and permanent fault. Figure 5.12 shows the simulink block diagram of the MG when all loads are constant power.

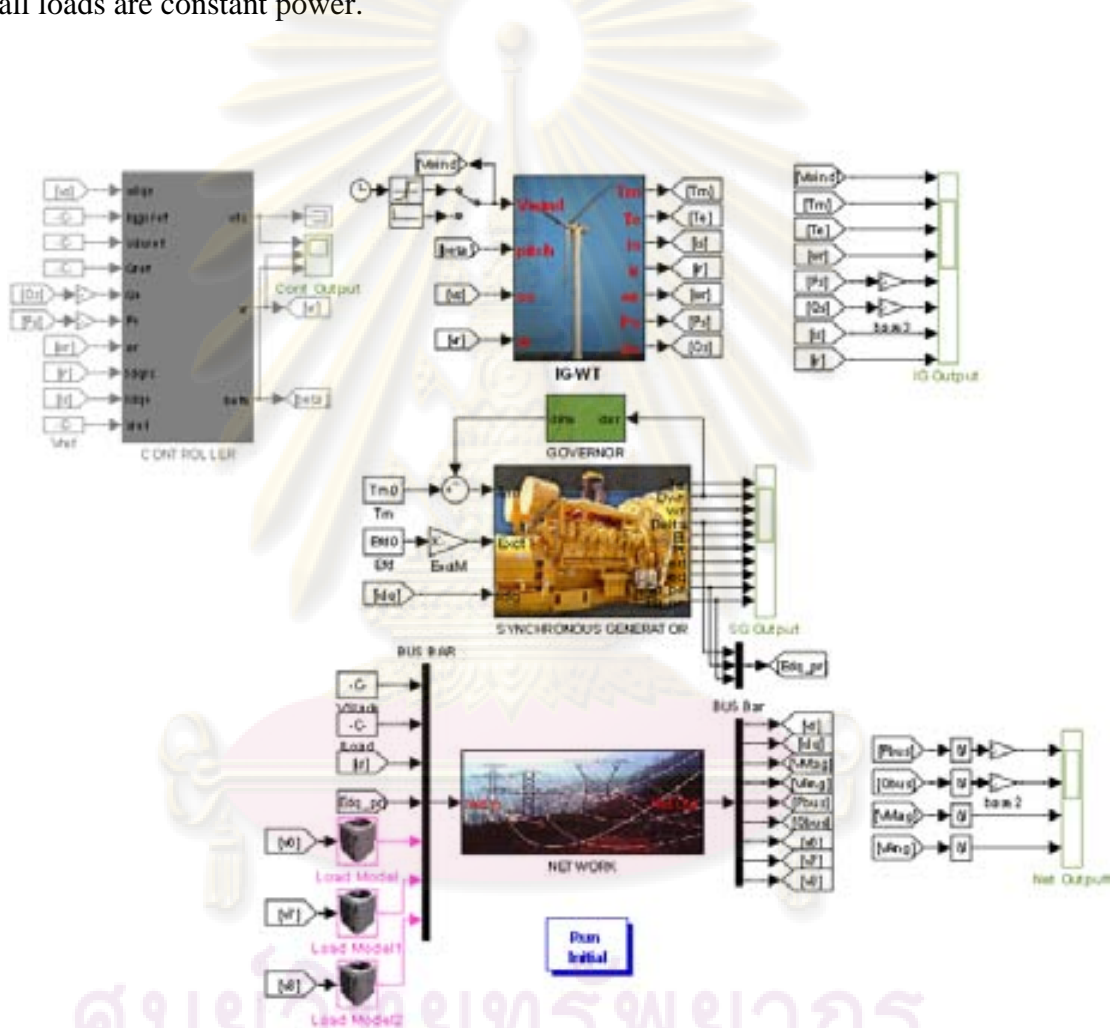


Figure 5.12 Simulink block of MG with all constant power loads

From the results of Figure 5.13, the frequency of the microgrid with all of loads being constant power is subjected to higher oscillation during temporary fault and becomes unstable under the permanent fault (islanding). The reason is that in the case of constant impedance load model, power is proportional to the  $V^2$ , whereas in the case of constant power load, the power is proportional to  $V^0$ . Hence, constant impedance loads can provide the damping to the system during the disturbance.



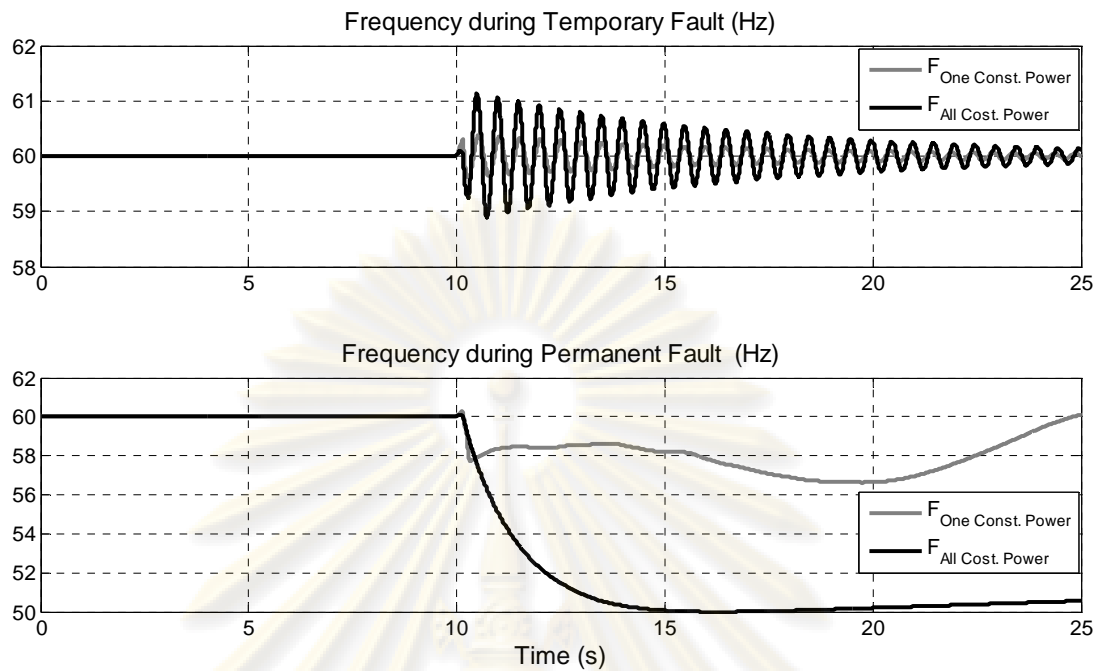


Figure 5.13 Frequency of the MG

### 5.7 Small Signal Analysis

Following the above time domain simulation, the small signal analysis of the linearized system has been conducted in order to examine the small signal stability of the microgrid in this case study. One of the various cases is selected to study its linearized model, it is the case that microgrid is encompassed with variable-speed wind turbine with VAR control and one constant power load model.

The order of all states of the modeled system is obtained from matlab using  $[sizes, x0, xstr] = sys([], [], [], 0)$ . The states are

```
xstr =
'simsys/CONTROLLER/DC BUS MODEL/Vdc'
'simsys/IG-WT/IG/Stator/fdqs'
'simsys/IG-WT/IG/Stator/fdqs'
'simsys/IG-WT/IG/Rotor/fdqr'
'simsys/IG-WT/IG/Rotor/fdqr'
'simsys/SYNCHRONOUS GENERATOR/Mechanical/delta'
'simsys/SYNCHRONOUS GENERATOR/State/Edq_pr'
'simsys/SYNCHRONOUS GENERATOR/State/Edq_pr'
'simsys/Load Model/P-const/G'
'simsys/IG-WT/IG/Electro-Mechanical/rotor speed wr'
'simsys/CONTROLLER/ROTOR-SIDE CONTROLLER/Power Regulator/PI/Iqrc*'
'simsys/CONTROLLER/ROTOR-SIDE CONTROLLER/Current Regulator/PI/vdq*'
'simsys/CONTROLLER/ROTOR-SIDE CONTROLLER/Current Regulator/PI/vdq*'
'simsys/SYNCHRONOUS GENERATOR/Mechanical/dwr'
'simsys/CONTROLLER/R-L BRANCH/IdqL'
'simsys/CONTROLLER/R-L BRANCH/IdqL'
'simsys/CONTROLLER/GRID-SIDE CONTROLLER/Vdc Regulator/PI/Idgc*'
'simsys/CONTROLLER/GRID-SIDE CONTROLLER/Current Regulator/PI/vdq*'
'simsys/CONTROLLER/GRID-SIDE CONTROLLER/Current Regulator/PI/vdq*'
'simsys/GOVERNOR/DROOP'
'simsys/CONTROLLER/ROTOR-SIDE CONTROLLER/Q Regulator/PI/Idrc*'
```

Table 5.9 Eigen values of the linearized model of the MG

N <sup>0</sup>	Eigen Value	Freq (rad/s)	Damping ratio	State
1	0.0000 + 0.0000i	0	1	I <sub>qrc</sub> *
2	-261.0434 + 511.0169i	511.0170	0.4549	$\lambda_{ds}, \lambda_{qs}$
3	-261.0434 - 511.0169i	-511.0170	0.4549	$\lambda_{ds}, \lambda_{qs}$
4	-2.6633e-05 + 377.0153i	377.0153	0.0000	I <sub>dL</sub> , I <sub>qL</sub>
5	-2.6633e-05 - 377.0153i	-377.0153	0.0000	I <sub>dL</sub> , I <sub>qL</sub>
6	-208.9609 + 31.9565i	31.9565	0.9885	$\lambda_{dr}, \lambda_{qr}$
7	-208.9609 - 31.9565i	-31.9565	0.9885	$\lambda_{dr}, \lambda_{qr}$
8	-63.5832 + 0.0000i	0	1	Conductance G
9	-32.4635 + 0.0000i	0	1	v <sub>drc</sub> *
10	-30.1350 + 0.0000i	0	1	v <sub>qrc</sub> *
11	-0.1133 + 12.7510i	12.7510	0.0089	$\delta, \Delta\omega_r$
12	-0.1133 - 12.7510i	-12.7510	0.0089	$\delta, \Delta\omega_r$
13	-9.8079 + 0.0000i	0	1	Governor
14	-3.4836 + 0.0000i	0	1	I <sub>drc</sub> *
15	-0.0049 + 0.8154i	0.8154	0.0061	V <sub>dc</sub> , I <sub>dgc</sub> *, v <sub>dgc</sub> *
16	-0.0049 - 0.8154i	-0.8154	0.0061	V <sub>dc</sub> , I <sub>dgc</sub> *, v <sub>dgc</sub> *
17	-0.5341 + 0.0000i	0	1	WT speed $\omega_r$
18	-0.0099 + 0.0000i	0	1	I <sub>qL</sub>
19	-0.0011 + 0.0000i	0	1	Eq'
20	-0.0048 + 0.0000i	0	1	Ed'
21	0.0000 + 0.0000i	0	1	v <sub>qgc</sub> *

Table 5.10 Participation factors

PARTICIPATION	EIGENVALUE												
	STATE	N <sup>0</sup>	1	2	3	4	5	6	7	8	9	10	11
V <sub>dc</sub>	1	1	0.0000	0.0000	0.0000	0.0001	0.0001	0.0000	0.0000	0.0000	0.0000	0.0000	0.0000
$\lambda_{ds}$	2	2	0.0000	0.6133	0.6133	0.0000	0.0000	0.4937	0.4937	0.0057	0.0055	0.0012	0.0000
$\lambda_{qs}$	3	3	0.0000	0.5812	0.5812	0.0000	0.0000	0.0726	0.0726	0.0017	0.0047	0.0017	0.0000
$\lambda_{dr}$	4	4	0.0000	0.1591	0.1591	0.0000	0.0000	0.7758	0.7758	0.0008	0.0235	0.1357	0.0002
$\lambda_{qr}$	5	5	0.0000	0.1829	0.1829	0.0000	0.0000	1.1912	1.1912	0.0023	0.2503	0.0115	0.0000
$\delta$	6	6	0.0000	0.0000	0.0000	0.0000	0.0000	0.0002	0.0002	0.0002	0.0000	0.0004	0.4939
E <sub>d-pr</sub>	7	7	0.0000	0.0000	0.0000	0.0000	0.0000	0.0000	0.0000	0.0000	0.0000	0.0000	0.0001
E <sub>q-pr</sub>	8	8	0.0000	0.0000	0.0000	0.0000	0.0000	0.0000	0.0000	0.0000	0.0000	0.0000	0.0000
Conductance G	9	9	0.0000	0.0023	0.0023	0.0000	0.0000	0.0101	0.0101	0.9920	0.0024	0.0022	0.0003
WT speed $\omega_r$	10	10	0.0000	0.0000	0.0000	0.0000	0.0000	0.0000	0.0000	0.0000	0.0000	0.0000	0.0000
I <sub>qrc</sub> *	11	11	1.0000	0.0000	0.0000	0.0000	0.0000	0.0000	0.0000	0.0000	0.0000	0.0000	0.0000
v <sub>drc</sub> *	12	12	0.0000	0.0083	0.0083	0.0000	0.0000	0.1232	0.1232	0.0081	0.9116	0.2979	0.0000
v <sub>qrc</sub> *	13	13	0.0000	0.0078	0.0078	0.0000	0.0000	0.0998	0.0998	0.0055	0.3296	0.8482	0.0002
$\Delta\omega_r$	14	14	0.0000	0.0000	0.0000	0.0000	0.0000	0.0002	0.0002	0.0002	0.0000	0.0004	0.5035
I <sub>dL</sub>	15	15	0.0000	0.0000	0.0000	0.5000	0.5000	0.0000	0.0000	0.0000	0.0000	0.0000	0.0000
I <sub>qL</sub>	16	16	0.0000	0.0000	0.0000	0.4999	0.4999	0.0000	0.0000	0.0000	0.0000	0.0000	0.0000
I <sub>dgc</sub> *	17	17	0.0000	0.0000	0.0000	0.0000	0.0000	0.0000	0.0000	0.0000	0.0000	0.0000	0.0000
v <sub>dgc</sub> *	18	18	0.0000	0.0000	0.0000	0.0000	0.0000	0.0000	0.0000	0.0000	0.0000	0.0000	0.0000
v <sub>qgc</sub> *	19	19	0.0000	0.0000	0.0000	0.0000	0.0000	0.0000	0.0000	0.0000	0.0000	0.0000	0.0000
Governor	20	20	0.0000	0.0000	0.0000	0.0000	0.0000	0.0000	0.0000	0.0000	0.0000	0.0000	0.0097
I <sub>drc</sub> *	21	21	0.0000	0.0014	0.0014	0.0000	0.0000	0.0280	0.0280	0.0005	0.0294	0.0021	0.0001

PARTICIPATION	EIGENVALUE										
N	N <sup>0</sup>	12	13	14	15	16	17	18	19	20	21
STATE	N <sup>0</sup>	12	13	14	15	16	17	18	19	20	21
V <sub>dc</sub>	1	0.0000	0.0000	0.0000	0.4999	0.4999	0.0000	0.0002	0.0000	0.0000	0.0000
$\lambda_{ds}$	2	0.0000	0.0000	0.0000	0.0000	0.0000	0.0000	0.0000	0.0000	0.0000	0.0000
$\lambda_{qs}$	3	0.0000	0.0000	0.0018	0.0000	0.0000	0.0000	0.0000	0.0000	0.0000	0.0000
$\lambda_{dr}$	4	0.0002	0.0000	0.0001	0.0000	0.0000	0.0000	0.0000	0.0000	0.0000	0.0000
$\lambda_{qr}$	5	0.0000	0.0000	0.0025	0.0000	0.0000	0.0000	0.0000	0.0000	0.0000	0.0000
$\delta$	6	0.4939	0.0122	0.0000	0.0000	0.0000	0.0000	0.0000	0.0000	0.0000	0.0000
$E_{d-pr}$	7	0.0001	0.0000	0.0000	0.0000	0.0000	0.0000	0.0000	0.0302	0.9698	0.0000
$E_{q-pr}$	8	0.0000	0.0000	0.0000	0.0000	0.0000	0.0000	0.0000	0.9698	0.0302	0.0000
Conductance G	9	0.0003	0.0000	0.0002	0.0000	0.0000	0.0000	0.0000	0.0000	0.0000	0.0000
WT speed $\omega_r$	10	0.0000	0.0000	0.0000	0.0000	0.0000	1.0000	0.0000	0.0000	0.0000	0.0000
I <sub>qrc</sub> *	11	0.0000	0.0000	0.0000	0.0000	0.0000	0.0000	0.0000	0.0000	0.0000	0.0000
v <sub>drc</sub> *	12	0.0000	0.0000	0.0027	0.0000	0.0000	0.0000	0.0000	0.0000	0.0000	0.0000
v <sub>qrc</sub> *	13	0.0002	0.0000	0.0000	0.0000	0.0000	0.0000	0.0000	0.0000	0.0000	0.0000
$\Delta\omega_r$	14	0.5035	0.0073	0.0000	0.0000	0.0000	0.0000	0.0000	0.0000	0.0000	0.0000
I <sub>dL</sub>	15	0.0000	0.0000	0.0000	0.0025	0.0025	0.0000	0.0049	0.0000	0.0000	0.0000
I <sub>qL</sub>	16	0.0000	0.0000	0.0000	0.4975	0.4975	0.0000	0.9946	0.0000	0.0000	0.0000
I <sub>dgc</sub> *	17	0.0000	0.0000	0.0000	0.4999	0.4999	0.0000	0.0001	0.0000	0.0000	0.0000
v <sub>dgc</sub> *	18	0.0000	0.0000	0.0000	0.5000	0.5000	0.0000	0.0001	0.0000	0.0000	0.0000
v <sub>qgc</sub> *	19	0.0000	0.0000	0.0000	0.0000	0.0000	0.0000	0.0000	0.0000	0.0000	1.0000
Governor	20	0.0097	0.9952	0.0000	0.0000	0.0000	0.0000	0.0000	0.0000	0.0000	0.0000
I <sub>drc</sub> *	21	0.0001	0.0000	0.9963	0.0000	0.0000	0.0000	0.0000	0.0000	0.0000	0.0000

From the eigenvalues obtained, the system is stable under the small signal analysis because all real parts are negative. It also shows that some modes 2,3,6,7,8,9,10 contribute to the fast dynamic responses and these modes are related to the states:

DFIG states:  $\lambda_{ds}$ ,  $\lambda_{qs}$ ,  $\lambda_{dr}$ ,  $\lambda_{qr}$

Control states: constant power load G,  $v_{drc}^*$  and  $v_{qrc}^*$

And other modes 11,12,13,14,15,16,17 contribute to the dominant modes and related to the states:

DFIG states:  $\omega_r$

SG states:  $\Delta\omega_r$ ,  $\delta$

Control states:  $V_{dc}$ ,  $I_{dgc}^*$ ,  $v_{dgc}^*$ ,  $I_{drc}^*$  and Governor

From the above, the states of DFIG could be candidates for model simplification with its fast dynamic responses. And the dominant modes 11, 12 of rotor angle of synchronous generator are the candidates for adding damping due to their low damping ratio, whereas the mode 17 of rotor of wind turbine provides the high ratio damping. It also observes that oscillation mode of the synchronous generator provides the high oscillation with frequency 12.7510 rad/s (2.03 Hz). This results from the small inertia of synchronous  $H = 2$  sec. However, the value of this frequency is reduced to 8.0370 rad/s (1.28 Hz) when  $H = 5$  sec and to 5.6702 rad/s (0.90 Hz) when  $H = 10$  sec.

## CHAPTER VI

### CONCLUSION

#### 6.1 Conclusion

The studies on stability performances of a microgrid application under various disturbances including the naturally fluctuation of the wind speed and the large disturbance of the fault have been conducted. The system modeled includes dynamics and control of the doubly-fed induction generator driven by the pitch-controlled wind turbine, the synchronous generator with droop characteristic, and the constant-power portion of the system load. The fluctuation of the wind speed has been represented using Weibull random distribution. Based upon simulated test results carried out using Matlab/Simulink, it can be concluded that the MG operates quite stably under normal operation with wind speed fluctuation and with non-islanding faults. Nevertheless, under disturbance operation which brings about isolation of the MG from the main grid, it reveals clearly the superiority of modern control design of wind turbine using DFIG to those of SCIG. Additionally, with no control on the rotor-side of an induction generator, as in the case of a squirrel cage-type induction machine, the local capacitor for voltage support is of necessity to ensure stable operation of the wind power station.

#### 6.2 Future Works

The microgrid system is a new concept of power system operation under the research and developing (R&D). Also it has various designs of microgrid systems depending on the different operational purpose so the stability of the system may also depend on the configuration of the system. And the future work will also

1. Try to address the control performance standard of the MG
2. Examine control design of DFIG to enhance the stability of the MG

ศูนย์วิทยทรัพยากร  
จุฬาลงกรณ์มหาวิทยาลัย

## REFERENCES

- [1] F. Katiraei, M.R. Iravani. **Transients of a Micro-Grid System with Multiple Distributed Energy Resources.** *International Conference on Power Systems Transients (IPST'05)*. Montreal, Canada, June 19-23, (2005).
- [2] N. Miller, **Report on Distributed Generation Penetration Study.** Subcontractor report, 1617 Cole Boulevard. Golden, Colorado 80401-3393: National Renewable Energy Laboratory, August 2003.
- [3] Mohamed, Faisal. **Microgrid Modelling And Simulation.** Thesis for the degree of Licentiate of Science in Technology, Helsinki University of Technology Control Engineering Laboratory, March 2006.
- [4] B. Kroposki, **DG Power Quality, Protection, and Reliability Case Studies Report.** Subcontractor report, 1617 Cole Boulevard Golden, Colorado 80401-3393: National Renewable Energy Laboratory, August 2003.
- [5] Lasseter, Robert H. **Control and Design of Microgrid Components.** Final Project Report, Board of Regents, University of Wisconsin System: Power Systems Engineering Research Center, January 2006.
- [6] Ned Mohan, Tore M. Undeland and William P. Roobins. **Power Electronics Converters, Applications, and Design.** 3rd edition. John Wiley & Sons, inc, 2003.
- [7] KNAZKINS, VALERIJS. **Stability of Power Systems with Large Amounts of Distributed Generation.** Doctoral Thesis, SWEDEN: KTH Electrical Engineering, October 2004.
- [8] A. P. Sakis Meliopoulos, George J. Cokkinides. **Small Signal Stability Analysis of the Integrated Power System - MicroGrid Model.** *Bulk Power System Dynamics and Control*. Cortina d'Ampezzo, Italy, August 22-27, (2004).
- [9] N. Jayawarna, X. Wu, V. Zhang, N. Jenkins, and M. Barnes. **Stability of a MicroGrid.** *The 3rd IET International Conference*. 4-6 April (2006): 316 - 320.
- [10] Ackermann, Thomas. **Wind Power in Power System.** John Wiley & Sons, Ltd, 2005.
- [11] The MatWorks, **SimPowerSystems For Use with Simulink,** User's Guide Version 4.
- [12] R.Patel, Mukund. **Wind and Solar Power Systems.** 2nd edition. Taylor & Francis, 2006.
- [13] R. Krishnan. **Electric Motor Drives Modeling Analyzing and Control.** Prentice Hall, 2001.
- [14] S.N. Bhadra, D. Kastha and S. Banerjee. **Wind Electrical Systems.** Oxford University, 2005.
- [15] P. Kundur. **Power System Stability and Control.** McGraw-Hill, Inc, 1994.
- [16] N. Hoonchareon, **Lecture Notes on Power System Stability.** Chulalongkorn University, 2008.
- [17] Peter W. Sauer and M.A. Pai. **Power System Dynamics and Stability.** Prentice-Hall, Inc, 1998.



**APPENDIX**

ศูนย์วิทยทรัพยากร  
จุฬาลงกรณ์มหาวิทยาลัย

## APPENDIX A

Table A. 1 Wind turbine and induction generator data [11]

Name	Value
Rated power [Mw]	2
Base wind speed (wind_base) [m/s]	6
Base rotational speed or rotational speed at maximum power for the base wind speed (speed_nom) [p.u.]	1.2
Nominal tip speed ratio $\lambda_{nom}$	8.1
Nominal power coefficient $Cp_{nom}$	4.8
Rated frequency (Hz)	60
Mutual inductance Lm (p.u.)	2.9
Stator resistance Rs (p.u.)	0.00706
Stator leakage inductance Lls (p.u.)	0.171
Rotor resistance Rr (p.u.)	0.005
Rotor leakage inductance Llr (p.u.)	0.156
Inertia H (s)	5.04

Table A. 2 Synchronous generator data

Name	Value
Rated power [Mw]	1
Armature winding resistance Ra (p.u.)	0.003
Stator leakage reactance Xls (p.u.)	0.15
Stator d-axis self reactance Xd (p.u.)	1.81
Stator q-axis self reactance Xq (p.u.)	1.76
Inertia H (s)	2

ศูนย์วิทยทรัพยากร  
จุฬาลงกรณ์มหาวิทยาลัย

## BIOGRAPHY

Sovannarith Leng was born on August, 06 1982 in Phnom Penh, the capital city of Cambodia. He spent most of his time in Phnom Penh from the primary school until he finished his undergraduate study. He studied in Department of Electrical Engineering, major of Electrical Engineering, Institute of Technology of Cambodia (ITC), Phnom Penh, Cambodia. He earned his Bachelor of Engineering degree in 2006. He was awarded AUN/SEED-Net scholarship to continue his study in Department of Electrical Engineering, Faculty of Engineering, Chulalongkorn University, Bangkok, Thailand in November 2006. His current research interests are in the stability of power system and microgrid.



ศูนย์วิทยทรัพยากร  
จุฬาลงกรณ์มหาวิทยาลัย